Experimental Study on *n*-Butane Partial Oxidation to Maleic Anhydride in a Solid Electrolyte Membrane Reactor

Experimentielle Untersuchung der partiellen Oxidation von n-Butan zu Maleinsäureanhydrid in einem Festelektrolytmembranreaktor

Dissertation

zur Erlangung des akademischen Grades

Doktoringenieur
(Dr.-Ing.)

von M.Sc. Yinmei Ye

geb. am 15. November 1972 in Hubei

genehmigt durch die Fakultät für Verfahrens- und Systemtechnik
der Otto-von-Guericke-Universität Magdeburg

Gutachter: Prof. Dr.-Ing. Kai Sundmacher
Priv.Doz. Dr.-Ing Roland Dittmeyer

Promotionskolloquium am 03.03.2006

Preface

This work was carried out at the Max Planck Institute (MPI) for Dynamics of Complex Technical Systems in Magdeburg between November 2001 and August 2005. It is a part of the research project “Membrane Supported Reaction Engineering Research” at Otto-von-Guericke University Magdeburg and MPI Magdeburg funded by the Deutsche Forschungsgemeinschaft (DFG, Project 447). I would like to take this opportunity to express my thanks to all people who supported this work.

I am most grateful to Professor Kai Sundmacher for providing me with the opportunity to do this project and for his excellent guidance and supervision throughout this work together with continuous encouragement. I extend my heartfelt thanks to Dr. Liisa Rihko-Struckmann for her precious advice and many fruitful scientific discussions during my work as well as for her valuable comments on this thesis.

I owe thanks to all colleagues at the MPI and the Otto-von-Guericke University of Magdeburg for their cooperation and discussions. Special thanks go to colleagues of “Electrochemical Membrane Reactor research” group (TP5): Professor Helmut Rau, Dr. Rene Frömmichen, Dipl.-Ing. Barbara Munder and Dipl.-Ing. Lyubomir Chalakov for their suggestions and valuable comments on my experimental work. Especially I wish to thank Dr. Frank Klose for his altruistic advice and Ms. Bianka Stein for her technical support. I additionally thank Professor Helmut Weiß and Dr. Yuri Suchorski at Otto-von-Guericke University Magdeburg for carrying out XPS measurement.

The financial support of the Max-Planck-Society for providing me with the Max-Planck-Scholarship is gratefully acknowledged.

Finally, my deepest thanks go to my husband, my daughter and my big family for their continuous support and encouragement throughout these years.

Magdeburg, September 2005

Contents

List of Symbols

A	electrode area (cm^2)
a_O	oxygen activity
C	capacitance (F)
E	potential (V)
E_a	apparent activation energy (kJ/mol)
$E_{cell,0}$	electromotive force of fuel cell at zero current (V)
E_{c_a}	terminal voltage between the cathode and the anode (V)
e	electron
F	Faraday's constant (96485 C/mol)
f	frequency (Hz)
$\Delta_R G$	Gibbs free energy of reaction (kJ/mol)
ΔH_a	association energy (kJ/mol)
ΔH_m	migration energy (kJ/mol)
h	electron hole
I	current (A)
i	current density (A/cm^2)
k	Boltzman constant, (1.3806×10^{-23} J/K)
L	membrane thickness (m)
n_i	number of moles (mol)
O_O^X	lattice oxygen
$O^{\delta-}$	electrophilic oxygen species
O^*	adsorbed oxygen species
q_i	charge number
r	reaction rate at close-circuit condition (mol/s or mol O/s)
r_0	reaction rate at open-circuit condition (mol/s or mol O/s)
r_+	reaction rate with positive current (mol/s or mol O/s)
r_-	reaction rate with negative current (mol/s or mol O/s)
R	universal gas constant (8.314 J/(mol K))

R	resistance (ohm)
S	selectivity (%)
T	temperature (K)
V_{VA}	charged vanadium vacancy
$V_{O}^{\cdot\cdot}$	oxygen vacancy
X	conversion (%)
Y	yield (%)
Z	impedance (ohm)
Z'	real part of impedance (ohm)
Z''	imaginary part of impedance (ohm)

Greek symbols

α	depression factor
υ_i	mobility ($m^2V^{-1}s^{-1}$)
η	overpotential (V)
Λ	rate enhancement factor
Λ_+	rate enhancement factor with positive current
Λ_-	rate enhancement factor with negative current
μ	chemical potential (kJ/mol)
θ	depression angle
ρ	enhancement ratio
ρ_+	enhancement ratio with positive current
ρ_-	enhancement ratio with negative current
σ	electrical conductivity ($ohm^{-1}cm^{-1}$)
ω	angular frequency (s^{-1})

Abbreviations

BET	Brunauer Emmett Teller
CFB	circulating fluidized-bed
CNLS	complex nonlinear least squares
CR	co-feed membrane reactor

EIS	electrochemical impedance spectroscopy
EMR	electrochemical membrane reactor
EOP	electrochemical oxygen pumping
FID	flame ionization detector
GC	gas chromatograph
LSGM	strontium and magnesium doped lanthana gallat
MA	maleic anhydride
MIEC	mixed ion-electron conductivity
MMR	mixed-feed membrane reactor
NEMCA	non-Faradaic electrochemical modification of catalytic activity
OCP	open-circuit potential
PB	phase boundary
PVD	physical vapor deposition
ScSZ	scandia stabilized zirconia
SE	solid electrolyte
SEMR	solid electrolyte membrane reactor
SEM	scanning electron microscopy
SEP	solid electrolyte potentiometry
SOFC	solid oxide fuel cell
TAP	Temporal-Analysis-Products
TCD	thermal conductivity detector
VPO	vanadium phosphorus oxide
XPS	X-ray photoelectron spectroscopy
XRD	X-ray diffraction
YSZ	yttria stabilized zirconia

Abstract

In this study the partial oxidation of *n*-butane to maleic anhydride (MA) in a solid electrolyte membrane reactor (SEMR) was investigated experimentally.

The electrical conductivity of solid electrolyte membrane materials and vanadium phosphorus oxide (VPO) catalyst was investigated with 2-probe impedance spectroscopy. 13% yttria stabilized zirconia was selected as the solid electrolyte membrane material due to its higher oxygen ion conductivity at low temperature. The electrical conductivity of VPO catalyst was found to be too low to directly serve as the anode, therefore an oxide-covered metallic anode structure was designed for the SEMR.

Prior to butane oxidation, the reactor was initially characterized with electrochemical methods. The measured oxygen flux through the membrane under electrochemical oxygen pumping agreed well with that predicted from Faraday's law at low current, while it slightly deviated at high current.

Butane oxidation in the SEMR was carried out in three different operation modes: (1) electrochemical membrane reactor (EMR), (2) co-feed membrane reactor (CR), and (3) mixed-feed membrane reactor (MMR). The feasibility of MA synthesis in the EMR was demonstrated with periodic redox and steady-state experiments. The selectivity to MA as well as the MA yield in the EMR was strongly influenced by the imposed current, reaction temperature and butane concentration as well as the anodic flow rate. The studied EMR gave a MA yield of 10% with MA selectivity up to 53% at a reaction temperature of 753 K.

The EMR operation gave higher conversion of oxygen but lower selectivity to MA than the CR operation. For the MMR operation, both the positive and negative currents led to a decrease in the MA selectivity compared to the CR operation. By means of comparing the three operation modes, the electrochemically pumped oxygen was found to be more reactive but less selective to MA than gas-phase oxygen, which is mainly related to the different reaction mechanisms between the CR and EMR operations.

A simplified reaction-mechanism scheme was finally proposed for butane oxidation carried out in the EMR. It involves not only the same catalytic reaction with well-known oxygen species such as O_2, O^* (adsorbed) and O_O^X (lattice oxygen in VPO catalyst) as in the CR but also an electrocatalytic reaction with O^{2-} and electrophilic oxygen species such as O_2^-, O_2^{2-} and O^-.

Zusammenfassung

In dieser Dissertation wurden experimentelle Untersuchungen der partiellen Oxidation von n-Butan zu Maleinsäureanhydrid (MA) in einem Festelektrolytmembranreaktor (SEMR) durchgeführt.

Die elektrische Leitfähigkeit von verschiedenen Festelektrolytmembranmaterialien und des Katalysators, Vanadylpyrophosphat (VPO), wurde mittels Impedanzspektroskopie nach der 2-Punkt-Methode untersucht. Das mit 13% Yttriumoxid stabilisierte Zirkonoxid wurde als Membranmaterial aufgrund der höheren Sauerstoffleitfähigkeit bei niedrigen Temperaturen gewählt. Die elektrische Leitfähigkeit von VPO war zu gering, um allein als Elektrodenschicht zu funktionieren. Aus diesem Grund wurde eine VPO-beschichtete metallische Anodenstruktur für den SEMR entwickelt.

Als Ergänzung zu den Untersuchungen des Butanoxidationsprozesses wurde der Reaktor mit elektrochemischen Methoden charakterisiert. Der gemessene Sauerstoffffluss durch die Membran bei niedrigen elektrischen Stromflüssen stimmte sehr gut mit der nach dem Faradayschen Gesetz errechneten Stromfluß überein, während er bei höheren Strom-dichten kleine Abweichungen aufwies.

Die Untersuchungen der Butanoxidation wurden in drei verschiedenen Operationsmodi durchgeführt: (1) elektrochemischer Membranreaktor (EMR), (2) Co-feed Membranreaktor (CR) und (3) Mixed-feed Membranreaktor (MMR). Die Machbarkeit der Maleinsäure-anhydrid-Synthese in einem Festelektrolytmembranreaktor wurde mit periodischen Redox- und mit stationären Untersuchungen demonstriert. Die Selektivität zu MA und die Ausbeute im EMR waren stark vom elektrischen Strom, von der Reaktionstemperatur und von der Butankonzentration sowie vom anodischen Gasfluss abhängig. Der untersuchte EMR hat bei der maximalen Selektivität von 53% eine Ausbeute von 10% für MA bei einer Temperatur von 753 K erreicht.

Beim Vergleich der unterschiedlichen Operationsmodi wurde offensichtlich, dass der elektrochemisch zugeführte Sauerstoff im EMR aktiver als der gasförmig zugeführte Sauerstoff im CR war. Die Selektivität und die Ausbeute zu MA im EMR wiesen insgesamt niedrige Werte auf. Im MMR-Modus, sowohl bei negativem als auch bei positivem elektrischen Strom, verkleinert sich im Vergleich zum Operationsmodus CR die Selektivität zu MA.

Der elektrochemisch zugeführte Sauerstoff war aktiver, aber weniger selektiv bezüglich MA als der gasförmig zugeführte Sauerstoff. Aus diesem Grund wurde ein mehrstufiger Reaktionsmechanismus für die Reaktionen im EMR vorgeschlagen. Dieser beinhaltet katalytische Reaktionen mit den bekannten Sauerstoffspezies O_2, O^* (adsorbierter Sauerstoff) und O_O^X (Sauerstoff in der VPO-Katalysatorstruktur) und elektrochemische Reaktionen mit O^{2-} und elektrophilen Sauerstoffspezies wie O_2^-, O_2^{2-} und O^-.

1. Introduction

1.1. Introduction to butane partial oxidation to maleic anhydride

1.1.1. Uses of maleic anhydride

Maleic anhydride (MA) is a versatile monomer and important chemical intermediate with many uses. The primary use of MA is in the manufacture of polyester and alkyd resins. These resins are added to fiberglass reinforced plastics to make a strong, lightweight, and corrosion resistant material that is found in boats, cars, trucks, pipelines and electrical devices. In a secondary capacity, MA is employed in the manufacture of lacquers, lube-oil additives, and agricultural products. The addition of MA to drying oils decreases the required drying time and improves the coating quality of lacquers: dispersants derived from MA prolong oil change intervals and improve the efficiency of automotive engines. Agriculture products made from MA include herbicides, pesticides, and plant growth regulators. Furthermore, fumaric and maleic acid are important MA derivatives used in paper sizing resins and as food and beverage acidulants. Moreover, MA can be used as a starting material for synthesis of 1,4-butanedial. The distribution of MA uses in 2000 year is summarized in Table 1-1 [1].

Table 1-1 Uses of maleic anhydride in year 2000.

Market uses of MA	Distribution, %
Unsaturated polyster resins	63
Lubricating oil additives	10
Copolymers	9
Alkenyl succinic anhydrides	5
Maleic acid	3
Fumaric acid	2
Agricultural chemicals	1
Others	7

The consumption and demand of MA in the world shows a growing tendency. Figure 1-1 reports the world consumption of MA from 1993 to 2000 [2]. In 2001, the worldwide maleic anhydride consumption totaled 1,329 thousand metric tons. Total worldwide consumption of MA is expected to grow at a rate of approximately 6-7% annually from 2001 to 2006, reaching a level of 1.5 million metric tons in 2006.

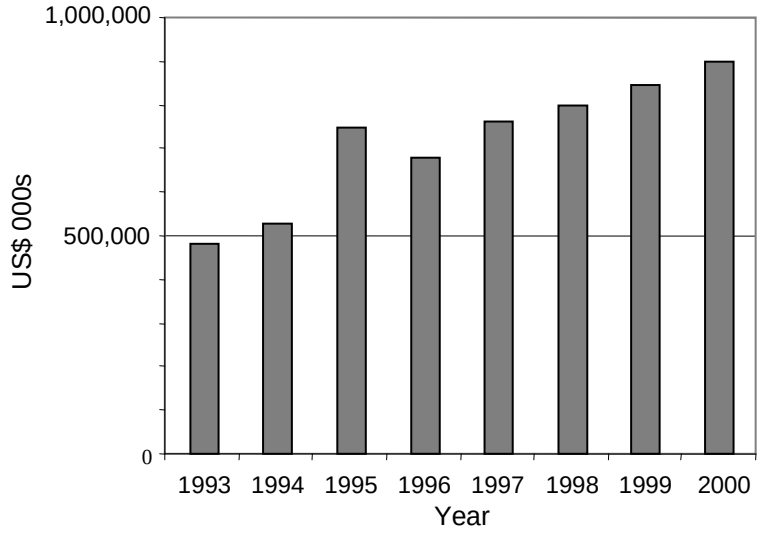

Figure 1-1 World sales of maleic anhydride, 1993-2000 (US$ 000s) [2].

1.1.2. Industrial production of maleic anhydride

MA was first synthesized in the 1830's, but was not manufactured commercially until about 1930. Initially, MA was produced by the partial oxidation of benzene using a vanadium-molybdenum oxide catalyst (V_2O_5-MoO_3). In brief, the process involved the oxidation of a low concentration of benzene in air followed by a separation step to recover MA from the reactor effluent. The conversion is high (97-99%) and the MA selectivity is near 75% with by-products CO and CO_2. However, benzene is a hazardous chemical. Over the years of efforts, *n*-butane has gradually replaced benzene for MA production, which was first realized by Monsanto in 1974. Compared to the benzene oxidation to MA, *n*-butane partial oxidation to MA was more economical, safer and more environmentally benign [3, 4].

n-Butane partial oxidation is still the only example of an industrially performed direct selective oxidation involving light alkanes. This catalytic reaction is recognized as one of the most complex selective oxidations [3-7], which involves eight hydrogen atoms abstraction and three oxygen atoms insertion with 14 electrons transferring. The reaction follows a series-

parallel reaction network (see Figure 1-2). Butane can be directly oxidized to the intermediate product MA accompanied by total oxidations to CO_x (CO and CO_2) in addition to H_2O, and MA can be over-oxidized to CO_x.

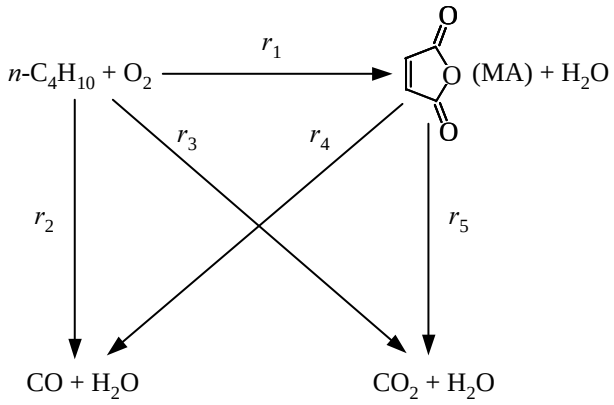

Figure 1-2 Reaction network of *n*-butane oxidation to MA.

There are several industrial processes for butane partial oxidation to MA where fixed-bed [8, 9], fluidized-bed [10], and circulating fluidized-bed (CFB) reactors [11] are employed. All reactions described in the network are highly exothermic (see Equations 1-1 to 1-5).

① $C_4H_{10} + 3.5O_2 \rightarrow C_4H_2O_3(MA) + 4H_2O$ $\Delta_R H = -1236\,\text{kJ/mol}$ (1-1)

② $C_4H_{10} + 4.5O_2 \rightarrow 4CO + 5H_2O$ $\Delta_R H = -1521\,\text{kJ/mol}$ (1-2)

③ $C_4H_{10} + 6.5O_2 \rightarrow 4CO_2 + 5H_2O$ $\Delta_R H = -2656\,\text{kJ/mol}$ (1-3)

④ $C_4H_2O_3 + O_2 \rightarrow 4CO + H_2O$ $\Delta_R H = -285\ \text{kJ/mol}$ (1-4)

⑤ $C_4H_2O_3 + 3O_2 \rightarrow 4CO_2 + H_2O$ $\Delta_R H = -1420\,\text{kJ/mol}$ (1-5)

The reaction temperature significantly affects the catalyst activity and selectivity. Therefore, the commercial fixed-bed reactor for butane oxidation is a multiple tube heat exchange reactor. The reactor is usually operated at the low temperature range from 673 to 723 K. Under low butane concentration in the feed (< 2 mol %), the butane conversion is in the range of 70-85% with the selectivity to MA around 67-75% [12, 13]. Due to the exothermicity of the reaction, the extent of the reaction in a fixed-bed reactor is limited by a low butane feed concentration (maximum 1.8 mol %) in order to avoid the formation of explosive mixtures and hot spots. Such a low butane feed concentration results in a low MA concentration in the effluent and thus increases the separation costs.

The fluidized-bed process developed in the early 1980s provides efficient heat removal. In a fluidized-bed reactor, the reaction gases flow upwards through a bed of fine catalyst particles. The fine catalyst particles and rapid mixing offer efficient heat and mass transfer, which avoids the formation of hot spots and provides a safe reactor operation at higher butane concentration (up to 4%). However, the major disadvantage of this type of reactor is the demand high attrition resistance of the catalyst to withstand the mechanical stress. The uses of attrition resistant catalysts often cause a loss in the MA selectivity. Furthermore, axial back-mixing of the catalyst causes gas back-mixing, which results in a decrease in the MA selectivity due to the consecutive combustion of MA especially at high butane conversion.

The company Dupont developed a new commercial process for butane partial oxidation to MA using a riser-regenerator circulating fluidized-bed reactor (CFB reactor). In this reactor, the oxidation of butane over the oxidized catalyst (reduction) and the regeneration (oxidation) of the reduced catalyst are carried out in separate reactors [14], i.e., in a riser reactor and a fluidized-bed regenerator, respectively. The CFB reactor offers several potential advantages over the alternative fixed- or fluidized-bed reactors for butane oxidation to MA: (1) high selectivity to MA because of essentially plug flow of the reactant gases in the riser reactor, optimal oxidation state of the catalyst and controlled oxygen concentration in the riser; (2) a very high butane concentration can be used since butane and oxygen are supplied separately and a highly concentrated product is usually obtained. However, this type of reactor requires attrition resistant catalysts with high oxygen storage capacity.

1.1.3. VPO catalyst

When introducing butane partial oxidation to MA, one has to say some words about the catalyst. Vanadium phosphorus oxide (VPO) is the unique catalyst used in the partial oxidation of *n*-butane to MA. The VPO catalyst is prepared via a multistep transformation from the precursor $VOHPO_4 \cdot 0.5H_2O$ [15, 16]. The activated VPO catalyst is known to have a complicated micro-structure often composed of numerous crystalline phases and some amorphous phases. The major crystalline phase is vanadyl pyrophosphate ($(VO)_2P_2O_7$). A second phase such as $VOPO_4$ could be present during the pretreatment and the reaction. The identified $VOPO_4$ phases are $\alpha, \alpha_{II}, \beta, \gamma, \delta$ -$VOPO_4$ [17]. $VO(PO_3)_2$ is another detectable crystalline phase in the VPO catalyst. The catalytic activity and selectivity of VPO are affected by many factors such as the crystalline phases, the vanadium oxidation state and the P/V ratio in the catalyst. In an extensive kinetics study, Buchanan and Sundaresan [18] found

that a catalyst with a P/V ratio of 1.0 was approximately twice as active as a catalyst with a P/V ratio of 1.1, while the selectivity to MA was similar.

Notwithstanding the complex nature of the active phase in the VPO catalyst, $(VO)_2P_2O_7$ appears to play a central role in the oxidation of butane to MA on the (100) crystalline face [3] since it is the dominating phase observed in the spent equilibrated VPO catalyst from the industrial fixed-bed process. It is commonly accepted that the vanadium oxidation state plays an important role in butane partial oxidation to MA. Based on the comparison between the X-ray diffraction (XRD) pattern and the radial electron distribution curve, Volta et al. [19] suggested that the active phase for the selective oxidation of *n*-butane consists of a mixture of well-crystallized $(VO)_2P_2O_7$ (V^{4+}) and an amorphous surface phase of V^{5+}. Zazhigalov et al. [20] proposed that the active catalyst must possess an optimal V^{4+}/V^{5+} ratio in order to obtain high selectivity in butane oxidation. By using a Temporal-Analysis-Products (TAP) reactor, Rodemerck et al. [21] investigated the catalytic behavior of the VPO catalysts having different vanadium oxidation states (+3.18 to +4.90). They found that catalysts with an average oxidation state of 3.7 or lower were not able to form MA, and only some intermediates such as butene, butadiene and furan in addition to the total oxidation products CO, CO_2 were observed. With a highly oxidized catalyst having an average vanadium oxidation state of 4.90, only CO_2 was formed initially and MA appeared subsequently as the catalyst was reduced under reductive conditions. For intermediate vanadium oxidation states (3.96 to 4.10), they found an increase in the MA yield with increasing vanadium oxidation state.

In brief, the MA formation needs a moderately high vanadium oxidation state. The average oxidation state of vanadium varies depending on the amount of V^{5+} present on the catalyst, which in turn is a function of the activation time and the reaction atmosphere [22]. The spent equilibrated VPO catalyst used in the industrial fixed-bed process typically exhibits a vanadium oxidation state of 4.00 to 4.03 [3].

1.1.4. Active oxygen species

Although it is generally accepted that the surface activation of butane is the rate-limiting step and that the oxidation of *n*-butane to MA occurs according to the Mars-van Krevelen mechanism [23], the nature of active oxygen species is still a subject of debate [3]. Gas-phase

oxygen, lattice oxygen and activated chemisorbed oxygen have been proposed as possible active species in the formation of the desired product MA and the undesired products CO_x.

In early works, Trifiro et al. [24] proposed that adsorbed oxygen is responsible for selective oxidation and that it is involved in the oxygen insertion steps for the formation of MA. Kruchinin et al. [25], Pepera et al. [23] and Misono et al. [26] concluded that lattice oxygen ions located in the top few surface layers are responsible for the oxidation of butane to MA and CO_x. Using the TAP reactor, Gleaves et al. [27] claimed that the VPO catalyst functions with two types of oxygen: surface lattice oxygen being responsible for the ring closure (furan formation) and activated chemisorbed oxygen involved in the further step of MA formation. Rodemerck et al. [28] reported that MA formation is associated with lattice oxygen according to the redox step, while CO_2 formation is due to a mechanism including both redox steps with lattice oxygen and steps in which the adsorbed oxygen is involved. In other words, the adsorbed oxygen is active but nonselective. Recently, Abon et al. [29] suggested on the basis of isotopic labeling results that only lattice oxygen is active for the formation of MA as well as of the other products. Using a novel oscillating microbalance reactor, Wang et al. [30] concluded that both lattice oxygen and adsorbed oxygen on the VPO catalyst could selectively oxidize butane to MA. In contrast to all these studies, Zazhigalov et al. [31] claimed that MA formation over the VPO catalyst is mainly due to gas-phase oxygen. The controversy in the literature about the role of oxygen in the selective and non-selective oxidations calls for further investigation and clarification.

1.2. Introduction to solid electrolyte membrane reactors

1.2.1. Types of membranes

Membrane reactors, as a comprehensive field of material science, catalysis and chemical engineering, have attracted increasing attention in the scientific research since the 1960s. This is because membrane reactors possess advantages in terms of enhanced catalytic activity and selectivity, combination of reaction and separation processes, simplicity in process design and safety in operation [32]. According to their most important characteristics, i.e., permselectivity and permeability, membranes can be classified into two types: porous and dense membranes.

Several excellent reviews on porous membranes have been published recently, e.g., by Marcano and Tsotsis [40], Coranas and Santamaria [32], Seidel-Morgenstern [33] and Julbe et al. [41]. Porous membranes offer a high permeability to molecules but with low permselectivity. The typical gas transport mechanisms in porous membranes are: molecular diffusion and viscous flow, capillary condensation, Knudsen diffusion as well as surface diffusion. Porous membranes have been widely and successfully employed in many oxidation reactions, such as oxidative coupling of methane [34], oxidative dehydrogenation of ethane [35], propane [36] and butane [37]. Butane partial oxidation to MA in a porous membrane reactor has been intensively investigated by the research group of Santamaria [38, 39].

Dense membranes have a rather high permselectivity to some special species but normally a lower permeability compared to porous membranes. The transport process in a dense membrane involves oxygen diffusion or ionic jumping in the lattice. Dense membranes include metallic membranes (e.g., Ag, Pd) and solid oxide dense membranes. The solid oxide dense membranes can be further classified into two types: solid electrolytes and mixed ion-electron conductors (MIEC). For the MIEC, the ionic and electronic conductivity are comparable. However, in a solid electrolyte the ionic conductivity dominates, being usually two or more orders of magnitude higher than the electronic conductivity.

The classification of a solid electrolyte is usually based on the conducting anion or cation. Nowadays, H^+, K^+, Na^+, Cu^+, Ag^+, Li^+, O^{2-}, and F^- conductors have been discovered and their properties have been studied in detail [42]. Out of all these, O^{2-} and H^+ conductors have been mainly used in solid electrolyte membrane reactors (SEMRs). Stoukides [43, 109] reviewed the current status of SEMR based on O^{2-} conductors. Recently, Iwahara et al. [44] published a prospect of hydrogen technology using proton-conducting ceramics. Very recently, Sundmacher et al. [45] reviewed the research work on SEMRs focusing on ceramic O^{2-} conductors, and high temperature as well as low temperature H^+ conductors.

1.2.2. Applications of solid electrolyte membrane reactors

The typical configuration of a SEMR is illustrated in Figure 1-3, where the membrane is an oxygen-ion conductive solid electrolyte. The cathode is exposed to oxygen-containing gas, e.g., air, and the anode is exposed to the reactants, e.g., hydrocarbons. The two electrodes are connected to a voltmeter (Case a), or to an external resistive load (Case b), or to an external

power source (Case c). The basic applications of the SEMR as shown in Figure 1-3 are the following:

(1) Solid electrolyte potentiometry,

(2) Solid oxide fuel cell, and

(3) Electrochemical oxygen pumping.

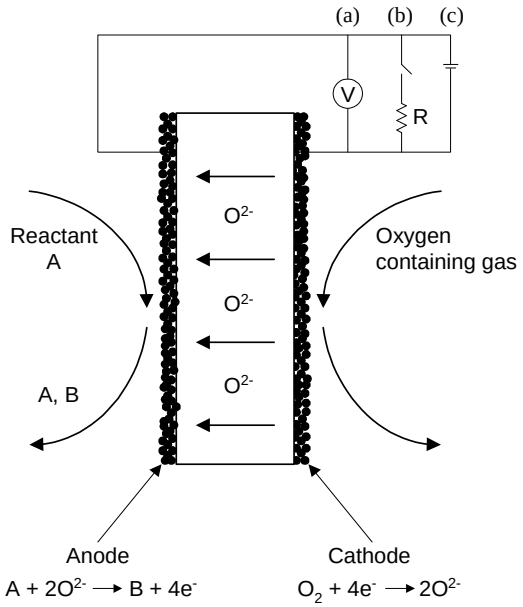

Figure 1-3 Configuration of an oxygen ion-conducting solid-electrolyte cell: (a) open-circuit operation; (b) closed-circuit operation in fuel cell mode; (c) closed-circuit operation in "pumping" mode.

1.2.2.1. Solid electrolyte potentiometry

Solid electrolytes can be applied to study the heterogeneous catalysis, which was first recognized by Wagner [46]. He proposed the use of solid electrolyte cells for the measurement of the activity of oxygen on metal and metal oxide catalysts. This technique, originally used to study the mechanism of SO_2 oxidation on noble metals [47], was subsequently termed Solid Electrolyte Potentiometry (SEP) [48]. To date it has been used in conjunction with kinetic measurements to study the mechanism of various catalytic reactions on metals [49, 50] or metal oxide catalysts [51-53].

The basic principle of SEP is the in-situ measurement of the chemical potential difference between the two electrodes on either side of a solid electrolyte at open-circuit conditions. One

of the electrodes exposed to the reactant mixture acts as both an electrode and a catalyst for the studied catalytic reaction. The other electrode exposed to air serves as a reference electrode. Under open circuit conditions (I = 0), the open-circuit potential (OCP) is measured by a voltmeter connected to the two electrodes (Case a in Figure 1-3). The OCP (E) is related to the chemical potential and can be written as:

$$E = \frac{1}{4F}\left[\mu_{O_2}(\text{catalyst}) - \mu_{O_2}(\text{reference})\right] \tag{1-6}$$

where $\mu_{O_2}(\text{catalyst})$ and $\mu_{O_2}(\text{reference})$ accordingly are the chemical potentials of oxygen at the catalyst and reference electrode surfaces; F is Faraday's constant, and 4 is the number of electrons involved in the electrode reaction.

The chemical potential of oxygen adsorbed on the reference electrode being exposed to ambient air is given by

$$\mu_{O_2}(\text{reference}) = \mu^0_{O_2}(g) + RT\ln(0.21) \tag{1-7}$$

where $\mu^0_{O_2}(g)$ is the standard chemical potential of gaseous oxygen at the temperature T and 0.21 (i.e., 0.21 atm/1 atm) corresponds to the gaseous oxygen activity in the reference gas (air).

In the same way, the chemical potential of oxygen adsorbed on the catalyst electrode [65] is

$$\mu_{O_2}(\text{catalyst}) = \mu^0_{O_2}(g) + RT\ln(a^2_O) \tag{1-8}$$

where a^2_o is the activity of oxygen adsorbed on the catalyst surface. From Equations 1-6, 1-7 and 1-8, one obtains

$$E = \frac{RT}{4F}\ln\frac{a^2_O}{0.21}. \tag{1-9}$$

When the thermodynamic equilibrium is established between oxygen in the gas phase and that adsorbed on the electrode surface, i.e., $a^2_o = P_{O_2}$ (atm)/1(atm), Equation 1-9 can be written as the Nernst equation:

$$E = \frac{RT}{4F}\ln\frac{P_{O_2}}{0.21} \tag{1-10}$$

From Equation 1-10, the unknown oxygen partial pressure can be determined. This has led to the use of solid electrolyte cells as oxygen sensors [54].

1.2.2.2. Solid oxide fuel cell

The primary application of solid electrolytes with oxygen ion conductivity is the solid oxide fuel cell (SOFC). In the SOFC, one electrode is exposed to the fuel and another to oxygen or air, and the cell works under closed-circuit conditions (Case b in Figure 1-3). The driving force, attributed to the difference of the oxygen chemical potential at the two electrodes, causes electrons to flow through the external circuit and thus electrical power is generated. Therefore, in a SOFC, the chemical reaction energy is directly converted into the electrical energy. The electromotive force $E_{cell,0}$ can be calculated from the following equation:

$$E_{cell,0} = -\Delta_R G / nF \tag{1-11}$$

where $\Delta_R G$ is the Gibbs free energy of the overall reaction and n is the number of transferred electrons.

When the external resistance load of the fuel cell is finite and electrical power is produced, the operating voltage E_{cell} generally drops below the electromotive force $E_{cell,0}$ due to the overpotential η:

$$E_{cell} = E_{cell,0} - \eta \tag{1-12a}$$

The cell overpotential η can be considered as the sum of three major components: (1) ohmic overpotential η_{ohm} arising from the ohmic resistances of membrane and electrodes, (2) concentration overpotential η_{con} caused by mass transfer resistances between the gas phase and the phase boundary at the two electrodes and (3) activation overpotential η_{act} due to the charge transfer resistances at the two electrodes:

$$\eta = \eta_{ohm} + \eta_{conc} + \eta_{act} \tag{1-12b}$$

The ohmic overpotential η_{ohm} is proportional to the cell current density i and can be written as

$$\eta_{ohm} = i\frac{L}{\sigma} \tag{1-13}$$

where σ is the oxygen ion conductivity of the membrane and L is the membrane thickness.

Figure 1-4 illustrates a typical current-voltage (I-V) curve of a fuel cell obtained by varying the external load [55]. The overall overpotential η increases with the current *I*. As indicated in Equations 1-12 and 1-13, in order to reduce the overpotential and thus to improve the efficiency of the cell, the membrane should be prepared as thin as possible and it should possess a high oxygen ion conductivity.

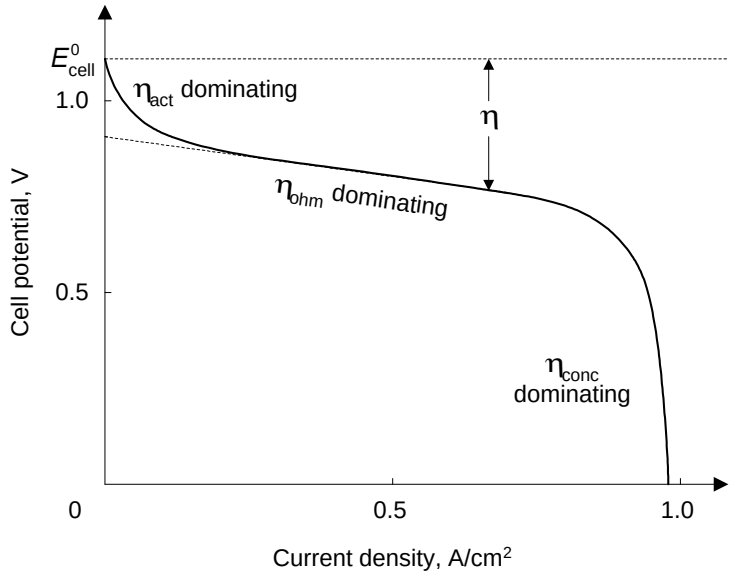

Figure 1-4 Typical current-voltage curve of a fuel cell obtained by varying the external load (adopted from literature [55]).

Due to the high operating temperatures (> 1073 K), in SOFCs various fuels can be used such as H_2, CO, CH_4, and CH_3OH. SOFCs are also attractive when valuable chemicals from the anodic reaction are produced with cogeneration of electrical energy instead of pure thermal energy. Chemical cogeneration, first demonstrated by Vayenas et al. [56] for the case of NH_3 conversion to NO, combines the concepts of a fuel cell and a chemical reactor. Recently, partial oxidation of methane over SEMR for cogeneration of electrical power and useful chemicals (i.e., synthesis gas, methanol, formaldehyde and C_2 products) has been studied [57-59].

1.2.2.3. Electrochemical oxygen pumping

The SEMR can be operated as an oxygen pump under close-circuit conditions (Case c in Figure 1-3) to carry out a reaction and produce useful chemicals rather than electrical energy.

If the spontaneously generated current is either very low or in the undesired direction, an external power source can be used to direct and control the current. The oxygen required for the reaction is then purely supplied electrochemically as O^{2-}. A current I corresponds to a flux of $I/4F$ moles of O_2 per second transported through the solid electrolyte membrane. Electrochemical oxygen pumping (EOP) has been used to study several important catalytic oxidation reactions, e.g., methane conversion to synthesis gas [60], catalytic conversion of ethane to acetaldehyde [61], and partial oxidation of C_2-C_4 alkanes [62].

Similar to the porous membrane reactor, the SEMRs provide a distributed and low local oxygen concentration compared to a conventional fixed-bed reactor, which can suppress the total oxidation. In addition, when oxygen is supplied as O^{2-}, the catalytic activity or selectivity to the desired products might be different. Lapeña-Rey et al. [63] studied the selective oxidation of methane to ethane and ethylene. They found that the electrochemically supplied oxygen gave higher overall C_2 (ethane and ethylene) selectivities than the co-feed gas-phase oxygen and they attributed this to the different local oxygen to methane ratios at the catalytic surface. Wang et al. [64] compared the catalytic and electrocatalytic oxidation of propane to propene. Their overall results suggested that the electrochemically supplied oxygen is more selective towards propene.

When the oxygen required for the reaction was supplied from both gas-phase oxygen and electrochemically pumped O^{2-}, the effect of non-Faradaic electrochemical modification of the catalytic activity (NEMCA) or electrochemical promotion might be induced. That means the change in the catalytic rate is not equal to the rate of O^{2-} transport through the solid electrolyte under the EOP condition.

The NEMCA effect has been studied for over 50 catalytic reactions on Pt, Pd, Rh, Ag, Ni, Fe, IrO_2 and RuO_2 catalyst-electrodes deposited on several types of solid electrolytes, e.g., O^{2-} conductors [65, 66], F^- conductors [67], and H^+ conductors [68]. More recently, the NEMCA effect was also found in reactions using MIEC conductors such as TiO_2 [69] and CeO_2 [70]. Work in this area has been reviewed extensively by Vayenas et al. [65, 71].

Vayenas et al. [65] attributed the NEMCA effect to changes in the catalyst work function caused by EOP. The NEMCA effect can be quantitatively expressed by two parameters [72]:

(1) The rate enhancement ratio ρ defined as

$$\rho = \frac{r}{r_0} \tag{1-14}$$

where r_0 is the catalytic reaction rate under open-circuit conditions, i.e., without EOP, and r is the NEMCA induced reaction rate under closed-circuit conditions, i.e., with EOP.

(2) The rate enhancement factor or Faradaic efficiency Λ defined as

$$\Lambda = \frac{\Delta r}{I/2F} = \frac{r - r_0}{I/2F} \tag{1-15}$$

where Δr is the change in the catalytic rate of oxygen consumption and *I/2F* is the imposed flux of O^{2-} transported through the solid electrolyte membrane, both with units of mol O/s. In the case of a pure Faradaic effect, all oxygen electrochemically transported through the membrane is consumed and thus $\Lambda = 1$, or only part of the pumped oxygen ions are reacted while the remaining part re-combines at the electrode to give molecular oxygen and thus $\Lambda <$ 1. In the case of a non-Faradaic effect, $|\Lambda| > 1$ and the reaction exhibits the NEMCA effect. When $\Lambda > 1$, the reaction is termed electrophobic; when $\Lambda < -1$, the reaction is termed electrophilic.

1.3. Scope of this work

As introduced above, MA production from butane oxidation has been commercialized either in fixed-bed or fluidized-bed reactors. However, all these reactors still suffer from disadvantages such as the demand for high attrition resistance of catalyst in fluidzed-bed reactors and possible hot spots and explosive mixtures in fixed-bed reactors. In order to overcome the limitations of these conventional reactors and simultaneously increase the MA selectivity and yield, research efforts have been carried out to develop either new promoted VPO catalysts or novel type of reactors. For example, the group of Santamaria [38, 39] investigated the application of a porous membrane reactor to MA synthesis from butane. However, butane partial oxidation in a solid oxide dense membrane reactor has not been demonstrated to our knowledge. Hence, this work will be the first study on the feasibility of butane partial oxidation to MA in a SEMR.

The principle of butane partial oxidation in a SEMR is illustrated in Figure 1-5. Gaseous oxygen (e.g., air) is supplied to the cathode and reduced to oxygen ions. Then these oxygen ions are transferred through the membrane to the anode on which the active oxygen species

react with the butane over the catalyst surface or directly discharge to form gaseous oxygen. The attractive operation is that this reactor might work in principle as a SOFC, thereby producing the valuable chemical MA at the anode with cogeneration of electrical power (Case a in Figure 1-5). The reactor can be operated under the EOP condition as well, i.e., the oxygen flux through the membrane is controlled galvanostatically by imposing an external current between the two electrodes (Case b in Figure 1-5). In order to know operational aspects of the reactor, the SEMR is initially characterized with electrochemical techniques such as SEP, I-V curve, EIS and EOP.

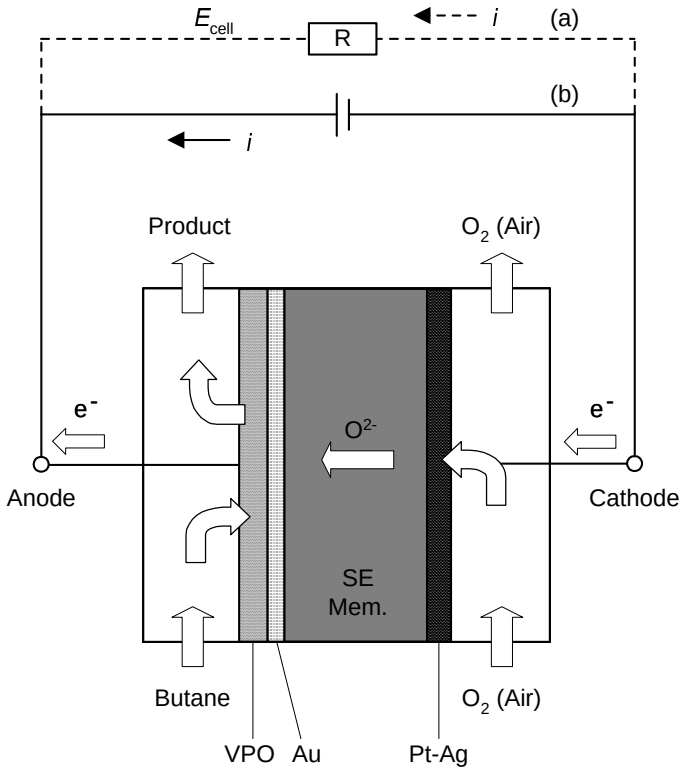

Figure 1-5 Principle of butane partial oxidation process in a solid electrolyte membrane reactor.

In butane partial oxidation, a high oxygen flux through the solid membrane is necessary to maintain the vanadium oxidation state, which plays an important role in the catalyst selectivity and activity as already introduced. The oxygen flux is directly related to the oxygen ion conductivity of the membrane that increases with increasing temperature. As introduced, butane partial oxidation to MA is usually carried out at the low temperature range, e.g., 673-723 K. Therefore, it is desirable to find a membrane material having a high oxygen ion conductivity at low temperature. This is the preliminary work before the preparation of the reactor for butane partial oxidation.

If the VPO catalyst not only has good activity and selectivity to MA but also possesses good electrical conductivity, the VPO catalyst can additionally work directly as the anode and thus the design of a SEMR for butane oxidation would be simplified. Otherwise, a complex anode structure is necessary. Therefore, the electrical conductivity of the VPO catalyst is measured before the SEMR was designed in the present work.

Compared to a conventional catalytic reactor using a mixture of butane and oxygen, one obvious advantage of the SEMR is that the explosion risk can be eliminated since butane and oxygen are totally separated by the gas-dense solid electrolyte membrane in the SEMR. Besides this, the SEMR provides a well-distributed, controlled and low local oxygen concentration compared to a conventional co-feed reactor, which usually can suppress the total oxidation. Furthermore, the active oxygen species in the SEMR might differ from those in the conventional reactor with supplying gas-phase oxygen, which possibly alters the selectivity to MA. Therefore, butane oxidation with electrochemically supplied oxygen ions is compared to that obtained with gas-phase oxygen. Based on the comparison, a tentative reaction mechanism of butane oxidation in the SEMR is proposed, which is a further goal of this work. In addition, the NEMCA effect in butane oxidation in the SEMR is examined with simultaneously supplying gas-phase and ionic oxygen, which is helpful for understanding the reaction mechanism in the SEMR.

In summary, the objectives of this work are:

(1) To screen the solid electrolyte membrane material aiming at the high O^{2-} conductivity at low temperature.

(2) To measure the electrical conductivity of the VPO catalyst.

(3) To characterize the SEMR with electrochemical techniques.

(4) To study butane partial oxidation in the SEMR with electrochemically supplied O^{2-}.

(5) To compare butane oxidation with electrochemically supplied O^{2-} to that with gas-phase O_2.

(6) To examine the NEMCA effect of butane partial oxidation with simultaneously supplying gas-phase O_2 and O^{2-}.

(7) To elucidate mechanistic aspects of butane partial oxidation in the SEMR under EOP conditions.

2. Experimental

2.1. Oxygen ion conductivity of solid electrolyte membranes

The oxygen ion conductivity of several membrane materials, i.e., yttria stabilized zirconia (13 mol % YSZ), scandia stabilized zirconia (7.5 mol %, 9 mol %, 10 mol % and 12 mol % ScSZ) (HTM Reetz, Germany) as well as $La_{0.9}Sr_{0.1}Ga_{0.85}Mg_{0.15}O_{3-\delta}$ (LSGM) (Max Planck Institute for Solid State Research at Stuttgart, Germany), were investigated as a function of temperature by means of 2-probe ac impedance spectroscopy (Zahner IM6, Zahner-elektrik GmbH, Germany). Two platinum (Pt) electrodes were prepared symmetrically by coating Pt paste (Chempur No. 900487, Germany) onto both faces of the solid electrolyte pellets, which were calcinated in air at 1173 K for 2 h. Electrochemical impedance spectroscopy (EIS) performed at OCP in air atmosphere at a temperature range from 693 to 1283 K in steps of 50 K with increasing and decreasing temperature. The exciting ac amplitude is 10 ~ 50 mV and the frequency is 1 Hz ~ 8 MHz. The connection resistance of Pt wires was subtracted from the measured impedance by initially measuring a blank cell.

2.2. Membrane reactor preparation

The tubular membrane reactor used in this work consists of three parts: (1) oxygen ion conducting solid electrolyte, (2) anode consisting of a VPO catalyst supported on a gold layer, and (3) cathode of a Pt-Ag alloy. The tubular membrane (Viking Chemicals, Denmark) had a length of 30 cm, and its inner and outer diameters were 10 mm and 10.4 mm, respectively. The inner and outer surfaces of the tube were first polished with SiC waterproof paper, then cleaned by distilled water and acetone, and finally dried at 423 K for 3 h. The cathode was prepared by depositing a thin layer of Pt-Ag paste mixture (weight ratio of Pt to Ag (Chempur, 009388) was around 1) to the inside of the YSZ tube and calcinating it in air for about 2 h at 1123 K. With the help of Pt-gauze (Chempur No. 900338) and Pt paste, a platinum wire of 0.125 mm diameter (Chempur, 009342) was affixed to the cathode. The anodic layer used as the current collector was prepared by depositing gold paste (Chempur, 902904) to the outer surface of the YSZ tube over 70 mm length from the closed-end side,

which was subsequently calcinated at 1173 K for about 2 h. The two electrodes were connected to the Potentiostat-Galvanostat with inert gold and platinum wires.

2.3. VPO catalyst preparation

The catalyst precursor, $VO(HPO_4)\cdot 0.5H_2O$, was synthesized by an organic medium method proposed by Johnson *et al*. [15]. 17.7 g V_2O_5 (Merck KGaA, Germany) was added to 375 ml isobutanol (Merck KGaA) and refluxed with 24.74g 85% H_3PO_4 (Merck KGaA) for 16 h. The light blue suspension was then separated from the organic solution by filtration and washed with 300 ml isobutanol and 225 ml ethanol. The resulting solid was refluxed in water (9 ml/g solid), filtered and dried in air at 383 K for 16 h.

The obtained precursor was mixed with distilled water (16 ml/g solid), and a slurry was formed after stirring for 24 h. The catalyst slurry was then sprayed onto the gold layer supported on the membrane and dried at 393 K for 12 h. In order to convert the precursor to the activated VPO catalyst, it was calcinated in N_2 flow for about 40 h at 823 K and subsequently activated in 1 mol % butane with air from 673 K to 753 K at 2 K/min and remained at 753 K over 10 h. The morphology and thickness of the electrodes as well as VPO catalyst layer were measured by scanning electron microscopy (SEM). The SEM images revealed that the prepared electrodes and the VPO catalyst layer were porous (Figures 2-1a, 2-1b, 2-1c) and their thickness was listed in Table 2-1.

2.4. Catalyst characterization

The specific surface area of the catalyst samples was measured by Brunauer Emmett Teller (BET) method with N_2 adsorption at 77 K with Micromeritics ASAP 2010 equipment. The determined BET surface area of the precursor and the activated VPO catalyst were listed in Table 2-1.

The electrical conductivity of the VPO catalyst was measured with 2-probe ac impedance spectroscopy as a function of temperature and atmosphere. Pellets, having 13 mm diameter and 1 mm thickness, were prepared by pressing about 300 mg powder of catalyst precursor ($VOHPO_4\cdot 0.5H_2O$) at pressure of 41 kN/cm^2. The two opposite surfaces of the pellets were coated symmetrically with platinum by physical vapour deposition (PVD) method (MED 020,

a. Pt-Ag cathode

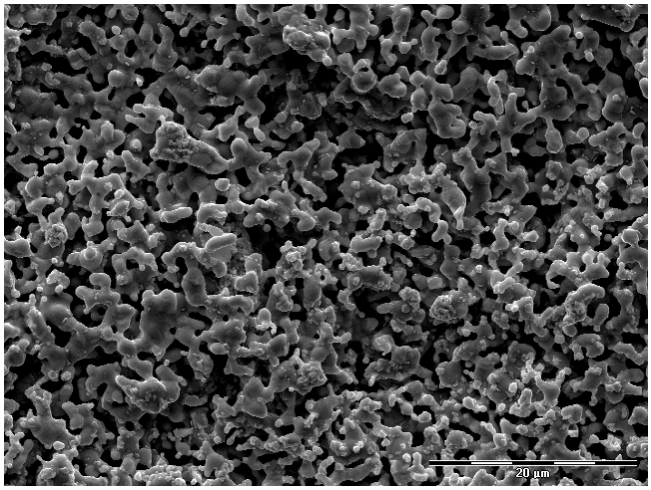

b. Au anode

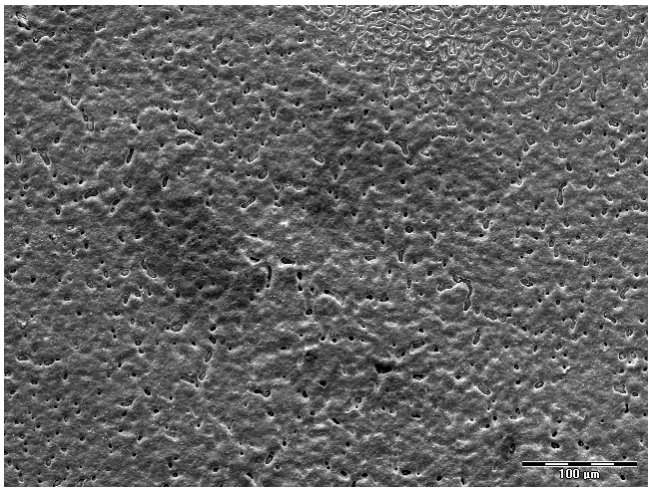

c. VPO catalyst

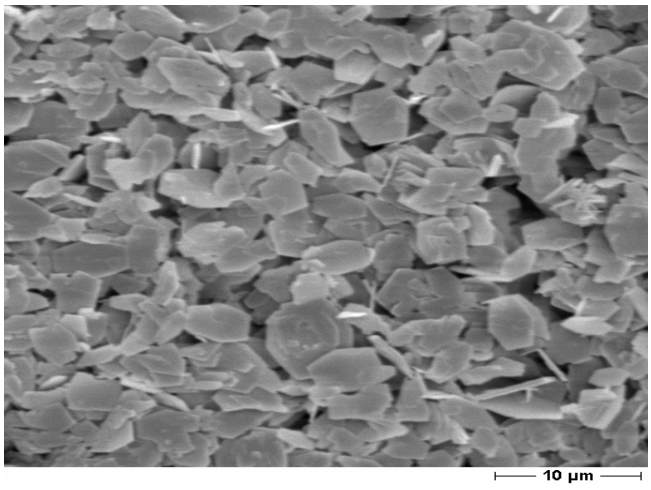

Figure 2-1 SEM of electrodes and VPO catalyst layer.

BAL-TEC, Liechtenstein). Before the conductivity measurement, the pellets were calcinated in N_2 at 673 K for about 65 h and were activated with about 1% butane in air at 693 K for about 12 h. Thus the precursor was transformed to the VPO catalyst, which was confirmed by X-ray diffraction analyses (XRD). Impedance spectra were recorded over the frequency range of 1 Hz ~ 8 MHz with 100 ~ 200 mV excitation voltage.

The carbon content in the used and fresh VPO catalyst was determined with a LECO CNHS-932 analyzer.

The crystal structures of the precursor and the fresh and used VPO were determined by XRD analysis. The analyses from powder samples were carried out using an X-ray diffract meter D5000 Bruker/AXS with a thin film attachment and Cu-Kα radiation at ambient temperature.

X-ray photoelectron spectroscopy (XPS) was used to determine the vanadium oxidation state on the surface of the fresh and used VPO catalyst. XPS analysis was performed in a stainless steel multi-chamber UHV system using a hemispherical electron energy analyzer (PHOIBOS 150, SPECS). The base pressure in the analysis chamber was lower than 5×10^{-9} mbar. A standard high-intensity Al/Mg twin anode X-ray source (XR-50, SPECS) was used, with pass energy of 10 eV. High-resolution spectra were corrected for charging effects by assigning a value of 284.5 eV to the C1s peak (adventitious carbon). Briefly, the percentage of surface V^{4+} and V^{5+} oxidation states was obtained by deconvolution of the V $2p_{3/2}$ peak as described in literature [73, 74].

2.5. Experimental setup

A schematic diagram of the experimental setup is shown in Figure 2-2, which includes four major parts: (a) the solid electrolyte membrane reactor and oven, (b) the gas chromatograph (GC) and data acquisition system, (c) the Galvanostat-Potentiostat, and (d) the mass flow controllers.

A SEMR with one end closed was constructed from a 13 mol % yttria-stabilized zirconia (YSZ) tube. The tubular membrane reactor was fixed inside a quartz glass tube, which was placed in an electrical furnace for temperature control. Air was introduced to the inside of the YSZ tube (cathode compartment). The butane diluted in N2 was always fed from the closed-end side to the anodic compartment formed between the inner wall of the quartz tube and the

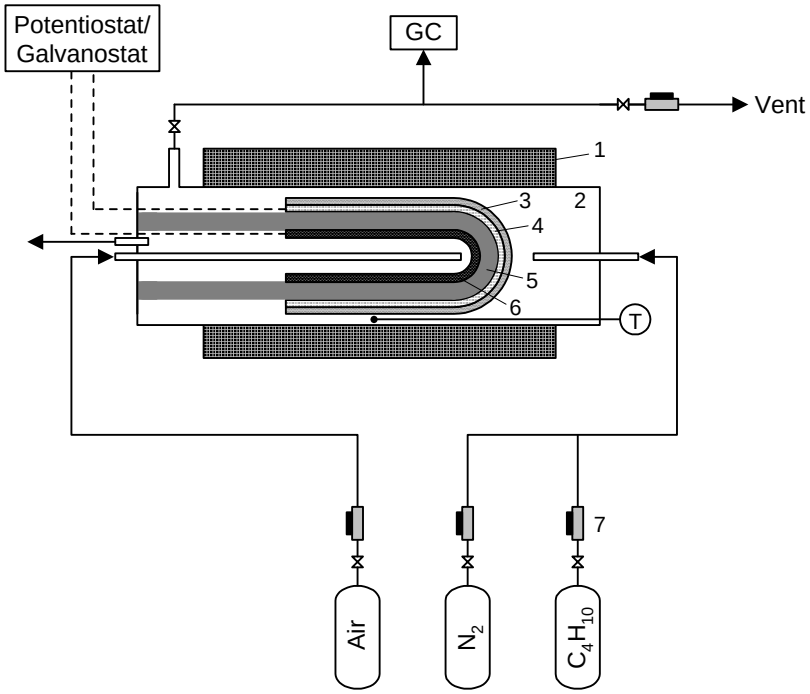

Figure 2-2 Schematic diagram of the experimental setup: (1) oven; (2) quartz glass tube; (3) VPO catalyst layer; (4) Au layer; (5) 13% YSZ membrane; (6) Pt-Ag layer; (7) mass flow controller.

Table 2-1 SEMR dimensions and butane oxidation conditions.

Parameter	Value
Membrane inner diameter	10.0 mm
Membrane outer diameter	10.4 mm
Electrode area	22.8 cm^2
Anode thickness	10 μm
Cathode thickness	15 μm
VPO catalyst layer thickness	50-100 μm
BET surface area of VPO precursor	4 m^2/g
BET surface area of VPO catalyst	11 m^2/g
Reaction temperature	723-784 K
Anode feed	0.35-1.16 mol % n-butane with N_2
Cathode feed	80-100 ml/min air
Current density	0.4-3.1 mA/cm^2
Weight hourly space velocity (WHSV)	8-40 h^{-1}

Note: WHSV=total mass feed rate in the anode (g/h) / weight of VPO catalyst (g)

outer wall of the YSZ tube at atmospheric pressure. The flow rates of inlet reactants and outlet products were regulated and measured respectively by mass flow controllers (measuring range, N_2: 10-500 ml/min, C_4H_{10}: 0.5-25 ml/min, Air: 2-100 ml/min, mixture vent: 10-500 ml/min). Constant current between the two electrodes was imposed by a Galvanostat-Potentiostat (Zahner IM6) with simultaneous recording of the terminal voltage. The experimental conditions are summarized in Table 2-1.

The reactants and the products were analyzed with an on-line GC equipped with a thermal conductivity detector (TCD) and a flame ionization detector (FID) (Agilent 6890N series) using the HP Chemstation program from Agilent to integrate data. MA and other hydrocarbons such as butane and butenes were analyzed by FID, while O2, N2, CO, CO2 and H2O were analyzed by TCD. More details are given in Appendix I. The GC was calibrated with liquid solutions of MA, dihydrofuran, furan and crotonolactone. For the gaseous component calibration, premixed calibration gases: (1) mixture of n-C4H10, N2, CO and CO2, and (2) mixture of O2, N2 were used (Westfalen AG, Germany). Electrically heated sampling lines (673 K) from the reactor to the GC were used to avoid the condensation and crystallization of MA.

The reaction results are mainly presented in terms of conversion of *n*-butane and oxygen, selectivity to the major products MA, CO, CO_2 as well as the yield of MA. The carbon and oxygen balance for the experimental results reported in this work were 97±5%. The butane conversion, $X_{C_4H_{10}}$, was calculated as follows:

$$X_{C_4H_{10}} = 1 - \frac{4Y_{C_4H_{10}}}{\sum n_i Y_i} \tag{2-1}$$

where n_i is the number of carbon atoms per molecule of the carbon containing products and reactants i, and Y is molar fraction in the effluent of the anode reaction chamber. The conversion of oxygen was calculated from

$$X_{\text{oxygen}} = 1 - \frac{2Y_{O_2}}{\sum m_j Y_j} \tag{2-2}$$

where m_j is the number of oxygen atoms per molecule of the oxygen containing products and reactants j.

The selectivities with respect to the carbon containing products *i* were calculated as the ratio of the carbon moles in a given product to the total carbon moles in the reaction products (Equation 2-3). The MA yield was calculated from the product of butane conversion and MA selectivity (Equation 2-4).

$$S_i = \frac{n_i Y_i}{\sum n_i Y_i},\ i \neq \mathrm{C_4H_{10}} \tag{2-3}$$

$$Y_{\mathrm{MA}} = X_{\mathrm{C_4H_{10}}} S_{\mathrm{MA}} \tag{2-4}$$

2.6. Operation modes

As illustrated in Figure 2-3, butane partial oxidation in the SEMR was carried out in three operation modes according to the different oxygen feeding to the anode compartment:

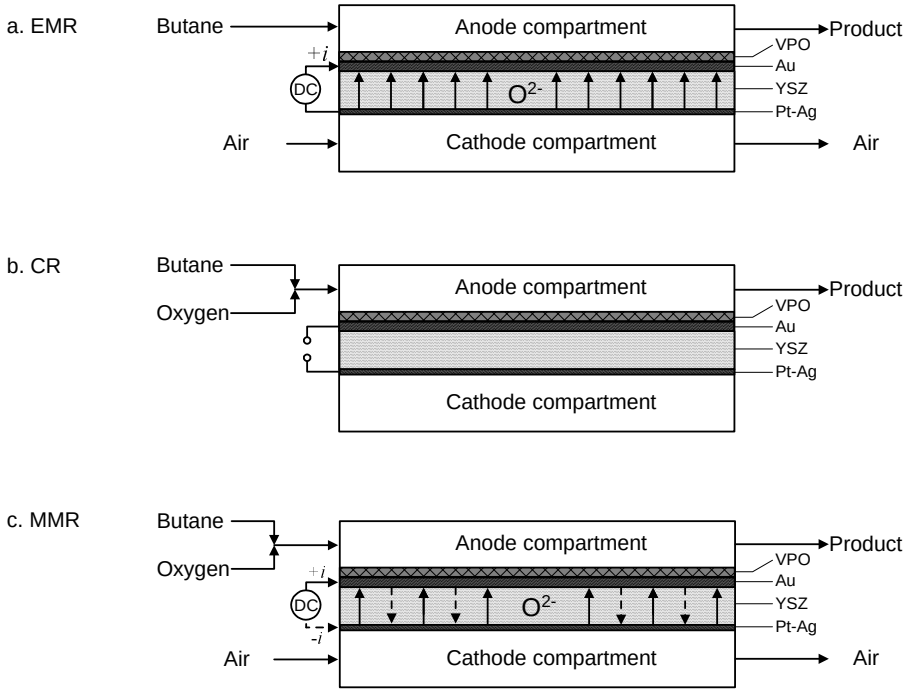

Figure 2-3 Illustration of three different operation modes, (a) Electrochemical membrane reactor, (b) Co-feed membrane reactor, (c) Mixed-feed membrane reactor.

(a) Electrochemical membrane reactor (EMR): butane was fed to the anode compartment and the oxygen required for the anodic butane oxidation was supplied in the form of O^{2-} by means of EOP, i.e., O^{2-} was pumped from the cathode to the anode by imposing

an external positive current to the reactor. In this mode, the SEMR was operated under closed-circuit conditions and the solid electrolyte membrane worked as an oxygen pump and as the catalyst support.

(b) Co-feed membrane reactor (CR): gas-phase oxygen (O_2) and butane were premixed and co-fed to the anode compartment, where the SEMR was operated under open-circuit conditions and the solid electrolyte membrane only worked as the catalyst support.

(c) Mixed-feed membrane reactor (MMR): the SEMR was operated under closed-circuit conditions. A mixture of O_2 and butane was fed to the anode compartment and O^{2-} was simultaneously supplied to or removed from the anode by imposing a positive or negative current to the reactor. Herein, positive currents ($+i$) mean O^{2-} was pumped to the anode side while negative currents ($-i$) mean O^{2-} was pumped away from the anode side.

3. Screening Membrane Materials

As introduced in Chapter 1, a low operating temperature is favorable for butane partial oxidation to MA. At low temperatures, the solid electrolyte membrane used in the reactor for the oxidation should have a high oxygen ion conductivity in order to increase the oxygen flux through the membrane. In this chapter, the oxygen ion conductivity of several solid electrolyte candidates was studied using the EIS technique.

3.1. Theoretical aspects

3.1.1. Impedance and EIS

When a sinusoidally varying potential $e(t) = E\sin(\omega t)$ is applied to a cell, the resulting steady state current $i(t) = I\sin(\omega t + \phi)$ is obtained. Here ω is the angular frequency with $\omega = 2\pi f$ (f is the conventional frequency in Hz), and ϕ is the phase difference between the voltage and the current. Similar to the Ohm's law, the impedance Z is defined as:

$$Z(t) = \frac{e(t)}{i(t)} \tag{3-1}$$

Impedance is a more general concept than resistance because it takes phase differences into account. In general, the complex impedance Z is frequency-dependent as defined above, and it can be divided into two components: the real part of the complex impedance, Z', and the imaginary part of complex impedance, Z'', i.e.,

$$Z = Z' - jZ'' \tag{3-2}$$

where $j = \sqrt{-1}$ is the imaginary number.

EIS is based on the measurement of the impedance Z as a function of f or ω over a wide frequency range. The impedance spectra are usually presented in the form of "Nyquist plots" or "Bode plots". The "Nyquist plot" shows the variation of the imaginary part of the complex impedance, Z'', against the real part of complex impedance, Z'. The "Bode plot" presents the

variation of the modulus of the complex impedance Z and the phase angle ϕ with respect to the frequency f .

3.1.2. Brick layer model and equivalent circuit

A real solid ceramic electrolyte is generally polycrystalline, which consists of many grains as illustrated in Figure 3-1a. The grains are usually termed bulk and the adjacency between the grains is called grain boundary. A simplified brick layer model [75] has been used to describe the ceramic microstructure (see Figure 3-1b). It assumes that the ceramic electrolyte consists of identical cubic grains and the grains are connected by grain boundaries. The grain boundary is oriented to be parallel or perpendicular to the electrode interface.

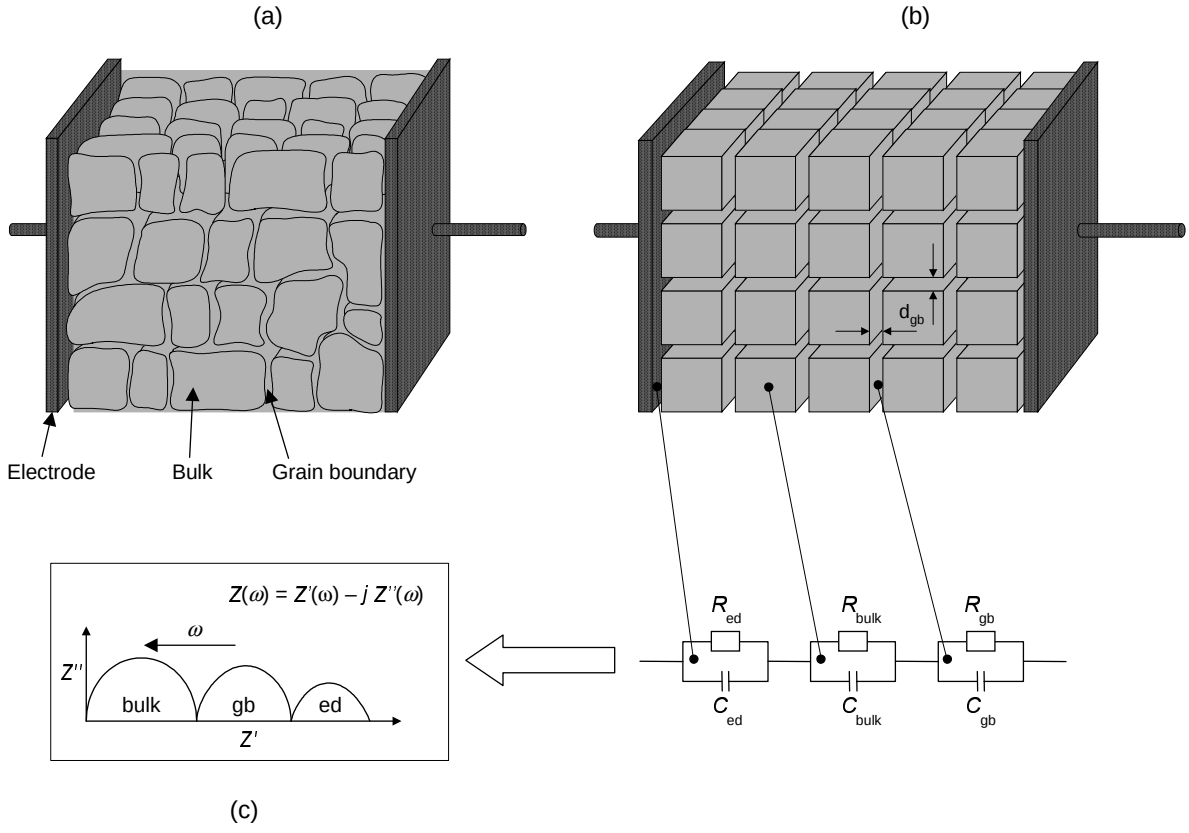

Figure 3-1 (a) Sketch of the real ceramic microstructure, (b) simplified brick layer model and equivalent circuit, (c) idealized impedance spectroscopy. Indices: ed = electrode-electrolyte interface, gb = grain boundary [76].

It is convenient to use an equivalent circuit to describe the brick layer model. As shown in Figure 3-1b, the first RC (resistor-capacitor) circuit (R_{bulk}, C_{bulk}), the second RC circuit (R_{gb},

C_{gb}) and the third RC circuit (R_{ed}, C_{ed}) accordingly correspond to the bulk, the grain boundary of the electrolyte and the interface between the electrode and the electrolyte. Each RC circuit gives rise to a semicircle and the corresponding idealized Nyquist plot is illustrated in Figure 3-1c. The semicircle at low frequencies corresponds to the behavior of the electrolyte-electrode interface, the intermediate frequency semicircle is due to the grain boundaries and the high frequency semicircle arises from the properties of the bulk material. It is worth mentioning that real polycrystalline electrolytes always show some anomalous frequency dispersion, therefore a constant phase element (CPE, $Z_{CPE} = A(j\omega)^{-\alpha}$, α is the depression factor [89]) is usually used to replace the pure capacitor C in the RC circuit. The reflection of the frequency dispersion in the Nyqusit plot is that the semicircle shown in Figure 3-1c becomes depressed or distorted.

Measurements of the electrical conductivity of solid electrolytes can be made using dc four-probe method [77] or using EIS. Compared to the four-probe dc measurement, a major advantage of EIS is its capability of resolving the bulk, grain boundary and electrode conduction processes by exhibiting successive semicircles in the impedance plot as described above.

3.1.3. Oxygen vacancy and oxygen ion conductivity

There are two types of solid oxides: the fluorite-type and the perovskite-type. The fluorite oxides are of the type MO_2, where M is a relatively large four-valent cation like Zr^{4+} and Ce^{4+}. Perovskites are of the type ABO_3, where A is a large ion like La^{3+} or Sr^{2+}, and B is a small ion like Ga^{3+} or Ti^{4+} [78]. The ionic conductivity of the solid oxides can be obtained by doping a suitable amount of lower valent cations, such as by doping Ca^{2+} or Y^{3+}, Sc^{3+} into fluorite-type CeO_2 or ZrO_2, and by doping Mg^{2+} and Sr^{2+} into perovskite-type $LaGaO_3$. The addition of such dopants to the solid oxides results in the creation of oxygen vacancies $V_O^{\bullet\bullet}$, which are responsible for the oxygen ion conductivity of solid electrolytes. Equations 3-3 and 3-4, respectively, express the formation of $V_O^{\ddot{}}$ in YSZ (doping Y_2O_3 to ZrO_2, an example of fluorite oxides) and in LSGM (strontium-magnesium-doped $LaGaO_3$, an example of perovskite oxides).

$$Y_2O_3 + 2Zr_{Zr}^{\times} + O_O^{\times} \rightarrow 2Y_{Zr}^{'} + V_O^{\bullet\bullet} + 2ZrO_2 \qquad (3\text{-}3)$$

$$2SrO + 2La_{La}^{\times} + O_O^{\times} \rightarrow 2Sr_{La}^{'} + V_O^{\bullet\bullet} + La_2O_3 \qquad (3\text{-}4a)$$

$$2MgO + 2Ga_{Ga}^{\times} + O_{O}^{\times} \rightarrow 2Mg_{Ga}^{'} + V_{O}^{\bullet\bullet} + Ga_2O_3 \quad (3\text{-}4b)$$

where the Kröger-Vink notation is used (see Appendix II).

The ionic conductivity is given by the sum of the products of the concentration n_i and the mobility υ_i of charge carriers with the charge number q_i:

$$\sigma = \sum_i n_i q_i \upsilon_i \quad (3\text{-}5)$$

In the case of oxygen ion conductors, the charge carrier is an oxygen vacancy $V_o^{\bullet\bullet}$ and $q_i = 2e$, the carrier concentration n_i is related to the dopant concentration.

The temperature dependence of the electrical conductivity σ can be empirically expressed as follows [89]:

$$\sigma(T) = \frac{A}{T}\exp(-\frac{E_a}{kT}) \quad (3\text{-}6)$$

where A is a pre-exponential factor, E_a is the activation energy of electrical conduction and k is Boltzman's constant.

Due to the effect of interaction between dopants and $V_o^{\bullet\bullet}$ defects such as Coulombic interaction, associates (clusters) might exist in the solid electrolyte, such as $(Y_{Zr}^{'}V_{O}^{\cdot\cdot})^{'}$ in YSZ [80]. Therefore, the activation energy E_a comprises the migration enthalpy ΔH_m of oxygen vacancies $V_o^{\bullet\bullet}$ and the enthalpy ΔH_a of associates formation [81].

3.2. Experimental results of O^{2-} conductivity of solid electrolytes using EIS

3.2.1. Typical impedance spectra

Figure 3-2 shows typical impedance spectra of a 7.5 mol % ScSZ electrolyte, whose behaviour is strongly dependent on the temperature. At lower temperatures, e.g., 673 K, three semicircles (or arcs) were clearly observed. As depicted in Section 3.1.2, the first high-frequency semicircle and the second intermediate-frequency semicircle are associated with the bulk and the grain boundary of the electrolyte, respectively. The low-frequency arc reflects processes occurring at the electrode-electrolyte interface. With increasing temperature, both the bulk and the grain boundary semicircle became smaller. At intermediate

temperature, e.g., 897 K, the bulk semicircle became incomplete. With further increasing temperature, e.g., 994 K, this bulk semicircle cannot be observed because the time constant ($\tau = RC$) of the bulk response becomes too short. At high temperatures, e.g., 1091 K, both the bulk and the grain boundary semicircles were invisible as they became indistinguishable and only the electrode semicircle was observed.

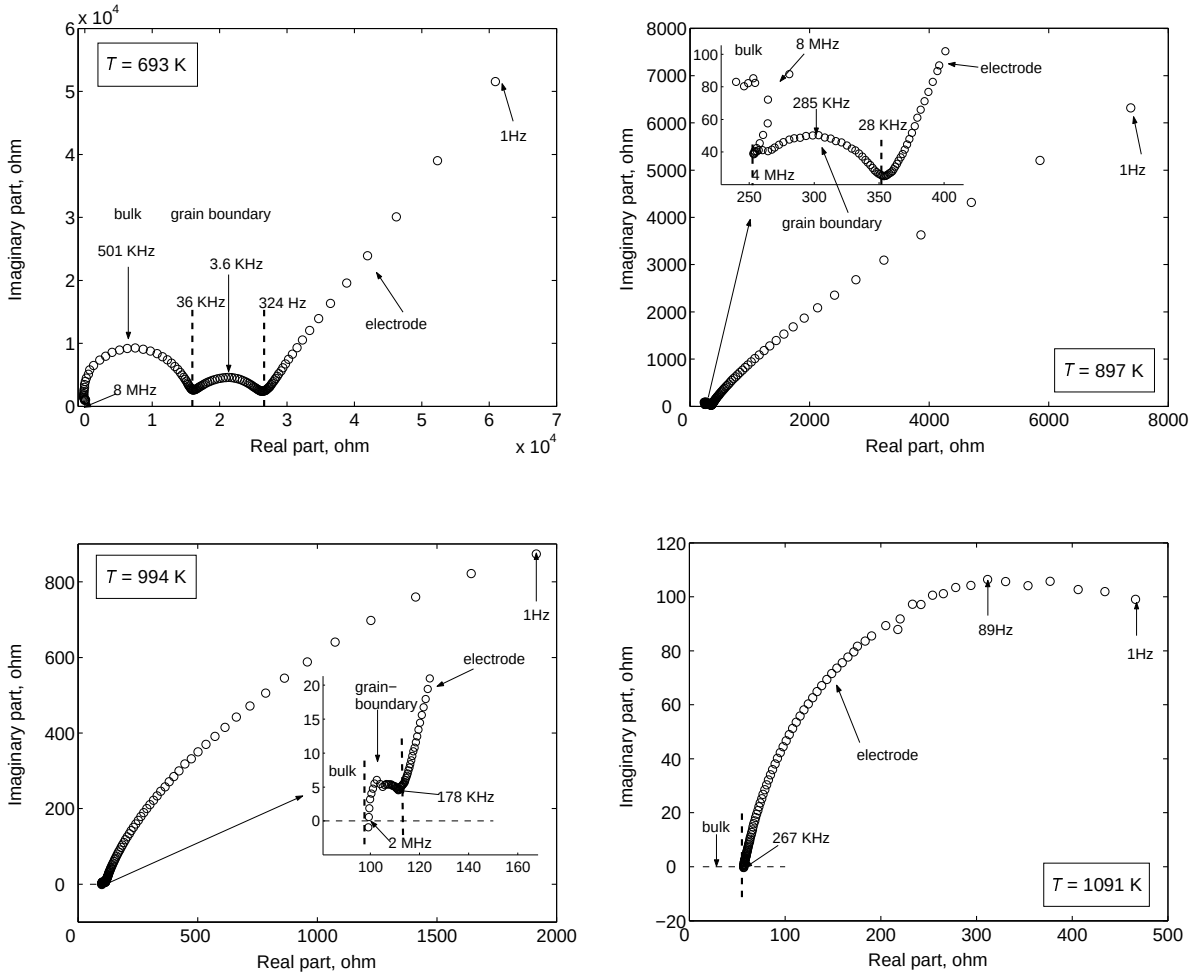

Figure 3-2 Impedance spectra of 7.5% ScSZ at different temperatures.

The impedance of the grain boundary is influenced by material impurities, sintering conditions, the preparation technology, the particle size and distribution, and the microstructure of the electrolytes [82]. Once the dopant concentration in the electrolytes is fixed, the contribution of the grain boundary resistance to the total electrolyte resistance should be rendered very small in order to obtain a high conductivity. Impedance spectra shown in Figure 3-2 represent the solid electrolytes such as 7.5 mol % and 9 mol % ScSZ, which have a considerable grain boundary resistance. Among the studied electrolytes, LSGM,

10 mol % and 12 mol % ScSZ exhibited a very small boundary resistance. The impedance spectra of LSGM at different temperatures are given in Figure 3-3. Similarly, the bulk and grain boundary semicircles gradually became invisible with increasing temperature.

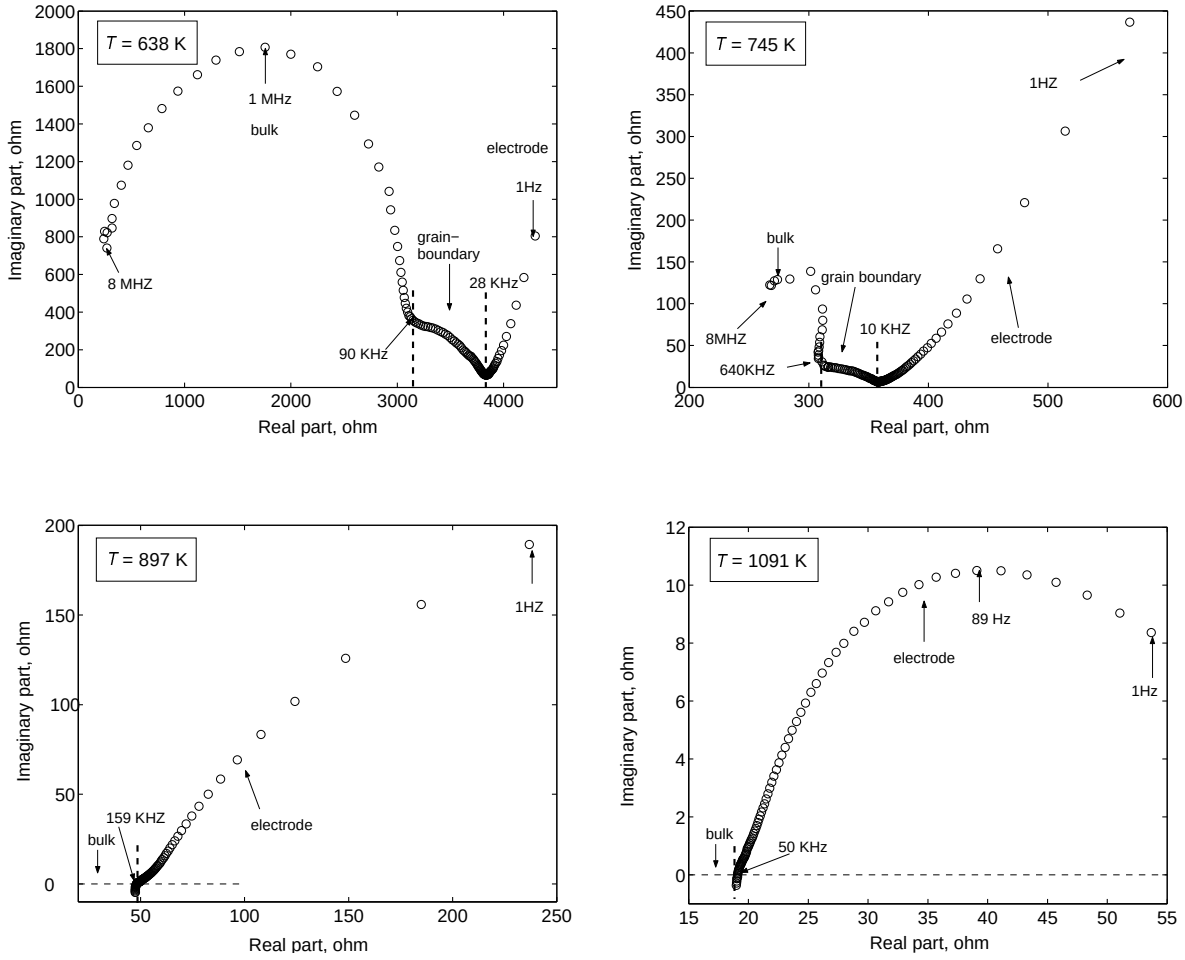

Figure 3-3 Impedance spectra of $La_{0.9}Sr_{0.1}Ga_{0.85}Mg_{0.15}O_{3-\delta}$ at different temperatures.

The impedance spectra of 13 mol % YSZ did not show any visible grain boundary resistance at the investigated temperature range as shown in Figure 3-4. As can be seen, the bulk semicircle decreased with increasing temperature and the semicircle can not be observed at higher temperatures (> 994 K).

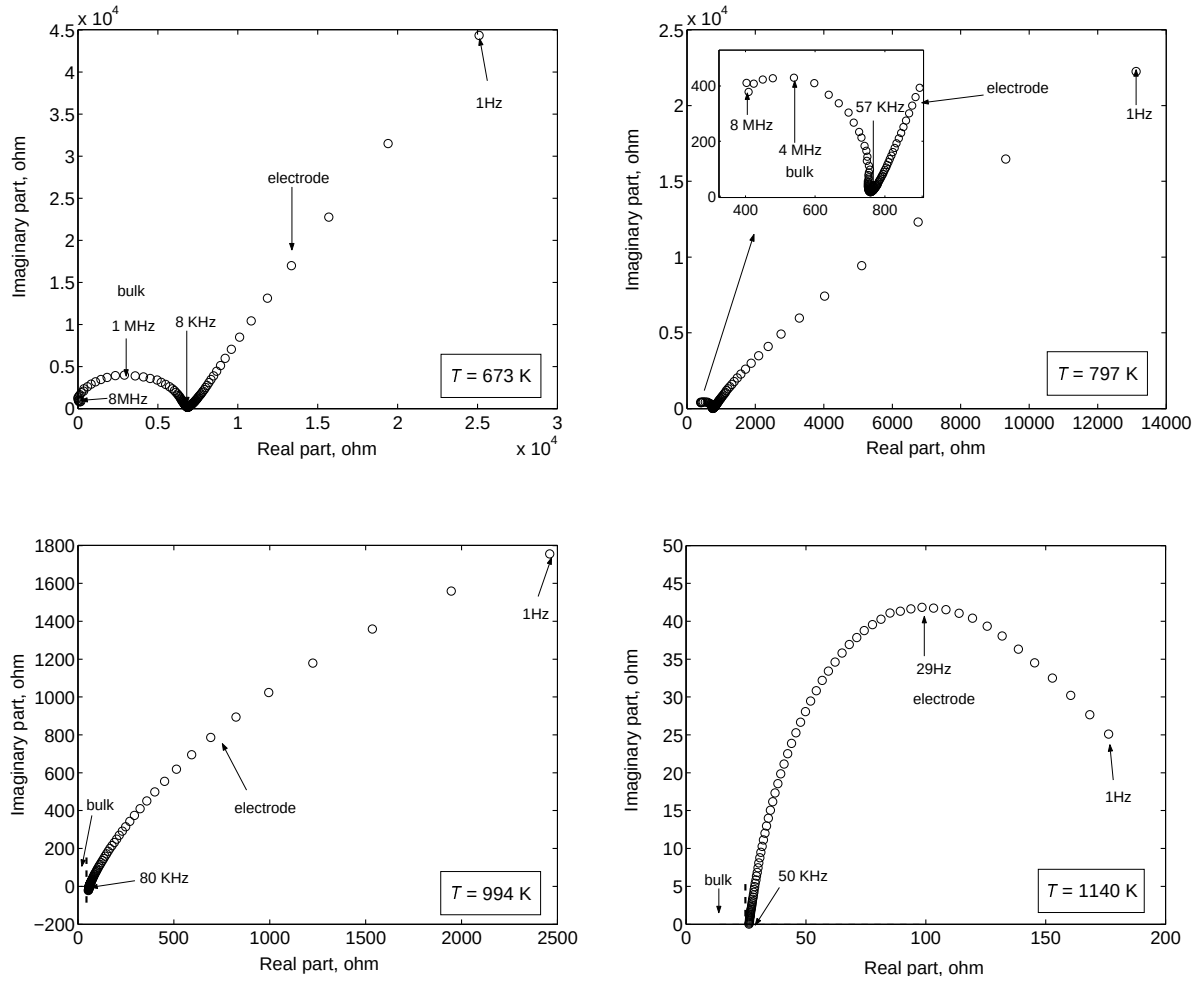

Figure 3-4 Impedance spectra of 13% YSZ at different temperatures.

3.2.2. Equivalent circuits for EIS fitting

A complex nonlinear least squares (CNLS) program (Zahner IM6, SIM software) with suitable equivalent circuits was used to fit the measured impedance spectra. Thereby the bulk resistance and the grain boundary resistance were obtained. For example, the equivalent circuits used to fit the impedance spectra of 7.5 mol % ScSZ (shown in Figure 3-2) are illustrated in Figure 3-5. From the fitting, three parameters can be obtained for each arc: the resistance R, the capacitance C and the depression factor α. The bulk and total electrical conductivity (contribution from both bulk and grain boundary resistances) of the electrolyte was calculated as follows:

$$\sigma = \frac{1}{R} \cdot \frac{L}{A} \tag{3-7}$$

where R is the bulk resistance or total resistance including bulk and grain boundary resistance, L is the thickness of the electrolyte and A is the electrode cross-section area. The fitting data for 7.5% ScSZ impedance spectra (shown in Figure 3-2) are compiled in Table 3-1.

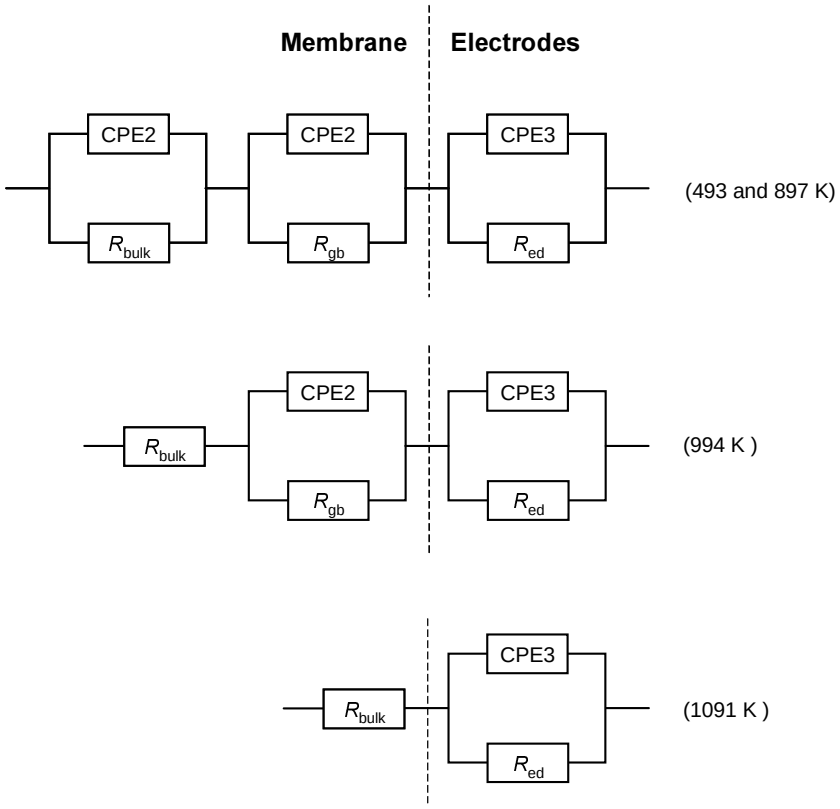

Figure 3-5 Equivalent circuits for CNLS fitting of 7.5 mol % ScSZ at different temperatures.

Table 3-1 CNLS fitting parameters and conductivity of 7.5 mol % ScSZ at different temperatures.

T (K)	Bulk			Grain boundary			Bulk conductivity σ_b (Ω^{-1}cm^{-1})	Total conductivity σ_t (Ω^{-1}cm^{-1})
	R_b (Ω)	θ (deg)	C (pF)	R_b (Ω)	θ (deg)	C (nF)		
673	1.6×10^{3}	7	12.3	1.0×10^{3}	10	4.7	2.14×10^{-4}	1.31×10^{-4}
897	245	8	3.7	114	12	10.3	1.41×10^{-2}	1.00×10^{-2}
994	88.7	-	-	13	41	230	3.89×10^{-2}	3.41×10^{-2}
1091	45.5	-	-	0	-	-	7.58×10^{-2}	7.58×10^{-2}

Note: θ is the depression angle, $\theta = \frac{\pi}{2}(1-\alpha)$.

3.2.3. Arrhenius plots

Figure 3-6 presents modified Arrhenius plots of the bulk conductivity and the total conductivity

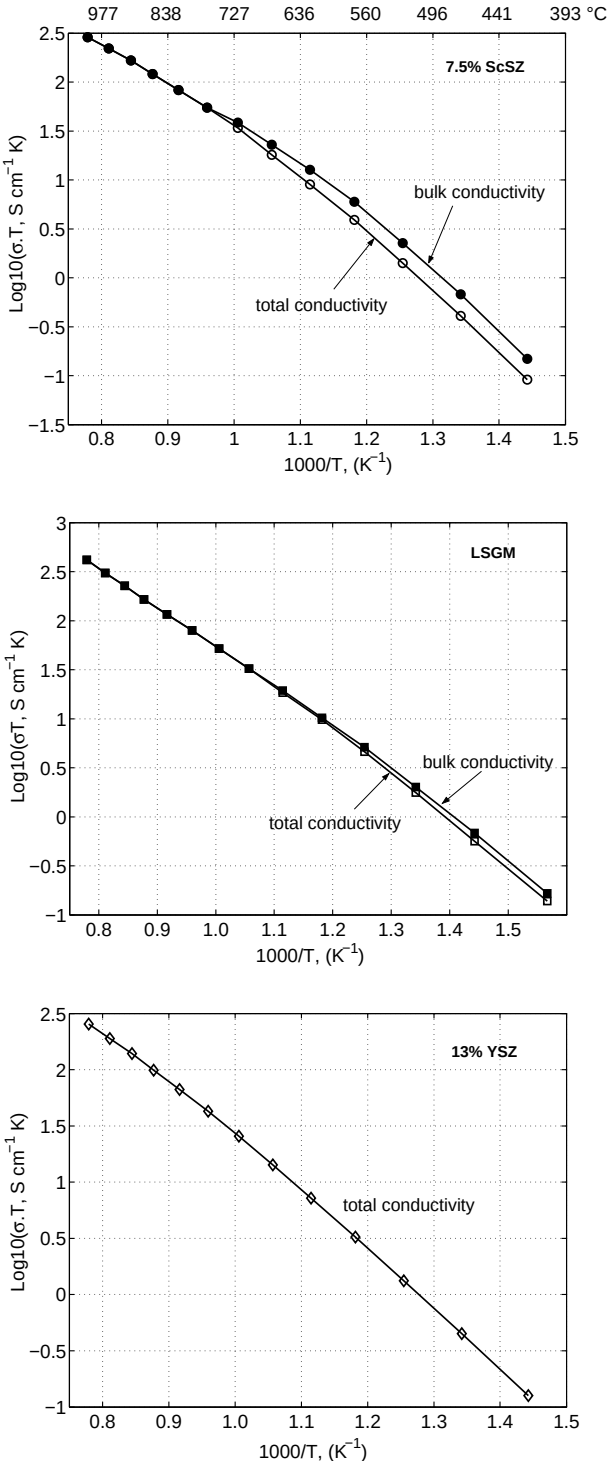

Figure 3-6 Arrhenius plots of bulk and total conductivity of solid electrolytes: 7.5% ScSZ, LSGM and 13% YSZ.

of typical solid electrolytes such as 7.5% ScSZ, LSGM and 13% YSZ. Due to the considerable grain boundary resistance in the 7.5% ScSZ, there is a remarkable difference between the bulk conductivity and the total conductivity at lower temperatures (T < 823 K). At higher temperatures (T > 873 K), the total conductivity is approximately equal to the bulk conductivity because the grain boundary resistance decreased with increasing temperature as shown in Figure 3-2. For the LSGM electrolyte, the total conductivity was only slightly lower than the bulk conductivity since the grain boundary resistance in the LSGM was minor. For 13% YSZ, the total conductivity is equal to the bulk conductivity since no grain boundary resistance was measured by EIS.

Some electrolytes (e.g., 9% SCSZ, LSGM, 12% ScSZ) conductivity measured with 2-probe ac EIS in this work was compared to the available literature values measured with the 4-probe dc method or 2-probe EIS [82, 83]. Good agreements are achieved. For instance, Figure 3-7 presents the comparison of the total conductivity of 9% ScSZ between this work and literature [82]. As can be seen, the total conductivity determined with EIS is in good agreement with the 4-probe dc measurement.

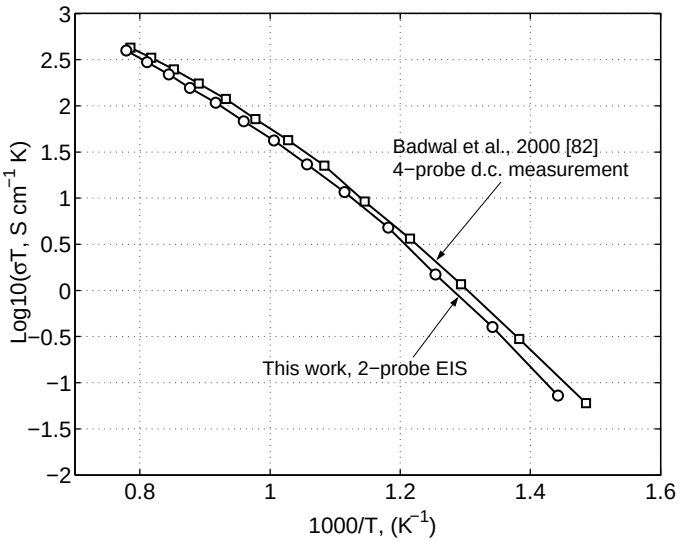

Figure 3-7 Comparison of the total conductivity of 9% ScSZ measured in this work to literature data.

3.2.4. Conductivity comparison of the solid electrolyte materials

The total conductivities of all membrane material candidates are compared to each other, as presented in Figure 3-8. As can be seen in Figures 3-6 and 3-8, the oxygen ion conductivity of all measured materials increased with increasing temperature. Generally, the Arrhenius

conductivity plots can be divided into two regions, i.e., high temperature region (973-1273 K) and low temperature region (623-823 K). Especially, a significant conductivity change around 873 K was observed for 12% ScSZ, which is ascribed to the phase transition from the β-phase to the cubic phase [83]. In the high temperature region, the oxygen ion conductivity of all investigated solid electrolytes sequenced as $\sigma_{\mathrm{LSGM}} > \sigma_{\mathrm{9ScSZ}} > \sigma_{\mathrm{12ScSZ}} > \sigma_{\mathrm{10ScSZ}} > \sigma_{\mathrm{7.5ScSZ}} > \sigma_{\mathrm{13YSZ}}$. However, in the low temperature region, the conductivity exhibited the decreasing order $\sigma_{\mathrm{LSGM}} > \sigma_{\mathrm{13YSZ}} > \sigma_{\mathrm{7.5ScSZ}} > \sigma_{\mathrm{9ScSZ}} > \sigma_{\mathrm{10ScSZ}} > \sigma_{\mathrm{12ScSZ}}$.

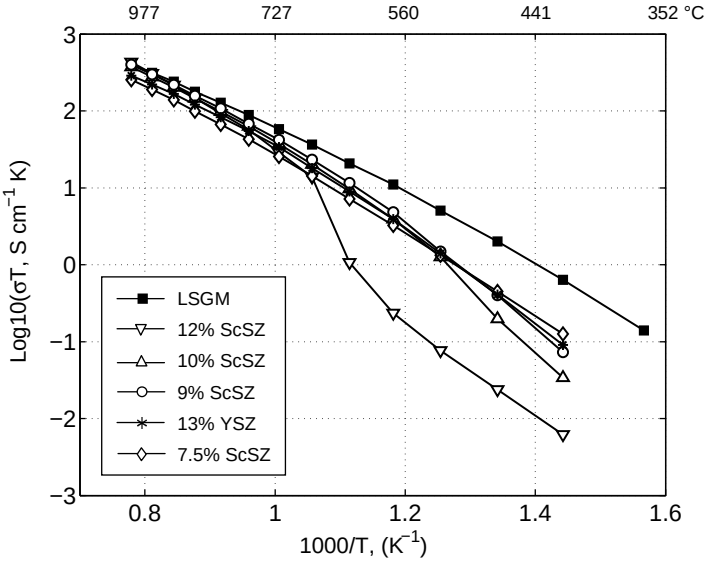

Figure 3-8 Conductivity comparisons of all investigated solid electrolytes at different temperatures.

From the slope of the Arrhenius plot, the activation energy E_a for the electrical conductivity can be calculated according to Equation 3-6. The calculation of the activation energy was performed separately in the high and low temperature regions. In the high temperature region, the activation energy is approximately equal to the migration enthalpy ΔH_m [81] since oxygen vacancies are almost isolated in the solid electrolytes. In the low temperature region, the activation energy is the sum of the migration enthalpy ΔH_m and the association enthalpy ΔH_a [81]. All activation energies determined from Arrhenius plots for the studied electrolytes were summarized in Table 3-2. The determined conduction activation energies of 9 mol % and 10 mol % obtained in this work were in agreement with the available values in literature [82].

Since butane partial oxidation in the SEMR is performed at low temperatures (T < 773 K), a reasonable oxygen ion conductivity at low temperatures is an important prerequisite for the feasibility of the reactor concept. As can beseen in Figure 3-8, LSGM exhibits clearly the highest oxygen ion conductivity in the low temperature region. Though 13% YSZ has the lowest conductivity at higher temperatures, it shows relatively high conductivity at lower temperatures, which is attributed to the negligible grain boundary resistance (too small to detect) as shown in Figure 3-4. This is also reflected in the activation energy. As can be seen in Table 3-2, in the low temperature region, the LSGM has the lowest activation energy followed by 13% YSZ. Considering the fact that the stability of LSGM in reducing atmosphere is still under discussion [116] and that membranes from this material are not commercially available yet, 13% YSZ was finally chosen as the membrane material for the SEMR in this work.

Table 3-2 Activation energy of the investigated solid electrolytes in low- and high-temperature regions.

Specimen	High-temperature region (973-1273 K)		Low-temperature region (623-823 K)	
	This work (eV)	Ref. [82] (eV)	This work (eV)	Ref. [82] (eV)
LSGM	0.75	-	0.99	-
13% YSZ	0.90	-	1.07	-
12% ScSZ	0.93	-	1.15	-
10% ScSZ	0.89	0.90	1.50	1.38
9% ScSZ	0.87	0.76	1.39	1.35
7.5% ScSZ	0.83	-	1.24	-

3.3. Concluding remarks

Aiming at a high oxygen ion conductivity at low temperatures, the oxygen ion conductivity of several solid ceramic electrolyte candidates was measured with 2-probe ac EIS at different temperatures. The obtained impedance spectra were analyzed by equivalent circuit based on

the brick layer model. The impedance spectra changed clearly with temperature. The bulk and grain boundary semicircles gradually became invisible with increasing temperature. Different types of solid electrolytes exhibited different magnitudes of grain boundary resistance. 7.5% ScSZ and 9% ScSZ have a significant grain boundary resistance, LSGM, 10% ScSZ and 12% ScSZ have small grain boundary resistances, while 13% YSZ shows negligible grain boundary resistance.

Form the measured impedance spectra, the oxygen ion conductivity of solid electrolytes were calculated and described by means of Arrhenius conductivity plots. The corresponding activation energies in the high and low temperature regions were determined by regression of the Arrhenius plot.

The oxygen ion conductivities of all solid electrolyte materials were compared to each other. The ranking is $\sigma_{\mathrm{LSGM}} > \sigma_{\mathrm{9ScSZ}} > \sigma_{\mathrm{12ScSZ}} > \sigma_{\mathrm{10ScSZ}} > \sigma_{\mathrm{7.5ScSZ}} > \sigma_{\mathrm{13YSZ}}$ in the high temperature region and $\sigma_{\mathrm{LSGM}} > \sigma_{\mathrm{13YSZ}} > \sigma_{\mathrm{7.5ScSZ}} > \sigma_{\mathrm{9ScSZ}} > \sigma_{\mathrm{10ScSZ}} > \sigma_{\mathrm{12ScSZ}}$ in the low temperature region. Since butane partial oxidation to MA is carried out at lower temperatures, solid electrolytes having high ionic conductivity at low temperature are preferred. 13% YSZ was finally chosen as the membrane material for the SEMR in this work due to its higher ionic conductivity at low temperature and a good stability under reducing atmosphere.

4. VPO Conductivity Measurements

In order to optimize the structure of the anodic layer in the SEMR to be designed for butane partial oxidation, the electrical conductivity of the VPO catalyst should be measured. If VPO catalyst possesses a high electrical conductivity, it can work not only as a catalyst for butane oxidation to MA but also directly as anodic current collector. Otherwise, an additional conductive electrode has to be constructed on the anode side to serve as anodic current collector. In short, the magnitude of the VPO conductivity will determine the complexity of the anodic structure.

If the VPO catalyst has either a high electron or high mixed ion-electron conductivity, the simple anodic structure as shown in Figure 4-1a can be used, where the VPO catalyst directly works as anode. If the VPO catalyst only has a high oxygen ion conductivity, an additional electronic conducting layer (e.g., a metal) has to be constructed on top of the VPO catalyst to serve as current collector (Figure 4-1b). When both the electronic and the ionic conductivities of the VPO catalyst are too low, a very complicated anodic structure is desirable (Figure 4-1c), where the anode is a metal-YSZ composite with a VPO catalyst being added to this layer to form a composite electrode. However, the preparation of such a composite electrode is very complex. Alternatively, an electronically conducting layer can be prepared between the solid electrolyte and the VPO catalyst layer to form an oxide-covered porous metal electrode (Figure 4-1d), where the metal serves as anodic current collector.

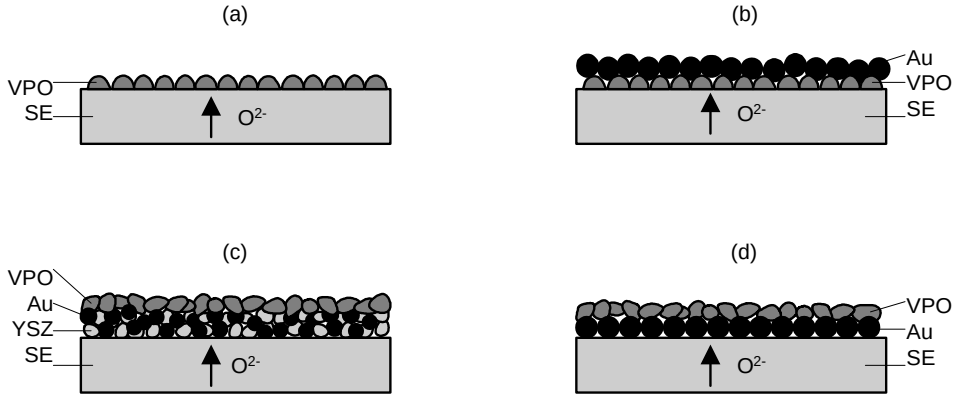

Figure 4-1 Anodic structure designs depending on the electrical conductivity of VPO catalyst.

4.1. Impedance spectra of VPO catalyst

Figures 4-2 gives two examples of experimental impedance spectra for VPO pellet measured at different temperature in environment of N_2 (0.007% O_2) and air (20.5% O_2), respectively. In any case, only one semicircle arising from the VPO catalyst was observed and no impedance from the electrode reaction was detected at low frequencies, which usually indicates that the electrical conductivity is due to the electronic conduction [84]. Thus, the measured impedance spectra can be interpreted by means of a simple RC equivalent circuit. As can be seen, it is clear that the impedance of the VPO catalyst decreased with increasing temperature. Under high oxygen concentration, the semicircle is not complete due to the short time constant.

(a)

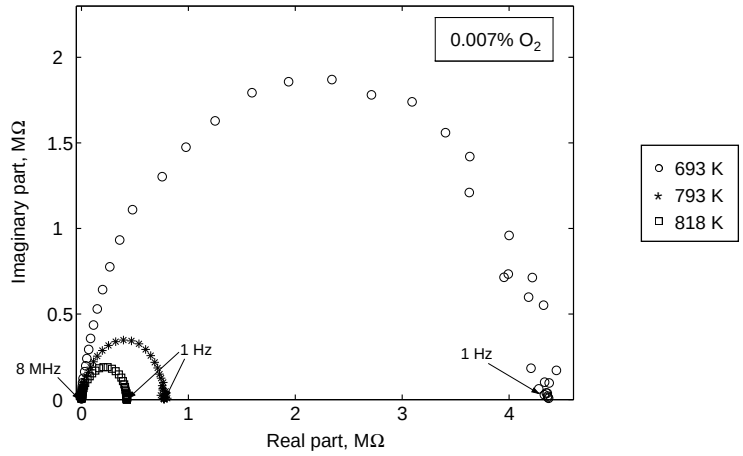

(b)

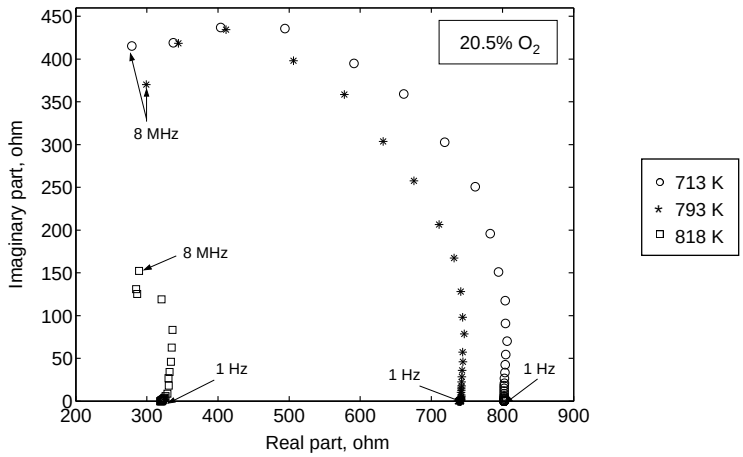

Figure 4-2 Typical impedance spectra of VPO pellet measured at different temperature and atmosphere.

4.1.1. Influence of temperature on VPO conductivity

The electrical conductivity σ of the VPO catalyst is calculated according to Equation 3-7. The variation of σ with respect to temperature is presented in the form of $\log(\sigma T)$ vs. $1/T$, as given in Figure 4-3. The electrical conductivity increased with increasing temperature and all curves are straight lines in plots, which are consistent with Arrhenius law (see Equation 3-6). The fitted activation energies are 1.29 and 1.67 eV under 0.007% and 20.5% O_2, respectively. It can be concluded that the electrical conductivity is very low, e.g., 1.1×10^{-6} S/cm in 0.007% O_2 and 1.0×10^{-4} S/cm in 20.5% O_2 at 763 K.

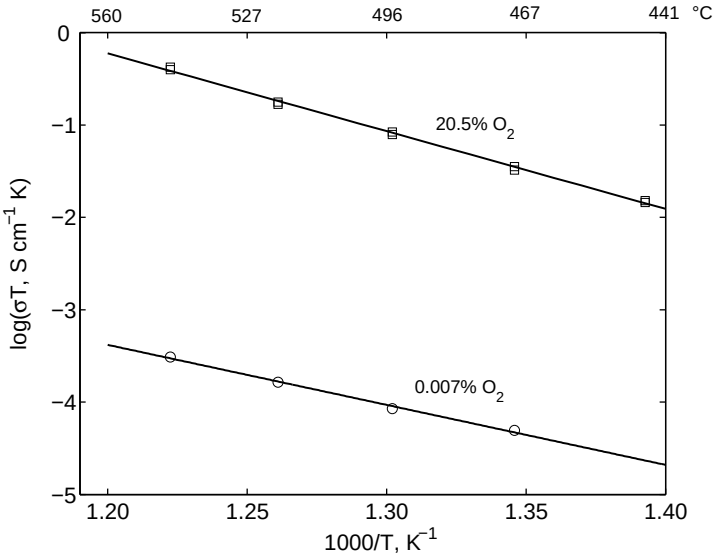

Figure 4-3 Dependence of electrical conductivity of the VPO catalyst on temperature.

4.1.2. Influence of oxygen pressure on VPO conductivity

As can be seen in Figure 4-3, the conductivity of the VPO catalyst at higher oxygen pressure was higher, which is further confirmed in Figure 4-4. It can be seen that the electrical conductivity increased with the oxygen partial pressure, i.e., $\frac{d\sigma}{dP_{O_2}} > 0$, which indicates that VPO catalyst is a p-type semiconductor [85]. The same conclusion has been reported by Herrmann et al. [86].

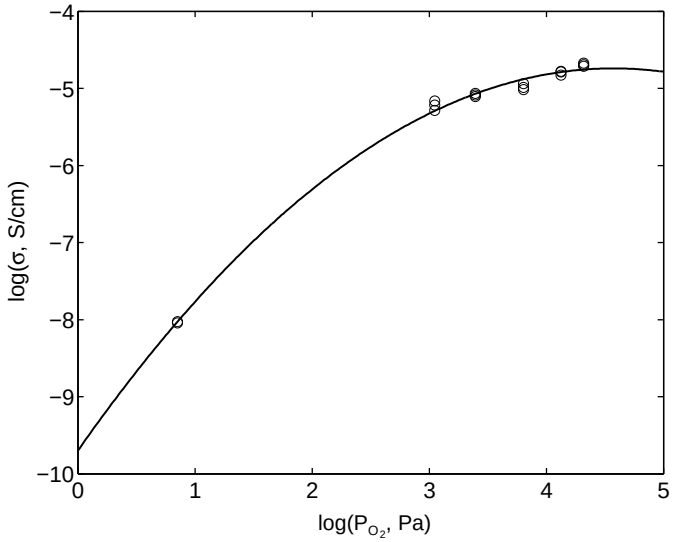

Figure 4-4 Variation of VPO conductivity as a function of the oxygen partial pressure, T = 693 K.

In the case of p-type semiconductor, the electronic conductivity is attributed to positive electron holes $h^{\cdot}$ and the main defects are cationic vacancies [85]. P-type semiconductive oxides tend to be nonstoichiometric because of oxygen excess, which is due to the fact that their cations are in a relatively stable low oxidation state but they can be partly oxidized to a higher oxidation state such as for Cu_2O, Cr_2O_3, NiO [87]. As introduced in Chapter 1, an activated VPO catalyst has a complicated microstructure and often contains the oxidized phase $VOPO_4$ together with the predominant reduced phase $(VO)_2P_2O_7$. As discussed by Busca [88], the proper formulation of the VPO catalyst could be $V_2P_2O_{9+\delta}$, with some excess of surface oxygen due to the presence of pentavalent vanadium (V^{5+}). Therefore, p-type conductivity of VPO catalyst must be related to the redox couple V^{4+}/V^{5+}. The positive holes $h^{\cdot}$ and cationic vacancy $V_{VA}^{'}$ are generated as V^{4+} being partly oxidized to V^{5+}:

$$\frac{1}{2}O_2(\text{gas}) \Leftrightarrow O_O^x + 2V_{VA}^{'} + 2h^{\cdot} \qquad (4\text{-}3)$$

where VA represents vanadium, $O_O^{\times}$ refers to oxygen on lattice sites and $V_{VA}^{'}$ is a charged vanadium vacancy.

The electrical conductivity of the VPO catalyst was also measured under varying gas phase composition (air and reaction mixture of 1.2 mol % butane in air) at a temperature of 693 K. As shown in Figure 4-5, the removal of butane caused a rapid increase in the conductivity

compared to that in the reaction mixture of butane and air, which is likely due to the reoxidation of the VPO surface being previously reduced in the reaction mixture. However, the introduction of butane again led to a decrease in the conductivity as a result of the reduction of the VPO catalyst surface. The VPO conductivity under air (oxidizing atmosphere) is about one order of magnitude higher than that under the reaction mixture (reducing atmosphere). This observation again confirmed the p-type character of the VPO catalyst. The increase in the conductivity under air and the decrease in the conductivity under the reaction mixture were found to be reversible, which is in agreement with the redox cycles of the VPO catalyst according to the Mars and van Krevelen mechanism, as already discussed by Herrmann [86].

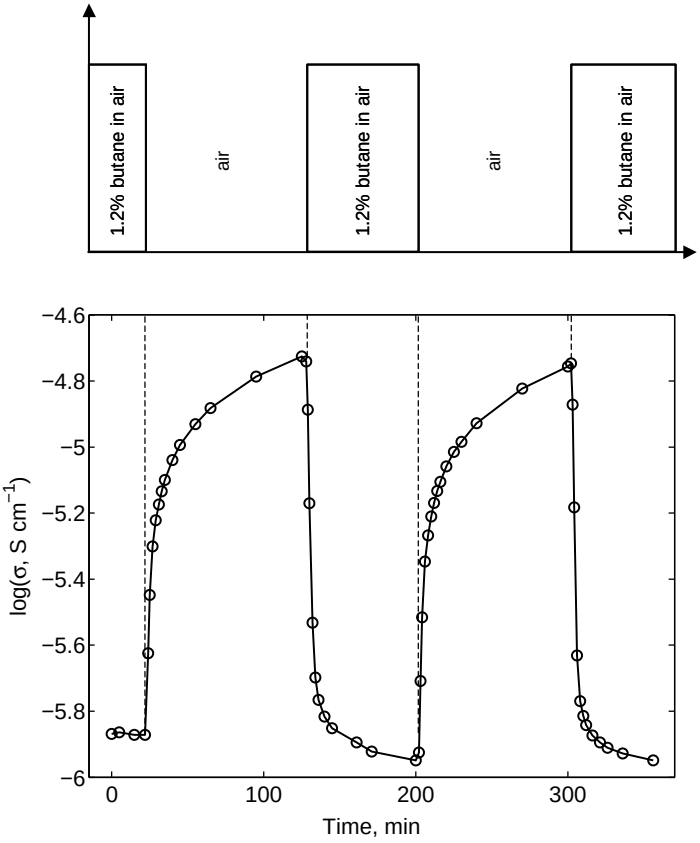

Figure 4-5 Variation of the VPO conductivity under different gas atmospheres: air and 1.2 mol % butane in air, T = 693 K.

4.2. Concluding remarks

The electrical conductivity of the VPO catalyst was measured by 2-probe ac impedance spectroscopy as a function of temperature and atmosphere. It was found that the electrical

conductivity is dominated by the electronic conductivity and that the VPO catalyst behaves as a p-type semiconductor since the conductivity increased with increasing oxygen pressure. The conductivity is rather low and therefore the VPO catalyst cannot directly serve as anode material in the SEMR to be used for butane partial oxidation. Based on this fact, a gold layer was used as the anodic current collector in this research work, i.e., an oxide-covered porous metal anodic structure was designed.

5. Characterization of the Solid Electrolyte Membrane Reactor with Electrochemical Techniques

Prior to butane partial oxidation, the SEMR was characterized with electrochemical techniques: SEP, EIS and I-V curve. The SEP measurement is helpful to evaluate the reactor preparation such as the contact between electrodes and membrane. The electrode resistance and membrane resistance can be estimated from the EIS. From the I-V curve, the operation mode of the reactor can be optimized. The EOP measurement is used to determine the oxygen evolution rate in the anode when the reactor is operated with an external energy supply.

5.1. SEP measurement

Figure 5-1 gives the OCP between the anode and the cathode (cathode is the reference electrode), which were measured with the SEP technique as a function of temperature and oxygen concentration using two reactor configurations:

(a) P_{O2} | Au | YSZ | Pt-Ag | Air, and

(b) P_{O2} | VPO | Au | YSZ | Pt-Ag | Air.

As introduced in Section 1.2.2.1, the OCP of the reactor cell is directly related to the oxygen activity on the anode (see Equation 1-9), and the OCP can be easily calculated from the Nernst equation (see Equation 1-10) when the thermodynamic equilibrium is established between gas phase oxygen and adsorbed oxygen on the electrode.

In the case of a low anodic oxygen concentration (e.g., 0.011% O_2), at lower temperature range (T < 850 K) there was a clear deviation of the SEP measurement from the Nernst equation for both reactor configurations, which indicates that the oxygen adsorption was not in equilibrium with the gaseous oxygen. The deviation decreased with increasing temperature. At temperatures above 900 K, for the blank reactor P_{O2} | Au | YSZ | Pt-Ag | Air, the measured SEP agreed well with the Nernst equation, which implied that the oxygen adsorption on the anode surface was in equilibrium with gaseous oxygen. It should be noted that for the reactor

P_{O2} | VPO | Au | YSZ | Pt-Ag | Air, temperatures above 823 K were not tested in order to avoid damaging of the VPO catalyst. In the case of a high anodic oxygen concentration (e.g., 2.49% O_2), a slight deviation was observed for the two reactor configurations, but it was smaller than that observed at lower oxygen concentration. The OCP measured with the SEP technique increased with increasing oxygen concentration as expected from Equation 1-10.

(a)

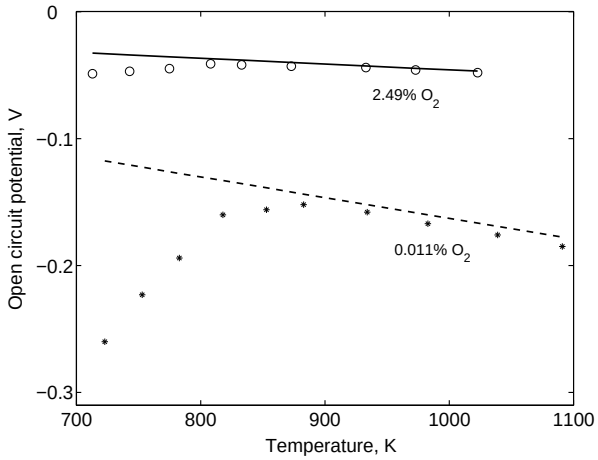

(b)

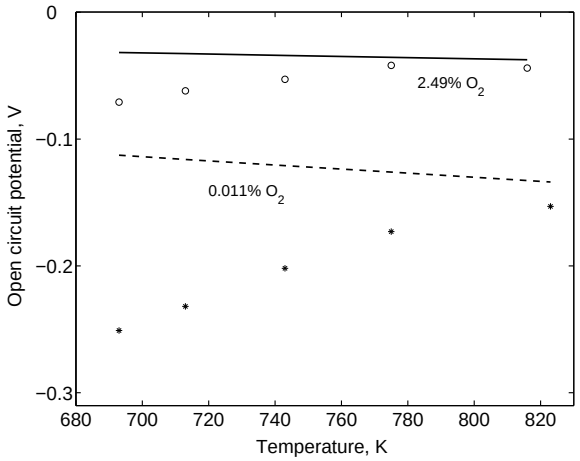

Figure 5-1 OCP results at different temperature in SEP measurements, (a) P_{O2} | Au | YSZ | Pt-Ag | Air, (b) P_{O2} | VPO | Au | YSZ | Pt-Ag | Air. Markers: experimental data, lines: calculated from Nernst Equation; Electrode area: 22.8 cm^2; anode: 40 ml/min 0.011% or 2.49% O_2 in N_2; cathode: 90 ml/min air.

The above results revealed that the SEP measurement at low operating temperature can qualitatively indicate the variation of the oxygen activity on the anode and that a quantitatively reliable measurement with SEP technique was only obtained above a certain temperature limit, i.e., 780 K and 850 K for 2.49% and 0.011% O_2, respectively. This low temperature limit is consistent with the minimum temperature of operating an oxygen sensor

(> 873 K), which is due to the low oxygen ion conductivity of the solid electrolyte and the slow charge-transfer reaction $O^{2-} \Leftrightarrow O_{(a)} + 2e^-$ at the electrode-electrolyte interface at low temperatures [89]. Therefore, it can be inferred that the preparation of the SEMR was successful.

5.2. EIS of the reactor

The electrochemical reactors Au|YSZ|Pt-Ag and VPO|Au|YSZ|Pt-Ag were characterized by 2-probe EIS at the OCP, as presented in Figures 5-2a and 5-2b. Generally the reactor impedance was very high at low temperature (T < 773 K). As can be seen, the ohmic resistance coming from the membrane and electrode wires was minor compared to the large

(a)

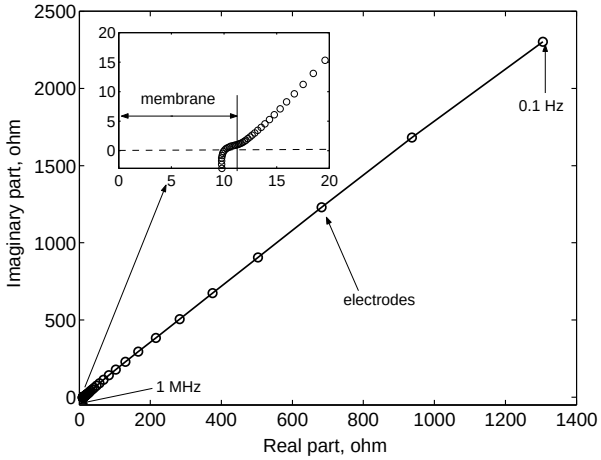

(b)

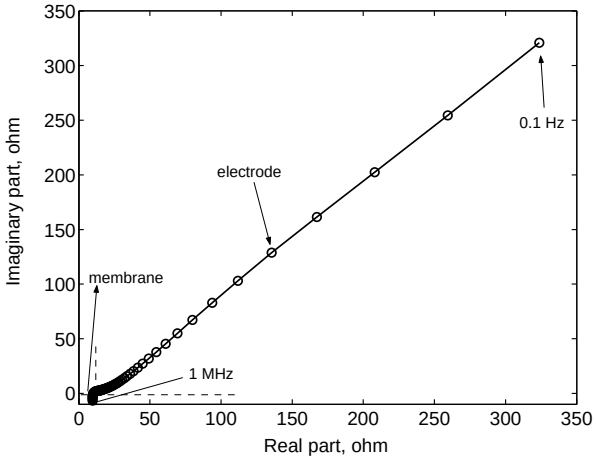

Figure 5-2 EIS of the reactors (a) N_2|Au|YSZ|Pt-Ag|Air and (b) N_2|VPO|Au|YSZ|Pt-Ag|Air. Electrode area: 22.8 cm^2; T = 755 K; anode: 40 ml/min N_2; cathode: 90 ml/min air.

impedance contributions of the electrodes. A Warburg impedance (a straight line with an about 45° angle) at low frequency was observed, which implied the electrode resistance is mainly ascribed to the diffusion limitation on the electrode. However, it is not possible to directly distinguish anodic and cathodic contributions to the overall electrode impedances since 2-probe EIS was performed here. To further reduce the overall electrical resistance of the reactor, the electrode material should be optimized (e.g., composite electrode) and the electrode preparation should be improved, e.g., to enhance the porosity.

5.3. I-V curve

The I-V curve of the reactor VPO | Au | YSZ | Pt-Ag was measured at a temperature of 755 K (Figure 5-3). E_{c_a} is defined as the terminal voltage between the cathode and the anode (herein the anode is defined as the reference electrode), and it can be written as

$$E_{c\_a} = E_{cell,0} - \eta \tag{5-1}$$

where $E_{cell,0}$ is the electromotive force of the cell at zero current (see Equation 1-11) and η is the overall electrochemical overpotential loss of the reactor as defined in Section 1.2.2.2.

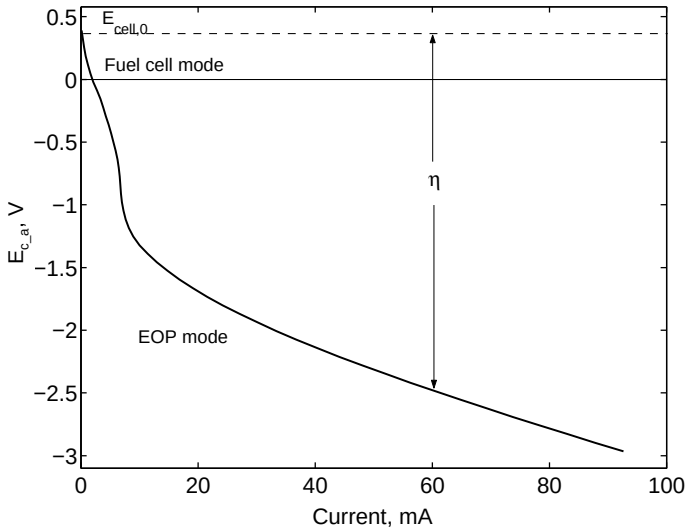

Figure 5-3 Experimental current-voltage curve of the solid electrolyte membrane reactor VPO | Au | YSZ | Pt-Ag. Electrode area: 22.8 cm^2; T = 755 K; anode: 40 ml/min 0.6 mol % butane diluted in N_2; cathode: 90 ml/min air.

The measured voltage $E_{c\_}$ at open-circuit condition (i.e., $E_{cell,0}$) was 0.45 V, which implies

that the SEMR can generate electric power and work as a SOFC ("Fuel cell mode"). However, under "Fuel cell mode" ($E_{c\_} \geq 0$ in Figure 5-3), the current across the membrane was below 2 mA ascribed to the high electrode resistance at low operating temperature, which can be seen in the EIS measurement of the reactor. For butane partial oxidation to MA over the VPO catalyst, a relatively high oxygen concentration is necessary to maintain the VPO catalyst oxidation state. When the SEMR is operated in "Fuel cell mode", the VPO catalyst will quickly lose its activity due to the low oxygen flux through the membrane to the anode at low currents. Therefore, the SEMR was operated in "EOP mode" ($E_{c\_} < 0$ in Figure 5-3) in this work, i.e., the circuit was closed and oxygen ions were pumped to the anode with an external imposed current/potential, in order to increase the oxygen flux towards the anode.

5.4. Electrochemical oxygen pumping

Since butane oxidation in the SEMR was operated in "EOP mode" in this work, the oxygen transport through the membrane with respect to the imposed current was determined experimentally prior to the oxidation experiment. As illustrated in Figure 5-4, the gaseous oxygen (O_2) was reduced to O^{2-} at the cathode. These oxygen ions permeated through the membrane and arrived at the anode where O^{2-} was oxidized to O_2 by releasing its electrons. The corresponding O_2 concentration in the anode chamber was measured with an on-line GC. Two electrochemical reactor configurations, i.e.

$N_2 \mid Au \mid YSZ \mid Pt\text{-}Ag \mid Air$, and

$N_2 \mid VPO \mid Au \mid YSZ \mid Pt\text{-}Ag \mid Air$

were used. Theoretically, the oxygen transport rate (J_{O_2}) through the membrane can be calculated according to Faraday's law:

$$J_{O_2} = I / 4F \qquad (5\text{-}2)$$

where F is Faraday's constant, I is the externally imposed current.

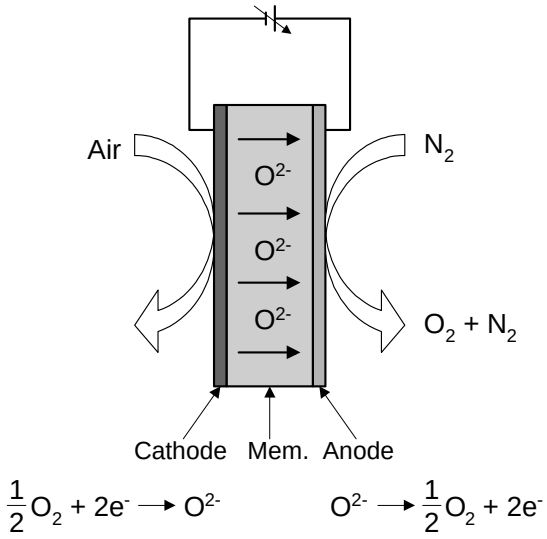

Figure 5-4 Schematic illustration of the EOP measurement.

As shown in Figure 5-5, the measured oxygen evolution rate as well as the terminal voltage increased with increasing current as expected. The data were obtained at steady state of each imposed current. The steady state conditions were confirmed by several comparable, consecutive analyses. It should be mentioned that the oxygen evolution rate was measured by first increasing and then decreasing the current systematically, and no hysteresis was observed during the measurement.

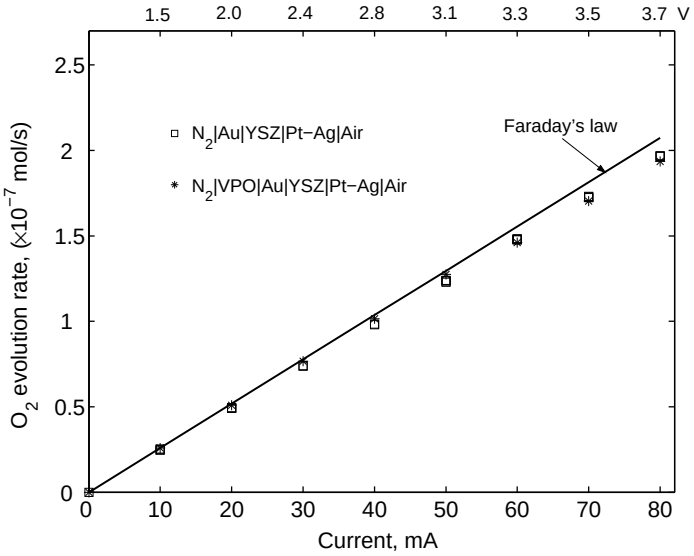

Figure 5-5 EOP results of the reactors: $N_2 \mid Au \mid YSZ \mid Pt\text{-}Ag \mid Air$ and $N_2 \mid VPO \mid Au \mid YSZ \mid Pt\text{-}Ag \mid Air$. Electrode area: 22.8 cm^2; T = 753 K; anode: 40 ml/min N_2; cathode: 90 ml/min air.

The experimentally measured oxygen evolution rate was compared to the value predicted from Faraday's law. As can be seen, at low imposed current the measured oxygen concentration in the anode chamber agrees very well with Faraday's law, while at the high current it shows a slight deviation. This deviation gradually increases with increasing current. The same results were obtained by varying the air flow rate in the cathode or even by introducing pure oxygen instead of air to the cathode, which indicated that the deviation at high currents is not due to the mass transfer limitation in the cathode.

A high voltage that exceeds the thermodynamic decomposition voltage of zirconia (2.5 V at 773 K) was applied in order to obtain the desired current at low operating temperature, as shown in Figure 5-5. Such a high voltage might result in the reduction of ZrO_2 [90] or traces of impurities in the membrane. After the oxygen pumping experiments, the color of the YSZ membrane surface at the anode side was found to change from gray-white to gray-black. Similar phenomena were also reported in literature [91-94]. Guo et al. [95] attributed such color changes to the formation of F-centers (oxygen vacancies having one or two electrons, e.g., $V_{\ddot{O}}e^{'}$) at the surface of the electrolyte. The reduction of the membrane and F-centers formation under the high voltage probably induced the electron conduction in the membrane, which might be responsible for the slight deviation of oxygen evolution at the higher imposed currents. In such a case, the transport number t_i of oxygen ions in the membrane would be below 1.0 and thus the effective oxygen transport should be corrected by the transport number, i.e., $J_{O_2} = t_i I / 4F$.

Table 5-1 O_2 evolution rate in the anode under EOP in the EMR Au | YSZ | Pt-Ag at different temperature (I = 70 mA).

Temperature (K)	Measured (mol/s)	Theoretical (mol/s)	Voltage (V)
753	1.72×10^{-7}	1.81×10^{-7}	3.49
1053	1.79×10^{-7}	1.81×10^{-7}	0.51

It is worth mentioning that the observed deviation at the same imposed current decreased with increasing temperature and the voltage between the two electrodes decreased as well. As

given in Table 5-1, compared to the case at 753 K, the measured O_2 evolution rates with 70 mA current at 1053 K was closer to that calculated from Faraday's law. The needed voltage decreased as the temperature increased, which probably reduced the risk of reduction of the membrane. The measured O_2 evolution rates were reversible during increasing and decreasing the temperature.

Additionally, the electrochemical reactor $N_2 \mid VPO \mid Au \mid YSZ \mid Pt\text{-}Ag \mid Air$ was found to behave similarly to the blank reactor $N_2 \mid Au \mid YSZ \mid Pt\text{-}Ag \mid Air$ at the oxygen pumping conditions as can be seen in Figure 5-5, which indicated that the fresh VPO catalyst was not easily oxidized by the pumped oxygen species. In other words, the rate of VPO oxidation was very low at this condition. As reported by Wang et al. [96], there are several factors affecting the rate of VPO oxidation. The rate of VPO oxidation r can be represented by:

$$r = k(T)P_{O_2}^{m}\theta^{n} \tag{5-3}$$

where k is the reaction rate constant, P_{O_2} is the oxygen partial pressure, and θ is the lattice oxygen vacancy concentration. As observed in the mentioned blank reactor, the amount of the pumped oxygen was low at the investigated temperature, i.e., P_{O_2} was low. The fresh VPO catalyst used in this experiment had a high oxidation state with a low concentration of lattice oxygen vacancies, i.e., θ was low. Therefore, the VPO oxidation rate is very low according to Equation 5-3.

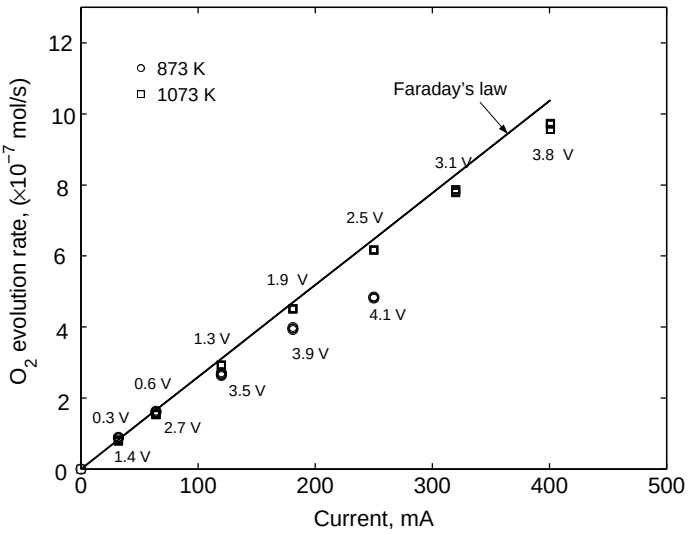

Figure 5-6 EOP results of the reactor: $N_2 \mid Pt \mid YSZ \mid Pt\text{-}Ag \mid Air$. T = 873 and 1073 K.

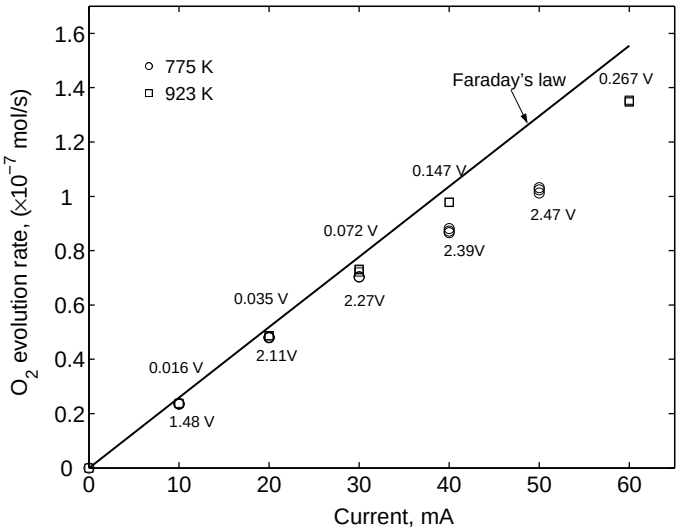

Figure 5-7 EOP results of the reactor: $N_2 \mid Ag \mid YSZ \mid Pt\text{-}Ag \mid Air$. T = 775 and 923 K.

For the EOP measurement, two other electrochemical reactors with Pt or Ag as anode were also tested. Figures 5-6 and 5-7 give the results of the oxygen pumping using the two reactor configurations $N_2 \mid Pt \mid YSZ \mid Pt\text{-}Ag \mid Air$ and $N_2 \mid Ag \mid YSZ \mid Pt\text{-}Ag \mid Air$, respectively, which generally show similar behavior to the reactor with Au as anode. At the lower operating temperature, it is clearly seen that the deviation between the measurement and Faraday's law was much more significant under the same magnitude of current. The terminal voltage decreased with increasing temperature as expected.

In the case of the reactor with Ag anode (see Figure 5-7), it is worth mentioning that an apparent deviation was observed at 923 K even though the external voltage between the two electrodes was 0.267 V. It might suggest that the reduction of the membrane and the formation of F-centers easily occurred at the interface between the membrane and Ag anode under the EOP condition, which would lead to an increase in the electronic conductivity of the membrane. The O_2 evolution rate was not reproducible for the same current during decreasing and increasing current. These phenomena were not observed in the reactors with Au or Pt as electrode. When the reactor with Ag as anode after the EOP measurement was calcinated in air for a certain time at high temperature, e.g., 975 K, the O_2 evolution rate can be restored, i.e., the oxygen evolution rate at low current agreed well with the theoretical value. In other words, the membrane can be reoxidized by being calcinated in oxygen atmosphere and thus recovered its oxygen ion conductivity, which seems to confirm that a reduction occurred in the membrane under EOP conditions. Therefore, in the following butane partial oxidation

experiments, Au was finally chosen as the anodic current collector due to its low catalytic activity and high stability under EOP conditions.

5.5. Concluding remarks

The SEMRs Au│YSZ│Pt-Ag and VPO│Au│YSZ│Pt-Ag were characterized by electrochemical techniques such as SEP, EIS, and I-V curve measurements. It was found that a minimum temperature was necessary to obtain a quantitatively reliable measurement with the SEP technique, which is due to the low oxygen ion conductivity of the solid electrolyte and to the slow charge-transfer reaction at the electrode-electrolyte interface at low temperature. Nevertheless, the reactor preparation was successful since the SEP measurement can qualitatively indicate the change of the oxygen concentration in the anode. The EIS revealed that the studied SEMR possesses a large electrical resistance at low operating temperature, which is mainly ascribed to the electrodes resistance. The I-V curve indicated that the reactor at low temperature has to be operated in the "EOP mode" in order to obtain a high current density with high oxygen flux through the membrane, which is necessary for maintaining the activity of the VPO catalyst.

EOP measurements with different reactor configurations demonstrated that the measured O_2 evolution rate was in good agreement with Faraday's law at low current, but it gradually deviated from Faraday's law with increasing current and this deviation was more pronounced at low temperature. The deviation is likely ascribed to the reduction of the solid electrolyte membrane and the formation of F-centers under a high external voltage.

The results from the SEP, EIS, I-V curve measurements indicated the same problem: there was a large electrochemical resistance of the studied SEMR, which was mainly due to the high electrode resistance at low temperature. Therefore, improvements on the electrode material and preparation, e.g., a composite anode as discussed in Chapter 4, have to be achieved to decrease the reactor resistance and thereby increase the current density.

6. Butane Partial Oxidation in an Electrochemical Membrane Reactor

In EMR operation mode, the reactor worked under closed-circuit conditions. The oxygen required for the anodic butane oxidation was generated as O^{2-} by means of EOP, as illustrated in Figure 6-1. In this mode, the solid electrolyte membrane served not only as a support for the catalyst but also as oxygen pump.

The blank reactor with the configuration Au/YSZ/Pt-Ag in the absence of a VPO catalyst was initially tested under conditions similar to those used in the reactor with VPO catalyst. Under the EOP condition, traces of CO_2 were detected but no CO was found as feeding 0.55 mol % butane. With high butane feed concentration (> 1.0 mol %) or high operating temperature (> 790 K), traces of butene were found in the effluent. However, the formation rate of CO_2 or butene in the blank reactor was negligible compared to the catalytic rates in the reactor with the VPO catalyst.

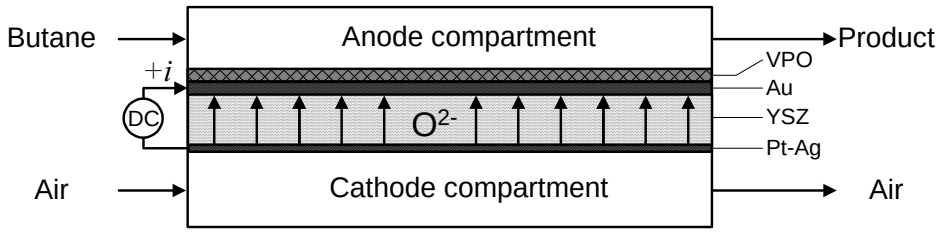

Figure 6-1 Illustration of the electrochemical membrane reactor applied for butane partial oxidation.

Butane oxidation in the EMR was performed with two different operating modes: (1) periodic redox operation and (2) steady-state operation. In the first operation, butane oxidation and oxygen pumping towards the catalyst were carried out sequentially. In the latter operating mode, butane oxidation and oxygen pumping were performed simultaneously.

6.1. Periodic redox experiments

Though the partial oxidation of *n*-butane to MA has been intensively investigated and realized in industry, the nature of active oxygen species is still far from being clear as indicated in

Chapter 1. When the oxidation was performed in the SEMR under the EOP condition, the active oxygen species become more complex and puzzling due to the fact that oxygen is supplied electrochemically in the form of O^{2-} to the catalyst and thus new active oxygen species might be formed. In order to approach active oxygen species involved in the butane oxidation in the SEMR, a periodic redox experiment was carried out. As illustrated in Figure 6-2a, there were five sequential periods with two separated processes, i.e., reduction (Steps 1, 3 and 5) and reoxidation (Steps 2 and 4) of the VPO catalyst in this set of experiments. During the reduction periods, butane was introduced to the anode under open-circuit conditions, while the reactor was operated under the EOP condition without butane feed during the reoxidation periods.

In the first step (Figure 6-2b), as 0.7 mol % butane was introduced to the fresh activated VPO catalyst, butane was oxidized to MA and CO_x in addition to H_2O (not shown here). Since the formation of MA and CO_x was found to decrease quickly, it can be concluded that the fresh VPO catalyst was reduced and deactivated fast. The active oxygen species for butane oxidation in this step mainly came from the stored surface lattice oxygen on the fresh VPO catalyst.

After flushing the reactor with N_2 for about 2 hours to clean the residual reactants, a constant current of 50 mA was imposed subsequently to the reactor (Step 2), which supplied oxygen ions to the anodic catalyst layer. As shown in Figure 6-2c, the gaseous oxygen formed in the anode increased steadily and approached a constant value, i.e., 1.25×10^{-7} mol/s, being close to 1.30×10^{-7} mol/s calculated from Faraday's law. During the reoxidation period with EOP, low concentrations of carbon dioxide were observed in the effluent, which likely originated from the combustion of carbonaceous deposits on the VPO catalyst surface being formed in the first step. At the beginning of EOP, the formation rate of gaseous oxygen was low because the pumped oxygen was firstly consumed for burning off carbonaceous deposits and for oxidising the surface of the reduced VPO catalyst.

After flushing the reactor with N_2 for about 3 hours to remove the residual oxygen, in the third step, butane was again introduced into the anodic compartment. Subsequently some MA and CO_x were detected in the effluent, as shown in Figure 6-2d. The re-formation of the products MA and CO_x (Step 3) confirmed that the reduced VPO catalyst (Step 1) was regenerated during the period of EOP (Step 2). As can be seen from Figures 6-2e and 6-2f, the whole periodic redox cycles were repeated and gave qualitatively similar results.

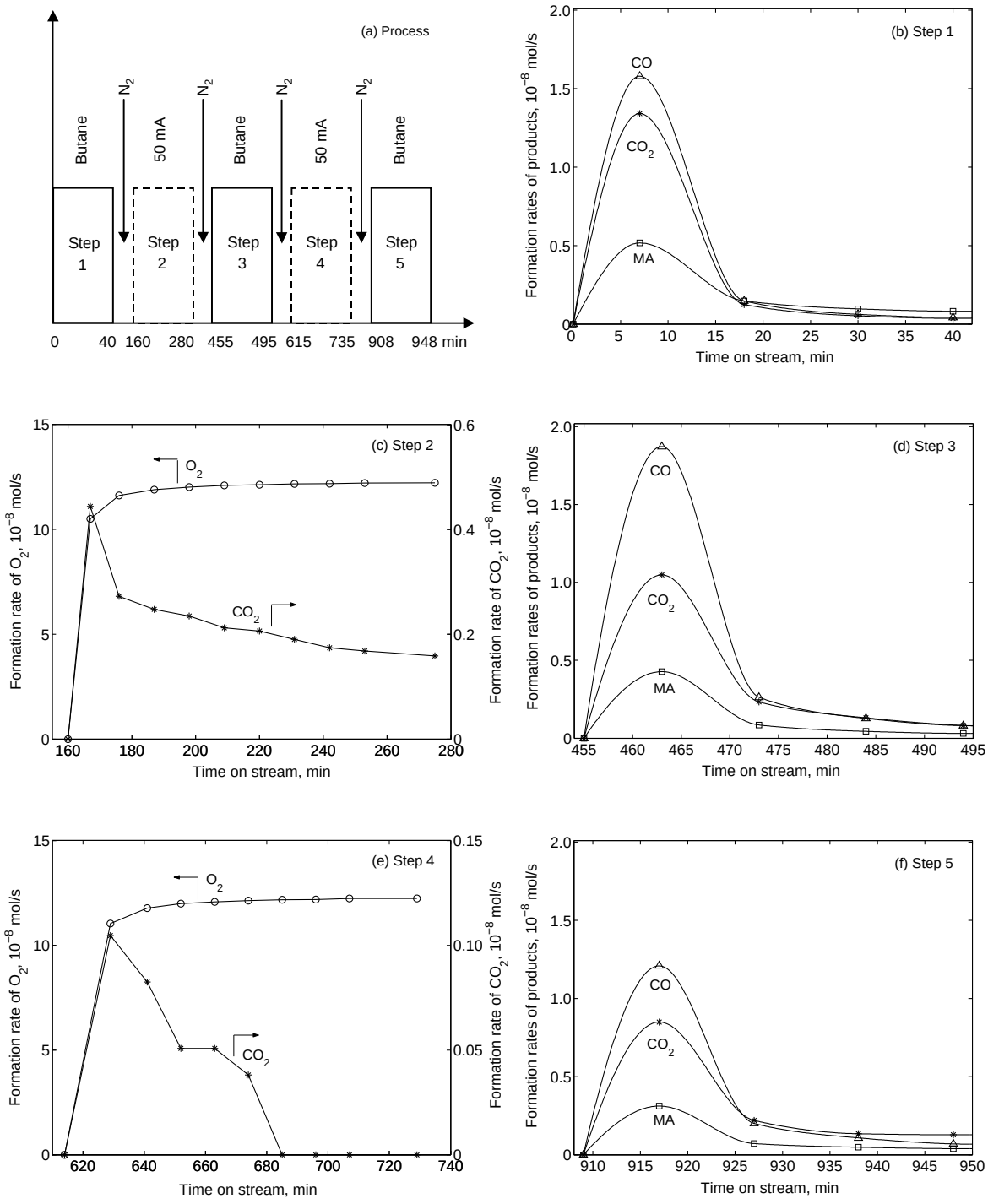

Figure 6-2 Periodic redox operation in the EMR: regeneration of the reduced VPO catalyst by the electrochemical oxygen pumping. T = 745 K; flow rate: 33 ml/min (STP); VPO catalyst loading: 6.6 mg/cm^2.

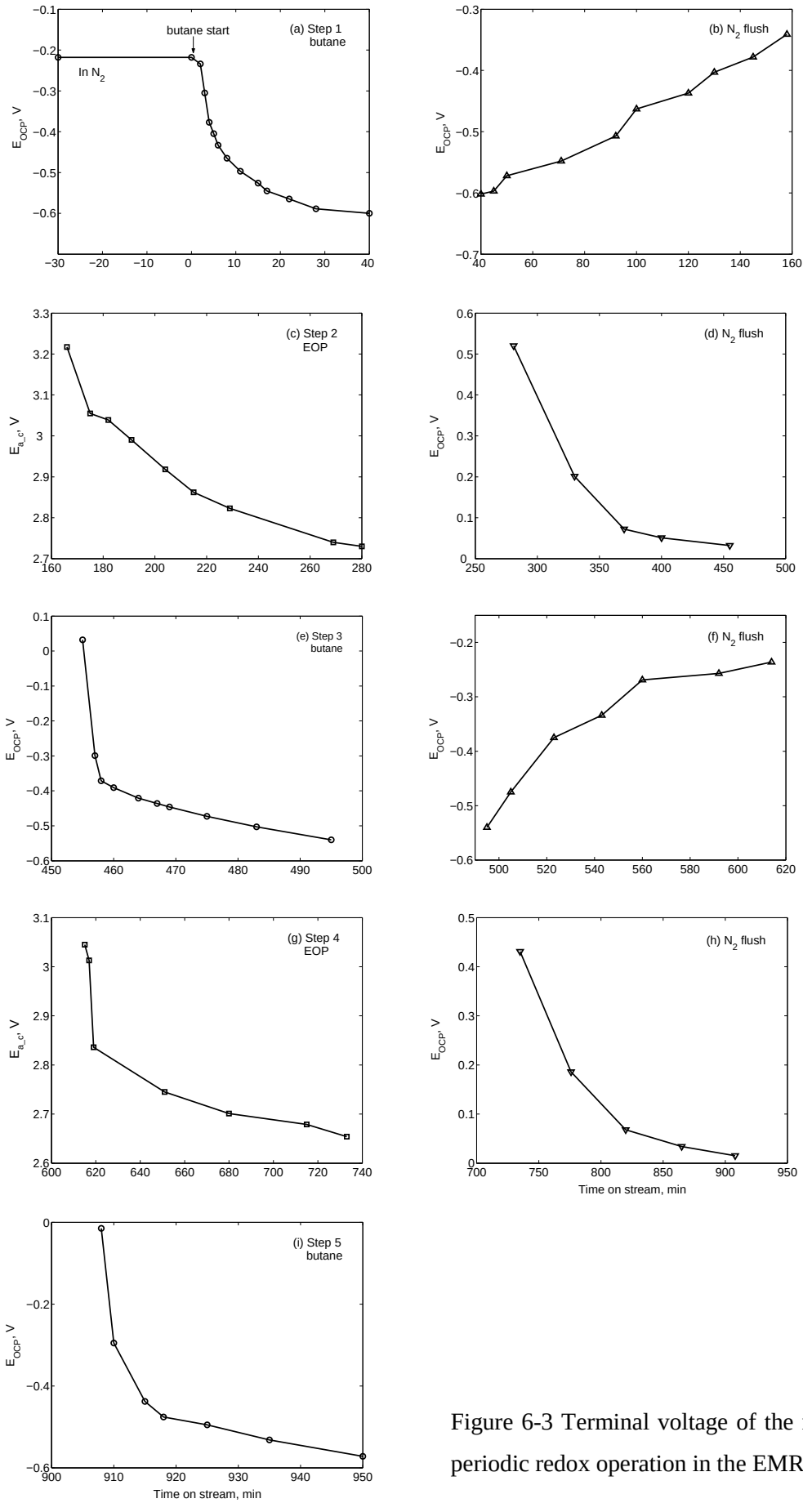

Figure 6-3 Terminal voltage of the reactor during periodic redox operation in the EMR.

During the periodic redox cycles, the terminal voltage between the anode and the cathode (cathode was defined as the reference electrode) was recorded as well (Figure 6-3). Figure 6-3a shows the variation of the OCP during the first reduction step (Step 1 in Figure 6-2). The OCP decreased with the time of reduction as butane was introduced to the anode compartment, which indicated that the surface oxygen was consumed and the activity of oxygen on the catalyst surface (a_o) decreased according to Equation 6-1:

$$a_O = \sqrt{0.21}\exp(2FE/RT) \tag{6-1}$$

The variation of the OCP was in agreement with the results shown in Figure 6-2b where the product formation rates were very fast (within 10 minutes of introducing butane to the anode) and then they slowly decreased and reached a steady level. Correspondingly, the OCP first dropped quickly and then the decrease became less pronounced.

With an isotopic exchange study, Pepera et al. [23] found that fast oxygen exchange on VPO catalyst can only occur in the near surface region corresponding to about five layers and lattice oxygen diffusion beyond this region was very slow. Therefore, the fast oxygen exchange being limited in a very few layers was the reason for the fast product formation rates and for the dramatic decline in the OCP at the beginning of the reduction. The diffusion of lattice oxygen from VPO bulk or subsurface regions to the surface layer is slow, which limited the further fast reduction of the VPO catalyst with butane. Therefore, the product formation rates were slow and the measured OCP became constant after a short reduction time.

When the butane was cut off and the anode was flushed with N_2, the OCP increased with the time of flushing, as shown in Figure 6-3b. This was probably because the flushing N_2 still contained about 0.01-0.02% O_2. This small amount of oxygen can be adsorbed on the Au or VPO catalyst surface, which resulted in an increase in the activity of oxygen on the catalyst surface and the OCP increased accordingly.

Figure 6-3c gives the variation of the terminal voltage E_{a_c} during the first reoxidation step (Step 2 in Figure 6-2) with a constant current of 50 mA. The terminal voltage slowly decreased with the time of oxidation. As the oxygen ions were pumped to the anode, the carbonaceous deposits in the anode were burned off and the reduced VPO catalyst was reoxidized. Simultaneously, the oxygen concentration increased with oxidation time (see Figure 6-2c). These two facts reduced the anodic polarization resistance by accelerating the

charge transfer reaction on the anode. Therefore, the overall reactor resistance decreased and the terminal voltage that was needed to obtain the same current became less.

When the current was switched off and the anode was flushed with N_2, the OCP decreased with flushing time, as shown in Figure 6-3d. However the OCP did not recover its original value –0.22 V (see Figure 6-3a) and it was about 0.03 V even after flushing the anode for approximately 3 hours. There are two possible reasons for this phenomenon. One is that the reactor cannot return to its original value quickly at a low temperature after a current treatment with a high external voltage. Another reason is that the VPO catalyst surface was reoxidized with EOP and the activity of adsorbed oxygen on the catalyst surface increased. When the periodic redox cycles were repeated, the terminal voltage as well as the OCP exhibited very similar results, which can be found in Figures 6-3e, f, g, h, i.

6.2. Active oxygen species

The above redox cycles of the VPO catalyst, i.e., reduction during the butane oxidation period and reoxidation during the EOP period, are illustrated schematically in Figure 6-4. A simple triangular reaction scheme is adopted to describe the reaction network. Butane reacts to MA or CO_x and MA can be further combusted to CO_x.

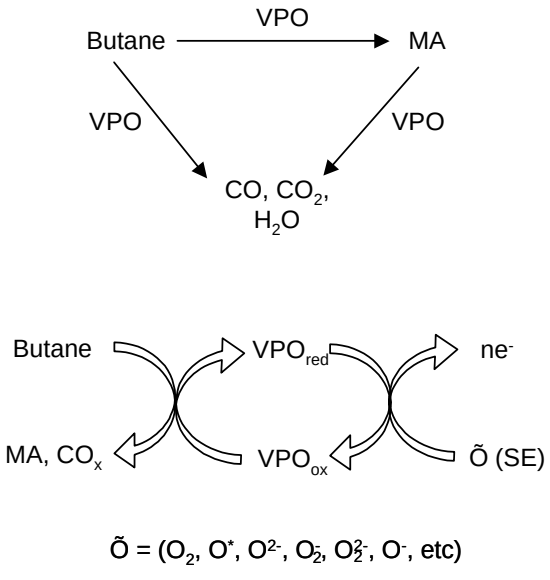

Figure 6-4 Proposed reaction scheme for butane partial oxidation in a solid electrolyte membrane reactor.

The results of the periodic redox experiments clearly demonstrated that the VPO catalyst was reduced during butane oxidation and could be reoxidized by oxygen ion pumping (see Figure 6-4). However, it is very difficult to identify and characterize the active oxygen species for reoxidation of the reduced VPO catalyst in Steps 2 and 4 (Figure 6-2). During the oxygen ion pumping, a number of oxygen species might be present in the anode, e.g., O_2, O_2^-, O^{2-}, O_2^{2-}, O^-, O^* (adsorbed). There are two possible mechanisms for reoxidation of the reduced VPO catalyst. One is the direct electrochemical oxidation: once the oxygen ions arrive at the anode, they will immediately and directly fill the VPO surface oxygen vacancies created in the reduction process. The second possible mechanism is the non-direct electrochemical oxidation: once the oxygen ions arrives at the anode, they will be quickly oxidized to form molecular oxygen at the anodic electrode (Au-layer) by releasing the electrons. This molecular oxygen will further fill the VPO surface oxygen vacancies created in the reduction process. Since the VPO catalyst used in this work was supported by a porous gold layer, the two proposed mechanisms might occur in parallel.

SEM images showed that the thickness of porous gold layer and VPO layer were about 10 μm and 50 μm, respectively. As illustrated in Figure 6-5, the VPO catalyst can be divided into two layers. The first very thin catalyst layer (Layer I) is in close contact with the gold and the membrane. The four-phase boundary (points of contact) is formed in this layer, which is defined as the locations where the YSZ membrane, the gold, the VPO catalyst and the gas phase are all in contact with each other. The second layer (Layer II) is superposed on Layer I and is isolated from the gold and membrane.

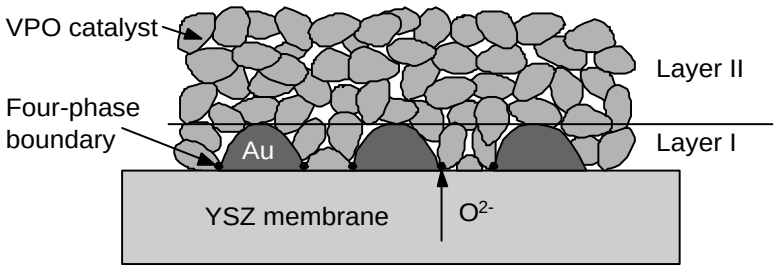

Figure 6-5 Schematic illustration of the anode structure, VPO catalyst/Au/YSZ membrane.

According to Brown et al. [97], the thickness of the three-phase boundary formed between anode, membrane and gas was estimated to be below 10 μm, which implies that Layer I containing the phase boundary in this reactor is thinner than Layer II. As the current was

imposed, the pumped ionic oxygen would first reoxidize the catalyst located at or around the four-phase boundary in Layer I. After the catalyst in Layer I is oxidised, the pumped ionic oxygen would be oxidised to form molecular oxygen at the phase boundary. The formed molecular oxygen then quickly diffuses to Layer II along the pores of the catalyst and simultaneously oxidizes the catalyst in this layer. Thus, the direct electrochemical oxidation with charged oxygen species (O_2^-, O^{2-}, O_2^{2-}, O^-) is restricted to Layer I and it can only occur at or around the phase boundary, while in Layer II only the non-direct electrochemical oxidation takes place. Generally, the non-direct electrochemical oxidation with conventional oxygen species (O_2, O^*) dominated the regeneration of the catalyst under the periodic operation, since Layer I is estimated to be clearly thinner than Layer II.

When the oxygen ion pumping and butane oxidation are carried out simultaneously, i.e., in steady-state operation, the direct electrochemical oxidation by non-conventional oxygen species (O^{2-}, O_2^-, O_2^{2-}, O^-) is more likely involved in the reaction compared to the periodic redox operation. This is because the products MA and CO could be oxidized to CO_2 by the electrophilic oxygen species such as O_2^-, O_2^{2-}, O^- coming from EOP, since the electrophilic oxygen species and products appeared in the anode simultaneously under the steady-state operation. The electrophilic oxygen species are usually believed to be very active for total oxidations [98]. A more detailed reaction mechanism will be proposed in the later chapter based on the comparison of the catalytic performances between the EMR and CR operations.

6.3. Steady-state experiments

A series of steady state experiments were carried out to assess the influence of the operating conditions on the membrane reactor performance, where EOP and butane oxidation on the anode were performed simultaneously. The experiments were carried out galvanostatically at atmospheric pressure varying the imposed current, reaction temperature, and butane feed concentration or flow rates.

6.3.1. Stability of the EMR operation

The molar ratio of oxygen to butane used in a fixed bed or fluidized bed reactor for butane partial oxidation to MA is usually around 12. However, it is much lower in the EMR due to the high electrical resistance at low temperature. The low oxygen/butane ratio might reduce

the VPO catalytic activity. So it is important to examine the stability of the operation under the EOP condition. Figure 6-6 illustrates the reactants (oxygen and butane) conversion,

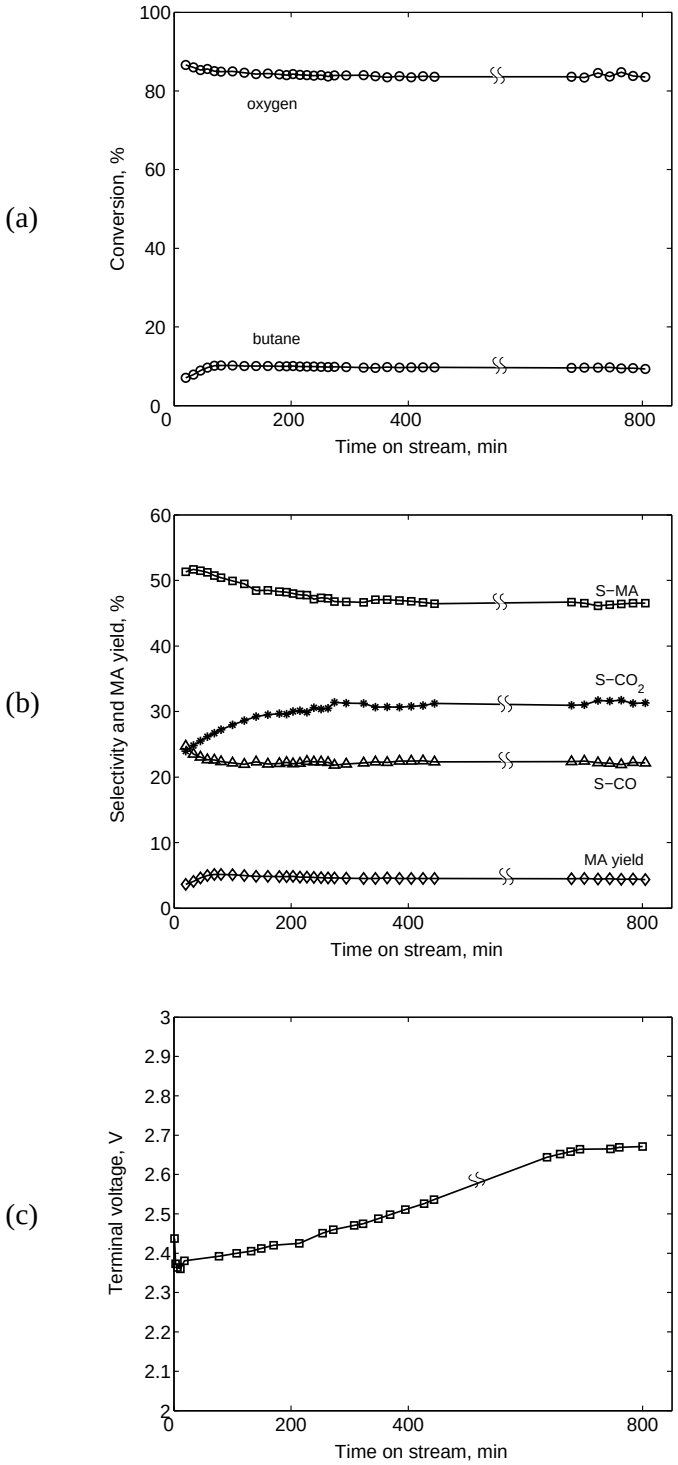

Figure 6-6 Stability of the EMR operation (a) conversions, (b) selectivities and MA yield, and (c) voltage in the EMR. I = 30 mA; T = 753 K; anode: 0.56 mol % butane in N_2 with total flow rate 35 ml/min; cathode: 80-100 ml/min air; VPO catalyst: 6.6 mg/cm^2.

products selectivity and MA yield in addition to the terminal voltage as a function of the reaction time at a current of 30 mA. The results were qualitatively similar for other studied currents.

During the initial 80 min, the butane conversion gradually increased and oxygen conversion decreased with time, as shown in Figure 6-6a. This was mainly due to the instability of the mass flow controller at the initial stage with an unstable butane concentration in the anode. At first, more butane was introduced into the anode, so more oxygen ions were consumed since the pumped oxygen was unchanged with a constant current. After about 100 min, the reactor approached a steady state with a very slow decline in the butane conversion. For instance, the butane conversion was 10.0% and 9.3% at 140 min and 800 min, respectively (see Table 6-1).

The MA selectivity (S-MA) has a higher initial value of 51% (before 50-70 min), as shown in Figure 6-6b. Meanwhile, the CO_2 selectivity (S-CO_2) increased apparently while the CO selectivity (S-CO) decreased. After about 140 min, the selectivities only changed slightly: the MA selectivity exhibited a weak decrease with reaction time, and the CO selectivity appeared to be constant but the CO_2 selectivity increased slightly. These tendencies can be clearly seen in Table 6-1. The MA yield increased at the initial stage due to the increase in the butane conversion. Afterwards, the MA yield somewhat declined with reaction time ascribed to the decrease in the MA selectivity.

Table 6-1 Variations of selectivities and conversions with reaction time in the EMR.

Time (min)	S-MA (%)	S-CO_2 (%)	S-CO (%)	X-butane (%)	X-oxygen (%)
20	51.3	24.0	24.7	7.1	86.5
140	48.5	29.2	22.3	10.0	84.3
800	46.5	31.3	22.2	9.3	83.5

The high initial MA selectivity was mainly due to the fact that the fresh VPO catalyst possessed a higher vanadium oxidation state and some lattice oxygen stored on the surface of VPO catalyst initially participated in the reaction. The slight decreases in the MA selectivity and in the butane conversion after the initial phase indicated the slow deactivation of the catalyst. As indicated in Chapter 1, the vanadium oxidation state was crucial for butane partial

oxidation to MA. In this study, the ratio of oxygen to butane was about 0.6, which was much lower than 12 that usually used in the industrial MA synthesis. The low oxygen/butane ratio might cause the reduction of the VPO catalyst and thus lowered the vanadium oxidation state of the catalyst. Even though the XRD spectra (see Figure 6-7) confirmed that the bulk catalyst remained the single-phase structure of vanadyl pyrophosphate [$(VO)_2P_2O_7$] without obvious change in crystallinity during the experiment, the color change of the catalyst (from brown before the reaction to gray-brown after the reaction) indicated a certain reduction on the catalyst surface [21].

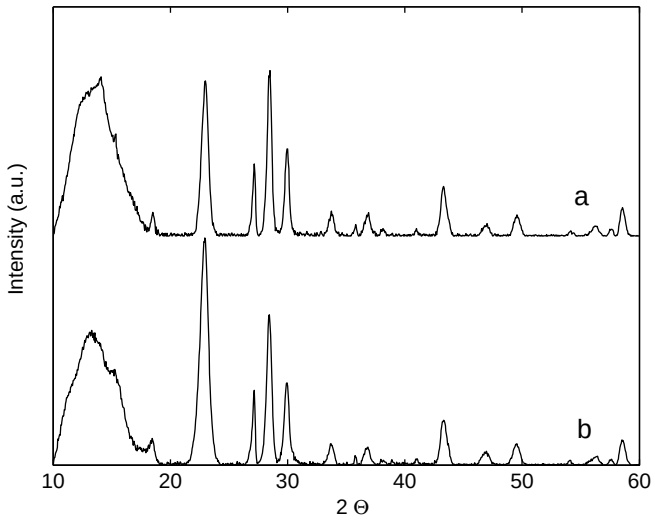

Figure 6-7 XRD spectra. (a) fresh catalyst, (b) used catalyst after about 13 hours' EMR reaction.

As indicated in Chapter 1, the oxidation state of vanadium greatly influences their catalyst performance for *n*-butane oxidation to MA and the desired catalyst requires an optimal V^{4+}/V^{5+} ratio [99]. The vanadium oxidation states on the surface of the fresh and used VPO catalyst were determined with the XPS technique, as shown in Figure 6-8. Compared to the fresh catalyst, some V^{5+} was reduced to V^{4+} or V^{2+} in the used catalyst. The surface vanadium oxidation state calculated from XPS results varied from 4.8 before the reaction to 4.6 after the reaction. The slight reduction of VPO catalyst surface after the EMR operation might be one reason for the slow catalyst deactivation. Additionally, the structure of the phase boundary between the YSZ membrane, Au and the VPO catalyst might be influenced with current treatment or calcinating time, as will be discussed in the following chapter.

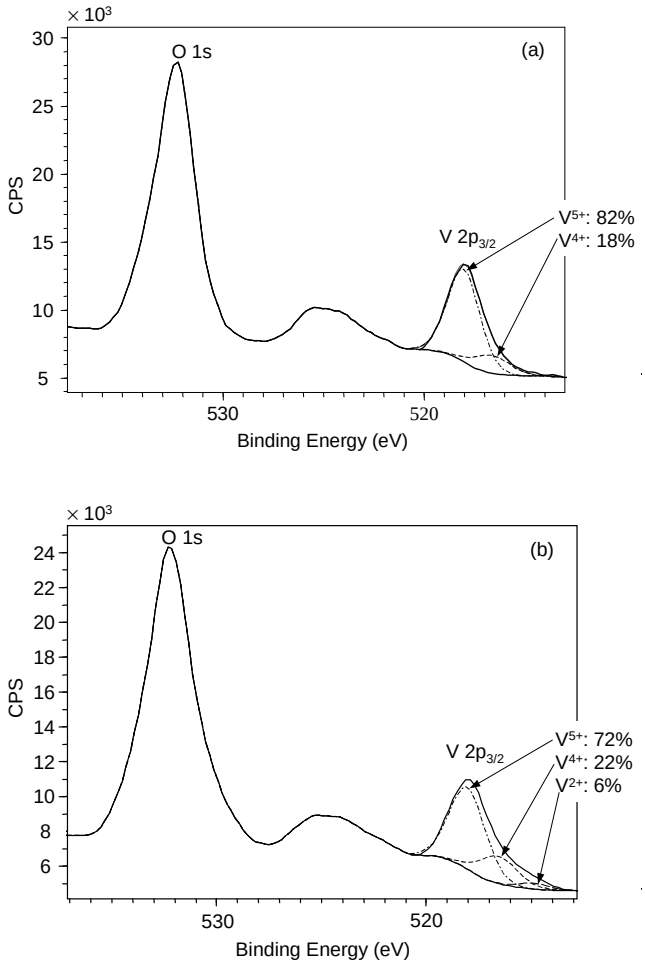

Figure 6-8 XPS results. (a) fresh catalyst, (b) used catalyst after about 13 hours' EMR reaction.

Carbonaceous deposits might also affect the activity of the catalyst. In this study the mass balance of carbon was around 95% indicating that traces of carbonaceous deposits probably formed on the catalyst. The existence of carbonaceous deposit on the anode was confirmed by measuring the carbon content of the fresh and used catalyst. The activated fresh catalyst showed a carbon content of 0.049% tracing from the activation procedure with butane. The carbon contents of the used catalysts were 0.072% to 0.134%. The highest carbon content was detected in the catalyst samples operated with lowest imposed current.

Figure 6-6c illustrates the terminal voltage of the reactor as a function of time. A fast initial voltage drop was observed, which was probably due to an abrupt charging of the reactor. After the initial phase, the terminal voltage slowly increased in the galvanostatic operation with a constant current. This was due to the growing electrical resistance of the reactor being induced by changes of the polarization resistances of the electrodes, which was confirmed by

the reactor EIS. As shown in Figure 6-9, the polarization resistance of the electrodes increased after the reaction compared to that before the reaction, which might be ascribed to the change of the phase boundary between the electrode and the membrane upon passing a current or upon the reduction atmosphere (butane) treatment, as reported by van Herle et al. [108].

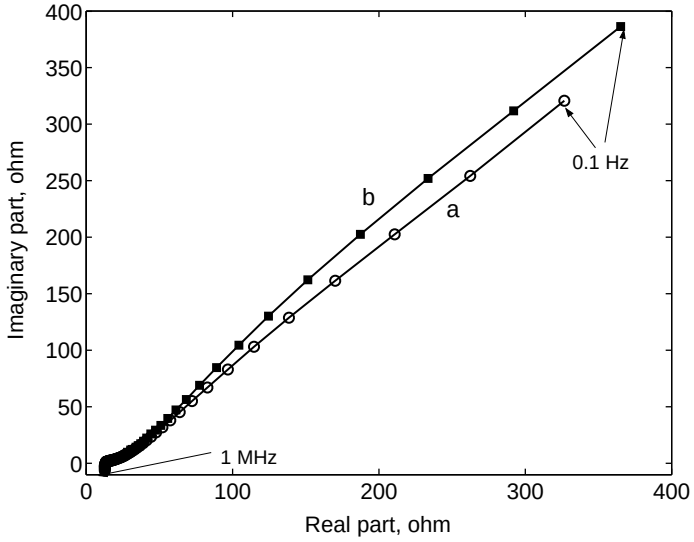

Figure 6-9 EIS of the reactor at the OCP: (a) before the reaction, (b) after about 13 hours' electrochemical reaction. T = 753 K; anode: 40 ml/min N_2; cathode: 80-100 m/min air.

6.3.2. Current effect

In the EMR, the effect of the imposed currents on the conversions, selectivities and MA yield was studied at the steady state with two different VPO catalyst loadings, i.e., 7.2 and 14.0 mg/cm^2 (Figure 6-10). The steady state was confirmed by at least three comparable GC analyses after about 2-3 hours' initial stabilization stage. The imposed currents varied from 10 to 70 mA, the corresponding current densities being 0.44-3.1 mA/cm^2.

With increasing current, the conversion of butane increased and the conversion of the pumped oxygen decreased (Figures 6-10a and 6-10b). Though the oxygen conversion was lower at higher current, more amount of oxygen was consumed at the higher current (not shown here).

Below 30 mA, the butane conversions were very similar with two catalyst loadings. For example, the butane conversions at 20 mA were 8.6% and 8.7% for the 7.2 mg/cm^2 and 14.0 mg/cm^2 catalyst loadings, respectively. At low oxygen pumping rates, the oxygen conversion in both cases approached to complete and thus the maximum amount of butane that can react is limited by the oxygen supply.

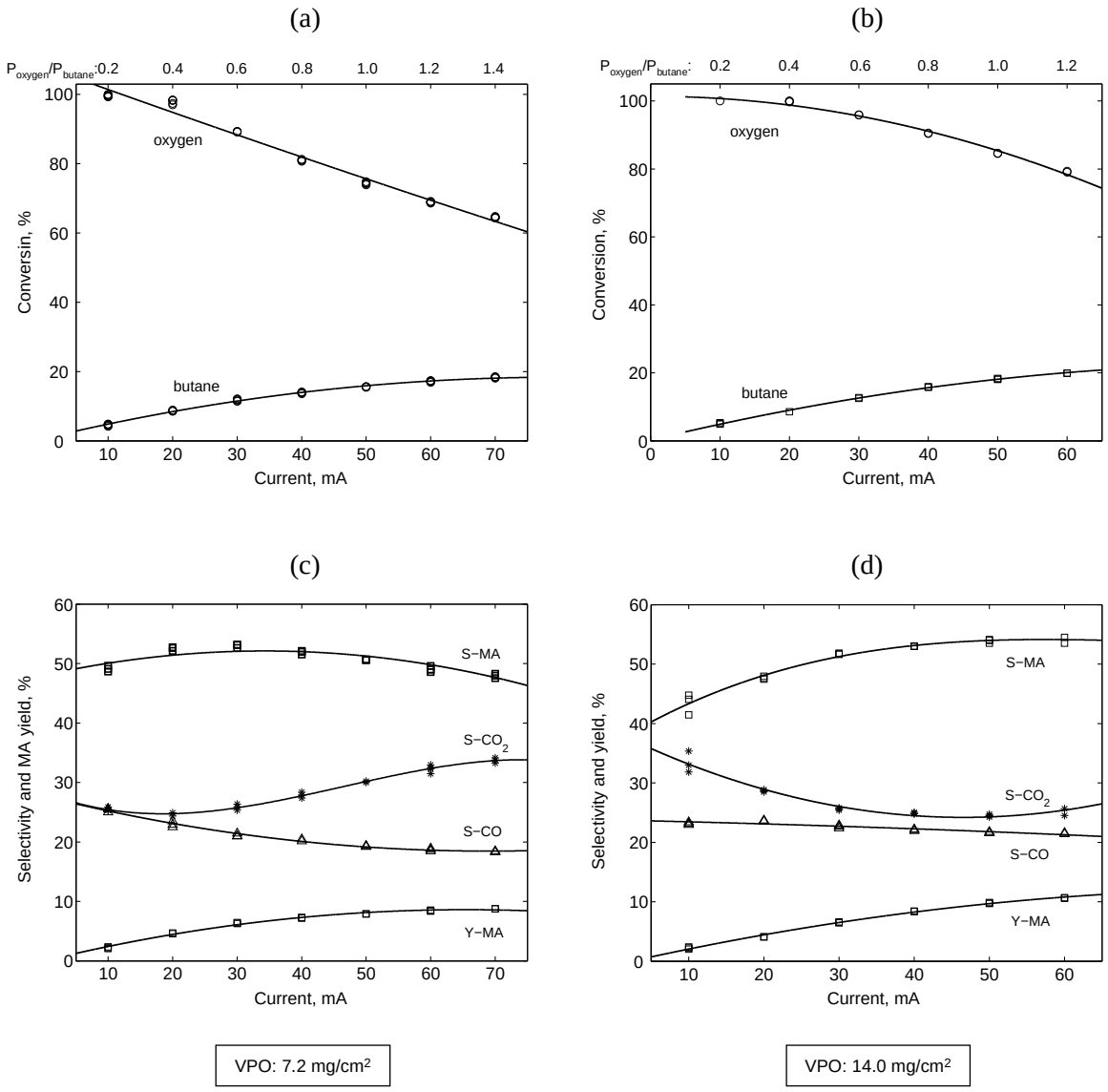

Figure 6-10 Butane partial oxidation in the EMR at different imposed currents. T = 753 K; anode: 0.55 mol % butane in N_2 with flow rate of 35 ml/min (STP).

Above 30 mA, the butane conversion at higher catalyst loading was higher. This is due to the fact that the oxygen conversion was now clearly below 100% with both catalyst loadings and thus the oxygen supply was not limiting the reaction. Therefore, the butane consumption was enhanced by the increased catalyst loading. For example, the butane conversions at 50 mA were 15.5% and 18.2% for the 7.2 mg/cm^2 and 14.0 mg/cm^2 catalyst loadings, respectively.

As shown in Figures 6-10c and 6-10d, at the lower imposed current, e.g., below 30 mA, the selectivity to MA increased with increasing current. This phenomenon was obvious especially at higher VPO catalyst loading (Figure 6-10d). The lower MA selectivity at the lower current

range is mainly due to the 100% oxygen conversion and no oxygen in the gas phase, which can dramatically reduce the VPO selectivity to MA, as discussed by Lorences and Rubio et al [100, 101].

At higher imposed currents, e.g., above 30 mA, the depletion of the pumped oxygen was not complete (Figures 6-10a and 6-10b) and the selectivity to MA was only weakly dependent on the current. Additionally, as shown in Figure 6-10c, there was a slight decline in the MA selectivity above 40 mA. This might be ascribed to the overoxidation of MA to CO_2, which became more likely as more electrophilic oxygen species and more MA were formed on the anode at the higher imposed current. This behavior was not observed at higher loading (Figure 6-10d) and it is likely due to the higher oxygen conversion (above 80%) even at the higher imposed current.

In addition, the selectivity to CO_2 was found to be higher than that to CO in all investigated reaction conditions, which indicated the reaction was probably performed in a reducing environment. As observed by Lorences et al. [102], the selectivity ratio of CO/CO_2 may reach 1.6 - 1.8 under oxidizing condition, whereas it dropped to 1.2 - 0.9 as the reaction condition became more reducing.

As discussed by Rodemerck et al. [21] and Ait-Lachgar et al. [103], the VPO catalyst selectivity to MA is strongly influenced by the vanadium oxidation state and the best selective catalysts need a moderately high oxidation state, e.g., 4.00 - 4.03 for the spent equilibrated catalyst. If the VPO catalyst is exposed to the oxidizing environment with a very high oxygen/butane ratio, the surface of the vanadium will be oxidized and the overoxidation of the intermediate product (MA) will be favored as a result of the high oxygen concentration and high vanadium oxidation state. In contrast, if the VPO catalyst is exposed to the reducing environment having a very low oxygen/butane ratio, the surface of the VPO catalyst will be strongly reduced. As discussed by Rodemerck et al. [21] and Schuurman et al. [104], the adsorption of MA on the reduced catalyst surface is stronger and the overoxidation of MA to CO_2 by any available oxygen species becomes more likely, which apparently reduces the VPO selectivity to MA. Therefore, a moderate oxygen/butane ratio seems to be necessary in order to obtain a reasonable MA selectivity.

In this set of experiments, the molar ratio of the pumped oxygen to butane in the feed was varied from 0.2 to 1.4 with increasing current. Being limited by the high electrical resistance of the reactor at the low temperature (753 K), the ratio used in the reactor is much lower

compared to a conventional fixed-bed reactor and it is even lower than that required stoichiometrically to react all butane, which indicates a reducing environment. However, it was found that the MA selectivity exhibited a maximum at a certain oxygen/butane ratio. Considering the fact that the overoxidation of MA to CO_2 is favored when more electrophilic or adsorbed oxygen species accumulated on the phase boundary with the higher current, it could be expected that the MA selectivity would decline significantly if a considerable higher current than that studied here were imposed to the membrane reactor. Nevertheless, the higher imposed current gave the higher MA yield, as shown in Figures 6-10c and 6-10d, so a further improved current would still be favorable in the studied EMR.

6.3.3. Temperature optimisation

n-Butane oxidation to MA is an exothermic reaction and it is conventionally carried out at low temperature (623-723 K), as introduced in Chapter 1. However, at the relative low temperature the electrical resistance of the EMR is too high, which will lead to a very low oxygen flux through the membrane. Therefore, the operating temperature has to be optimized for this special type of reactor.

As shown in Figure 6-11, the effect of temperature on butane partial oxidation is studied at the imposed currents of 40 and 20 mA. As expected, the conversions of the butane and the oxygen pumped increased with increasing temperature (Figures 6-11a and 6-11b). The increment of butane conversion with increasing temperature at higher current (40 mA) was more significant compared to that at lower current (20 mA). It is due to the fact that the oxygen conversion at the lower current (20 mA), which often approached to 100%, was higher than that at the higher current (40 mA). Thereby, the consumption rate of butane at the lower current was limited stronger by the supplying rate of oxygen compared to that at the higher current.

As can be seen in the Figures 6-11c and 6-11d, the selectivity to MA decreased and the selectivity to CO_x increased with increasing temperature indicating that the activation energy for MA formation is lower than that for the reaction to combustion products CO_x. By using the reported activation energies [105], i.e., 80, 92 and 113 kJ/mol respectively for the MA formation, the butane total oxidation to CO_x and the MA combustion to CO_x, the process was simulated and a good agreement was obtained in the investigated temperature range [106].

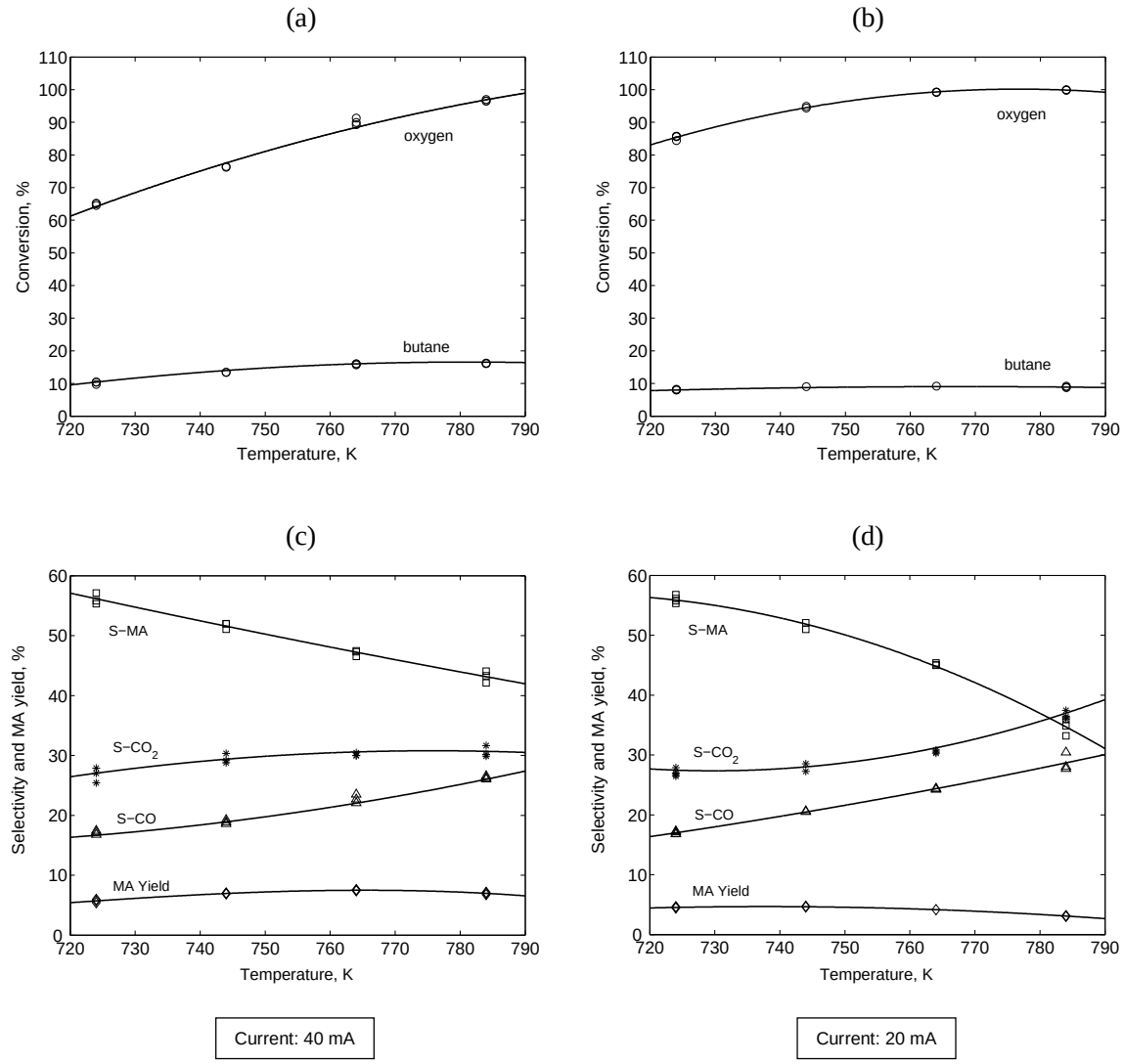

Figure 6-11 Butane partial oxidation in the EMR at different temperatures. Anode: 0.55 mol % butane in N_2 with flow rate of 35 ml/min (STP); VPO catalyst: 7.2 mg/cm^2.

For 40 mA, the selectivity to MA linearly decreased with increasing temperature. On average, a 20 K temperature rise reduced the MA selectivity by 4%. For 20 mA, there is a steep decline in the selectivity to MA at higher temperature (785 K) due to the fact that the pumped oxygen is depleted and the surface of the VPO catalyst was reduced rapidly. The CO_x formation on the reduced VPO catalyst surface was favored, as shown in Figure 6-11d, the selectivity to CO_x obviously increased (785 K). Mallada et al [107] also reported that the catalyst near the effluent became less selective to MA, and the CO_x selectivity increased as the gas-phase oxygen was depleted in fixed-bed reactors. Since the temperature influenced the butane conversion and MA selectivity conversely, the MA yields exhibited slight maxima with respect to temperature, e.g., at 763 K for 40 mA and at 743 K for 20 mA.

The oxygen flux through the membrane is mainly controlled by the reactor temperature once the electrodes as well as the membrane composition are optimised and well prepared. The oxygen flux is greater at higher temperatures thanks to the higher oxygen ion conductivity of the solid electrolyte membrane. The high oxygen flux is necessary to maintain the activity and selectivity of the VPO catalyst. Taking into account the temperature effects on the oxygen flux and MA selectivity as well as on the MA yield, the optimal temperature was 753 ± 5 K for the studied solid electrolyte membrane reactor.

6.3.4. Butane concentration effect

The effect of butane concentration in the feed on the catalytic performance in terms of conversion and selectivity as well as the reaction rates was studied at a fixed imposed current of 50 mA, as illustrated in Figure 6-12. Regarding the low oxygen flux at low temperature (753 K), i.e., 5.6×10^{-5} mol/m^2/s at 50 mA, the investigated butane concentration (0.35-1.2 mol %) was lower than usually used in a conventional fixed-bed reactor (1.2-2 mol %). As expected, the oxygen conversion increased with increasing butane concentration since the oxygen-supplying rate was unchanged at a constant current (Figure 6-12a). Although the butane conversion decreased with increasing butane concentration, the overall consumption rate of butane (Figure 6-12c) was enhanced by the higher butane concentration since more oxygen reacted at the higher butane concentration.

With increasing butane concentration, the selectivity to MA slightly declined but the selectivity to CO_x gradually increased (Figure 6-12b). The MA yield was lower at the higher butane concentration since both butane conversion and MA selectivity decreased with increasing butane concentration. As already discussed in Figure 6-4, *n*-butane oxidation is a serial-parallel reaction. There are two possible reasons for the decline in the MA selectivity. On the one hand, more formed MA might be overoxidised to CO_x as the MA concentration in the anode increased with increasing butane concentration. On the other hand, the catalyst surface might change under the increased partial pressure of hydrocarbons. The feed ratio of oxygen/butane decreased from 1.5 to 0.5 with increasing butane concentration. The catalyst surface gets reduced more deeply under a lower oxygen/butane ratio, which could lead to a decrease in the VPO selectivity to MA. These two possible reasons could well explain the tendency of the MA formation rate, as shown in Figure 6-12c, which had a maximum with respect to the butane concentration.

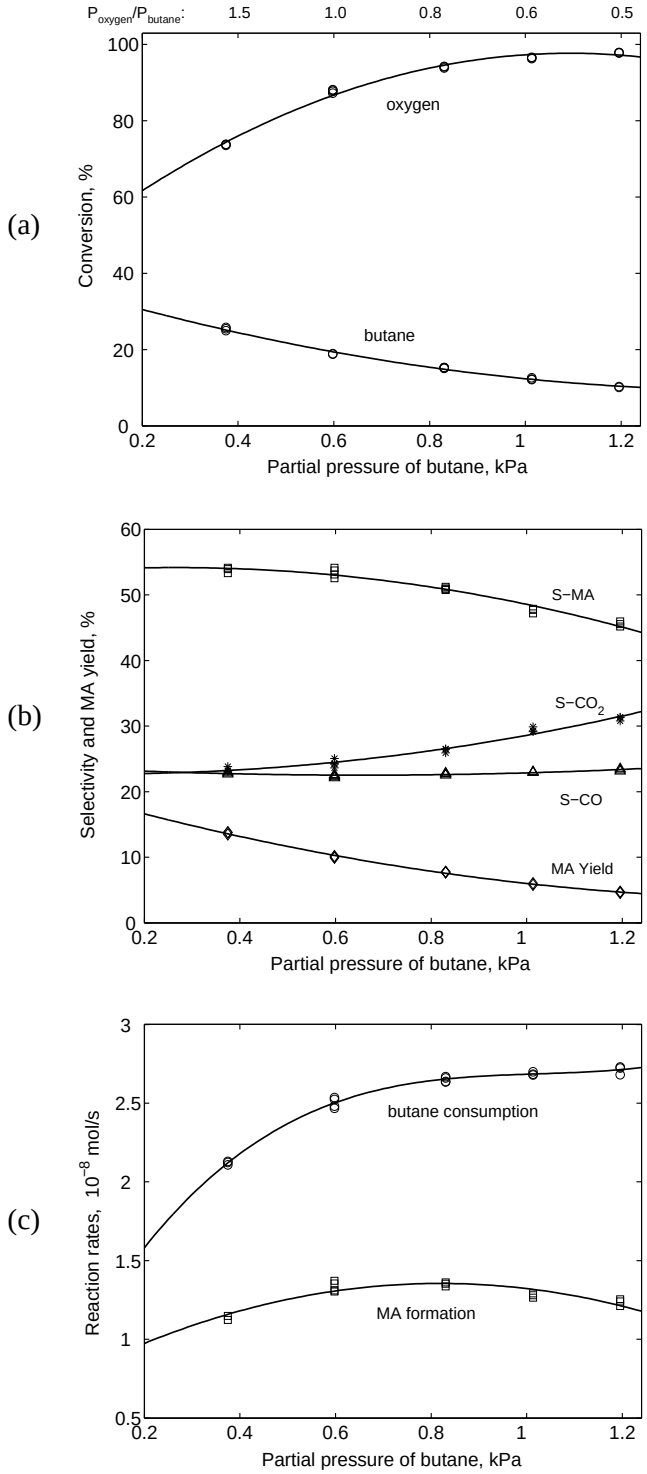

Figure 6-12 Butane partial oxidation in the EMR at different butane concentrations. T = 753 K; I = 50 mA; anode: butane in N_2 with flow rate of 34 ml/min (STP); VPO catalyst: 14.0 mg/cm^2.

6.3.5. Flow rate effect

As presented in Figure 6-13, the effect of flow rates (F) on the conversion, selectivity and MA

yield was studied at two different imposed currents of 20 and 50 mA. In this set of experiments, the butane concentration in the feed was fixed at 0.55 mol % and the catalyst loading (W) was fixed at 7.2 mg/cm^2. The butane conversion was higher at the lower flow rate (corresponding to higher W/F) due to the increased contact time of butane with VPO catalyst, as shown in Figures 6-13a and 6-13b. The oxygen conversion was nearly constant over the measured flow range, exhibiting only a weak decline at low flow rate (W/F > 0.005 g·min/cm^3).

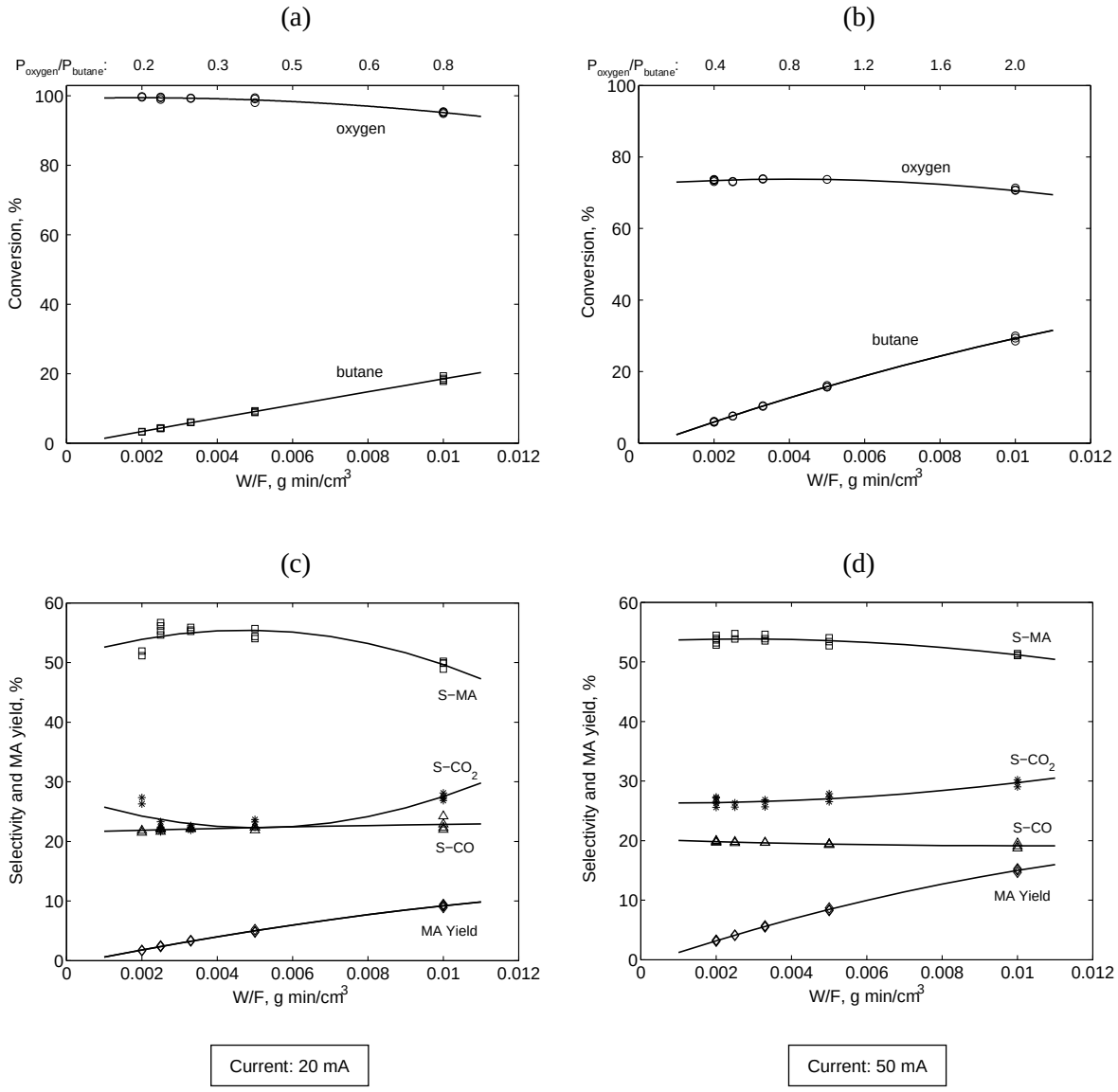

Figure 6-13 Butane partial oxidation in the EMR at different feed flow rates. T = 753 K; anode: 0.55 mol % butane in N_2; VPO catalyst: 7.2 mg/cm^2.

n-Butane oxidation to MA follows a series-parallel reaction network with a desired intermediate product MA and undesired products CO_x. Generally, the selectivity to the

intermediate product should benefit from the higher flow rate because the further oxidation of the intermediates would be suppressed by short residence time of the intermediates in the reactor. It can be seen in Figures 6-13c and 6-13d that this desired effect of the flow rate on the MA selectivity is only realized at the lower range, i.e., $W/F \geq 0.005$ g·min/cm^3. At higher flow rates, i.e., $W/F < 0.005$ g·min/cm^3, the MA selectivity did not increase further (for 50 mA) and sometimes even decreased with increasing flow rate (for 20 mA). It should be noted that increasing the feed flow rate not only reduces the residence time of the products in the reactor but also lowers the oxygen concentration in the anode at given current. The dilution of the oxygen content decreases the ratio of oxygen/butane, e.g., from 2.0 to 0.4 as the flow rate increased from 17 ml/min to 85 ml/min for 50 mA current. At high flow rate, the ratio of oxygen/butane is low and the catalyst surface is reduced, which results in a loss of catalyst selectivity to MA as discussed in Section 6.3.2. So there are two competitive effects of the flow rate on the selectivity to MA in the EMR. The MA yield benefited from the low feed flow rate mainly thanks to the increase in butane conversion with decreasing flow rate. In order to obtain a higher MA selectivity and MA productivity in an EMR, a moderate feed flow rate is favored.

6.4. Concluding remarks

The partial oxidation of *n*-butane to MA was carried out in the EMR under periodic redox and steady-state operations. The experimental results clearly demonstrated that it is feasible to synthesize MA in EMR mode with periodic or steady-state operation.

The results of periodic redox operation confirmed that reduced activity of VPO catalyst in the butane oxidation could be regenerated by oxygen ion pumping. The OCP with SEP measurements qualitatively revealed the oxygen activity variation on the anode surface. Two possible oxidation mechanisms are proposed for the VPO reoxidation: direct electrochemical oxidation in the first VPO layer and non-direct electrochemical oxidation in the second VPO layer. However, the nature of the active oxygen species for the regeneration of the VPO catalyst is still under discussion.

The stability of the catalytic performance in the EMR was investigated. It was found that the VPO catalyst exhibited slow deactivation, i.e., the MA selectivity slightly decreased but the CO_2 selectivity increased. The deactivation was mainly ascribed to the reduction of VPO surface under the low oxygen/butane ratio.

The results of steady-state experiments demonstrated the influence of the operating conditions such as the imposed current, reaction temperature, butane concentration and flow rate on the conversion of reactants and selectivity to products as well as yield of MA. The selectivity to MA was 50-53% and the butane conversion was 15-18% with the MA yield of 8-10% in the studied EMR under the following operating conditions: reaction temperature of 753 ± 5 K, butane concentration of 0.55 mol % and current density of 2.2 mA/cm^2 with 16 h^{-1} WHSV. The catalyst-mass-based and membrane-area-based MA productivity of this reactor were accordingly 1.22×10^{-4} $mol/(h\cdot g_{cat})$ and 0.017 $mol/(m^2\cdot h)$.

The MA yield in the investigated non-optimized lab-scale EMR is lower compared to that in an industrial conventional reactor due to the low oxygen flux of the membrane at the low reaction temperature. Nevertheless, the study of butane oxidation in the EMR can bring new insight into the investigation of the mechanism for butane partial oxidation, since oxygen species supplied to the VPO catalyst in the EMR differ from those in the conventional co-feed reactors. A more detailed reaction-mechanism scheme will be proposed in Chapter 8 based on the comparison of EMR and CR operations.

7. Comparison of Electrochemical Membrane Reactor and Co-feed Membrane Reactor

As indicated in Chapter 1, since oxygen is supplied electrochemically in the form of O^{2-} in the EMR, the selectivity to the desired product might differ from that obtained in the co-feed reactor by directly supplying gas-phase oxygen. In order not only to know the difference between the EMR and CR operations, but also to investigate the reaction mechanism of butane oxidation in the EMR under EOP conditions, a CR operation with the same reactor configuration as the EMR was investigated and the results were compared to those of the EMR operation.

7.1. Co-feed membrane reactor for butane partial oxidation

The CR operation is illustrated in Figure 7-1 where the reactor is operated under open-circuit conditions. The solid electrolyte membrane only serves as a catalyst support. The reactants are gas-phase oxygen (O_2) and butane, which are co-fed to the anode compartment.

Similar to the EMR operation, butane oxidation in the CR was performed with two different operating modes: (1) periodic redox operation and (2) steady-state operation. In the first mode, butane oxidation and feeding of gas-phase oxygen to the anode were carried out sequentially. In the second mode, butane oxidation and gas-phase oxygen feeding were performed simultaneously.

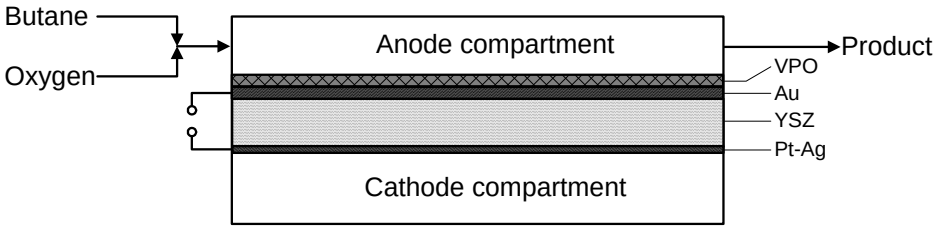

Figure 7-1 Illustration of the co-feed membrane reactor for butane partial oxidation.

7.2. Catalytic activity of the blank reactor

The catalytic activity of the blank reactor Au/YSZ/Pt-Ag without the VPO catalyst was initially tested with co-feeding of butane and gas-phase oxygen. No CO or CO_2 was detected. Traces of butene were found at higher butane concentration (> 1.0 mol %) or high temperature (> 790 K), which was probably attributed to the oxidative dehydrogeneration or thermal dehydrogeneration of butane. However, the formation rate of butene in the blank reactor was negligible compared to the catalytic rates in the reactor with VPO catalyst.

As depicted in Chapter 6, traces of CO_2 were formed by the direct oxidation of butane under EOP conditions in the blank EMR. The CO_2 formation rate increased with increasing current. For instance, the CO_2 formation rates with 10 and 70 mA were 9.0×10^{-10} and 2.9×10^{-9} mol/s, respectively, at 753 K with feeding of 0.55 mol % butane. Since no CO_2 was detected in the CR as mentioned above, one can conclude: compared to the gas-phase oxygen supplied in the CR, the electrochemically pumped oxygen in the EMR seems to be active for directly catalyzing butane to CO_2 at the three-phase boundary between Au, the YSZ membrane and gas phase.

7.3. Periodic redox experiments

Similar to the periodic redox cycles in the EMR, there are five sequential periods with two separated processes of reduction (Steps 1, 3 and 5) and reoxidation (Steps 2 and 4) of the VPO catalyst in this set of experiments (see Figure 7-2a). The difference between the periodic redox experiments in the CR and in the EMR is that gas-phase oxygen instead of oxygen ions was used to reoxidize the VPO catalyst. During the reduction periods, butane was introduced to the anode without gas-phase oxygen, while only gas-phase oxygen was fed to the anode without butane during the reoxidation periods.

The results of the periodic redox experiments in CR operation (Figures 7-2b to 7-2f) appear to be qualitatively similar to those in EMR operation (Figures 6-2b to 6-2f). As shown in Figure 7-2b, once butane was introduced to the catalyst layer in the anode, the VPO catalyst was quickly reduced and lost its activity as indicated by the formation of MA and CO_x, which decreased dramatically. Subsequently, the reduced VPO catalyst in the first step was gradually reoxidized with recovering the catalyst activity in step 2 by introducing gas-phase

oxygen (Figure 7-2c), which was confirmed by renewed formation of MA and CO_x (Figure 7-2d) as butane was added to the catalyst layer again (step 3). The whole periodic redox results could be qualitatively reproduced, as presented in Figures 7-2e and 7-2f.

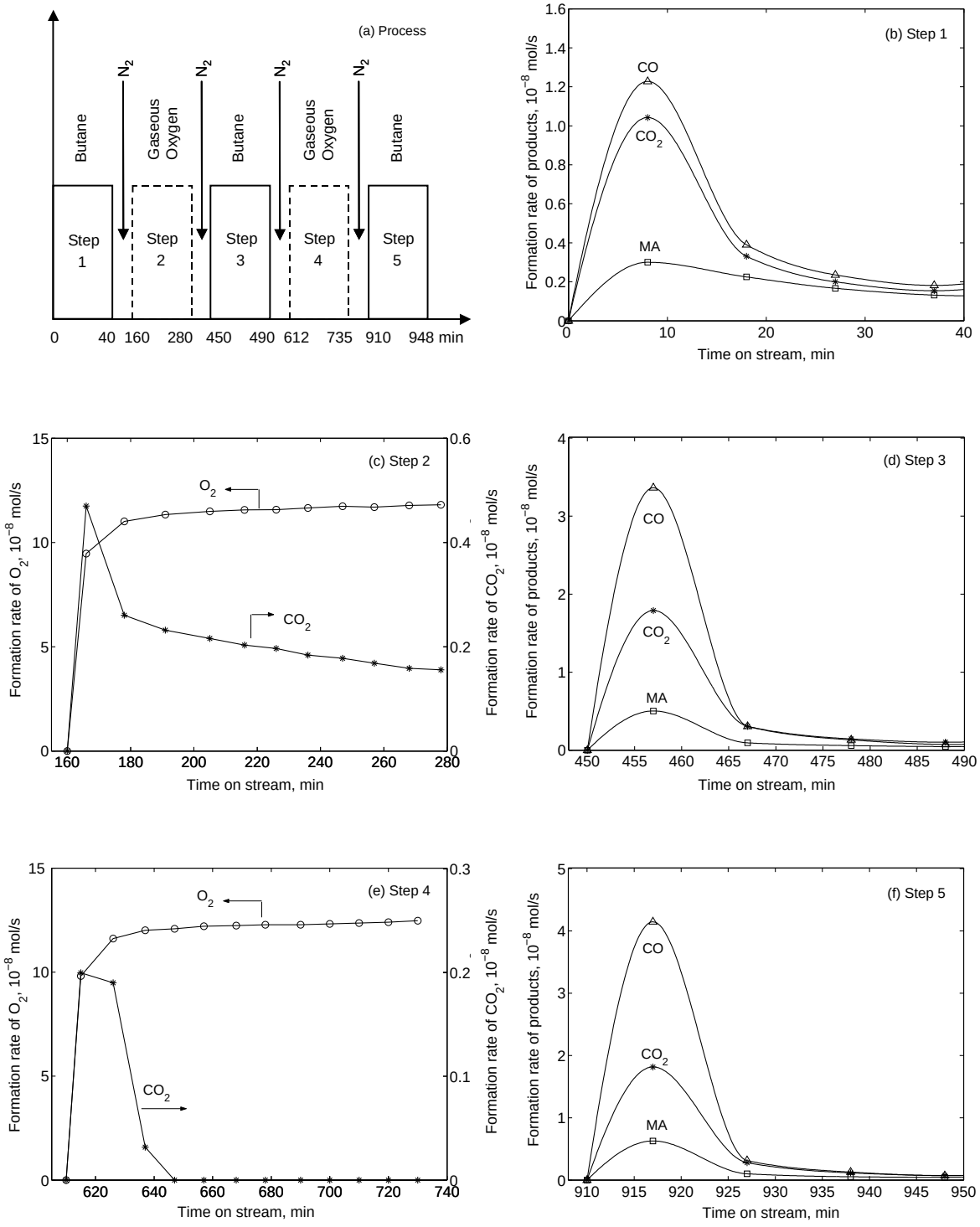

Figure 7-2 Periodic redox operations in the CR: regeneration of the reduced VPO catalyst by gaseous oxygen. T = 745 K, flow rate: 33 ml/min (STP), VPO catalyst: 13.2 mg/cm^2.

The redox process, i.e., the reduction of the VPO catalyst with butane and the reoxidation of the reduced VPO catalyst with gas-phase oxygen, was further confirmed by recording the OCP between the anode and the cathode (Figure 7-3). It is worth emphasizing that all OCP values in the CR can be recorded during the redox periods since the CR was always operated under open-circuit condition. However, the OCP recording with SEP technique in the EMR can only be realized during the reduction period, while during the reoxidation period only the terminal voltage was recorded since two electrodes without a reference electrode were used in the studied EMR.

The OCP variation in the CR during the reduction period was qualitatively similar to the EMR, as shown in Figures 7-3a, e, i. For instance, the OCP quickly dropped from –0.17 V to –0.59 V within the first 10 min as butane was introduced and then it slowly decreased from –0.59 V to –0.68 V within the final 30 min (see Figure 7-3a), which was consistent with the formation rates of products observed in Figure 7-2b. A similar behavior was observed in the EMR operation (see Section 6.1). After the butane treatment, the OCP of the reactor under the same atmosphere (N_2) decreased from the original value –0.17 V (Figure 7-3a) to about –0.47 V (Figure 7-3b), which implied that the oxygen activity on the catalyst surface decreased according to Equation 6-1 and therefore the VPO catalyst must have been reduced in step 1.

Figure 7-3c gives the variation of the OCP during the first reoxidation step (step 2 in Figure 7-2) with gas-phase oxygen. The OCP increased with the time of oxidation, which indicates that the VPO catalyst was gradually reoxidized. At first the OCP increased quickly with time (from –0.47 V to –0.16 V within the first 30 min). Afterwards, it increased slowly and approached a constant value (from –0.025 V to –0.014 V within the final 30 min). This behavior, being in agreement with the formation rate of O_2 (step 2 in Figure 7-2c), implies that the surface of the reduced VPO catalyst was quickly reoxidized and then the reoxidation was nearly saturated due to the slow diffusion of oxygen from the surface to the VPO bulk or subsurface regions. After the gas-phase oxygen treatment, the OCP of the reactor under N_2 increased from –0.47 V (Figure 7-3b) to about –0.06 V (Figure 7-3d). Hence, the OCP qualitatively indicated that the reduced VPO catalyst in step 1 was reoxidized by gas-phase oxygen in step 2. When the periodic redox cycles were repeated, the OCP exhibited a very similar behavior, which can be found in Figures 7-3e, f, g, h, i.

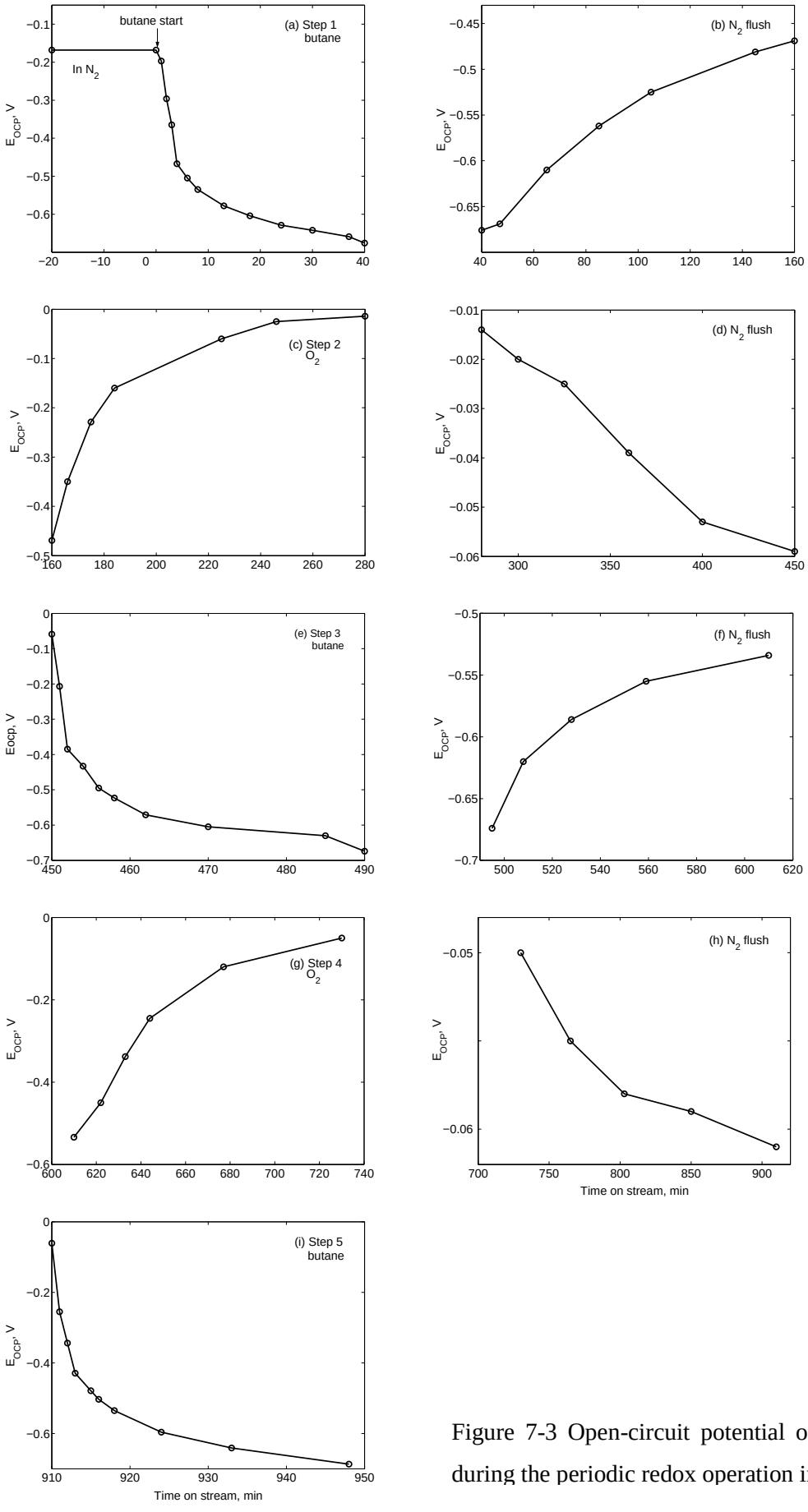

Figure 7-3 Open-circuit potential of the reactor during the periodic redox operation in the CR.

In the CR it is clear that the active oxygen species for the reoxidation of the catalyst is molecular oxygen from the gas phase, whereas in the EMR the active oxygen species involved in the reoxidation of the reduced VPO catalyst is not easily characterized and determined, as discussed in Section 6.2. Nevertheless, similar observations in periodic redox cycles might imply that the active oxygen species were same in these two types of reactors.

7.4. Stability comparison between the CR and EMR

7.4.1. Stability of the CR operation

In order to obtain the direct comparison between the EMR and the CR, the oxygen/butane ratio used in the CR was set to a similar value as in the EMR. So it was also necessary to examine the stability of the operation in this reactor. Figures 7-4a and 7-4b presented the catalytic performance in terms of conversion, selectivity and MA yield as a function of reaction time.

After the initial stage (60-80 min), the catalytic performance reached a steady state. Some typical values of selectivity and conversion at different reaction time are summarized in Table 7-1.

Table 7-1 Variations of selectivity and conversion with reaction time in the CR.

Time (min)	S-MA (%)	S-CO_2 (%)	S-CO (%)	X-butane (%)	X-oxygen (%)
10	50.2	15.7	34.1	11.0	89.6
143	62	11.9	26.1	15.5	84.3
766	62.1	12.2	25.7	15.8	83.9

In addition, the corresponding variation of the OCP with reaction time was recorded, as plotted in Figure 7-4c. The OCP variation was consistent with the catalytic performance. After the initial fast drop, the OCP reached a stationary value of –0.45 V. The OCP was higher at the beginning of the reaction (about –0.19 V) indicating the high initial oxygen activity on the VPO catalyst surface being related to a high vanadium oxidation state. From

the XPS measurements, the surface vanadium oxidation state was found to decrease from 4.8 on the fresh VPO catalyst to 4.7 on the used VPO catalyst.

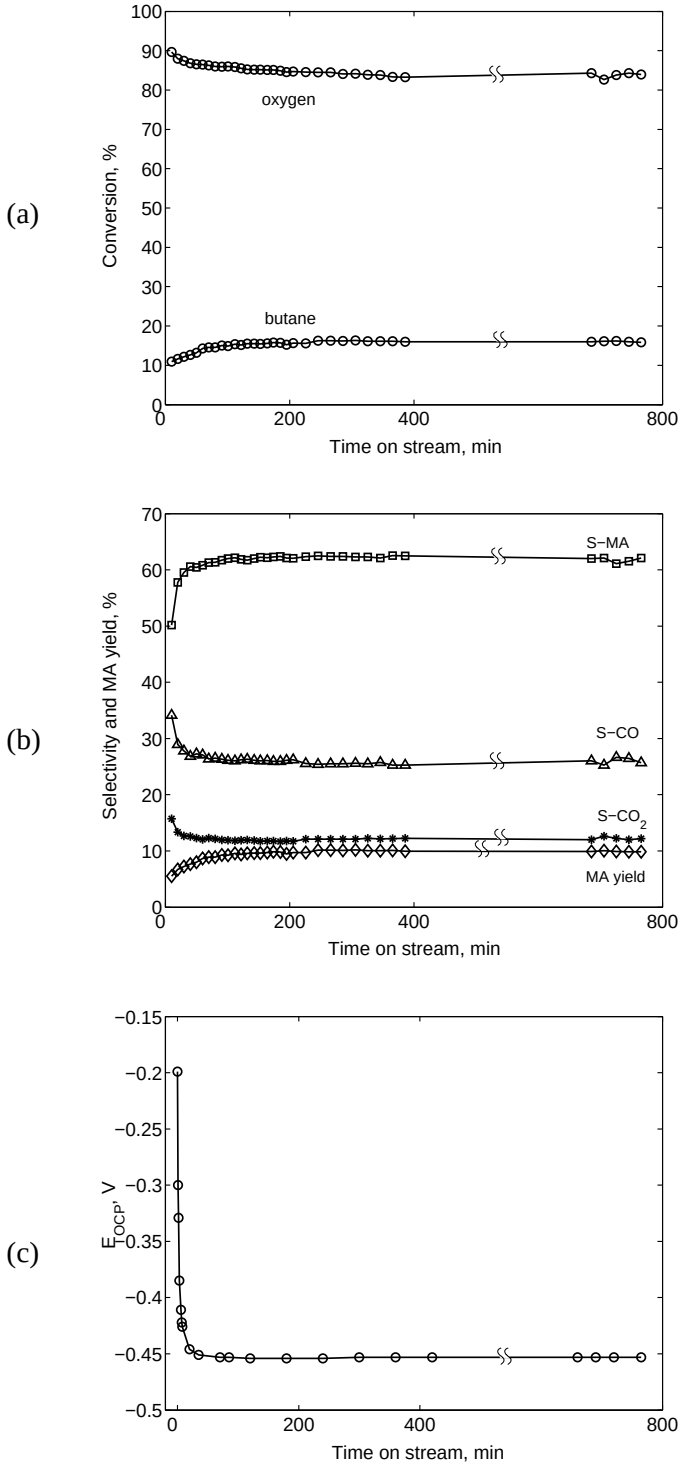

Figure 7-4 Stability of the CR operation (a) conversions, (b) selectivities and MA yield, (c) open circuit potential in the CR. T = 753 K; anode: 0.60 mol % butane and 0.48 mol % O_2 in N_2 with total flow rate 37 ml/min; cathode: 80-100 ml/min air; VPO catalyst: 13.2 mg/cm^2.

7.4.2. Comparison of the stability between the CR operation and EMR operation

When comparing Figure 7-4 to Figure 6-6, one can easily find that in the CR the MA selectivity at the steady state was higher than that at the initial state, while in the EMR it behaved conversely. The reason for this difference is still not clear. In the EMR the selectivity to CO_2 was higher than that to CO. However, in the CR the selectivity to CO_2 was lower than that to CO. These phenomena will be further discussed in the later sections. Comparing Table 6-1 to Table 7-1, it can be concluded that the VPO catalyst slowly deactivated during the EMR operation, which was reflected in the slight decrease of MA selectivity as well as the MA yield after the initial phase. However, the operation in the CR was stable after 2-3 hours' initial stage.

It should be noted that the VPO catalysts used in both reactors were initially activated at similar conditions (1 mol % butane in air) and stable catalyst activity and selectivity was obtained after about 8-10 hours of activation. Since no deactivation was observed in the CR during the investigated time, it can be inferred that the aging problem of the catalyst usually encountered in the catalytic reactions was not the main reason for the deactivation observed in the EMR.

One possible reason for the slow deactivation of the EMR operation is the change of the structure of phase boundary between the YSZ membrane, Au and the VPO catalyst. The microstructure of the Au electrode and the corresponding phase boundary might change under the dc current treatment or the reducing atmosphere, as reported in literature [110]. Additionally, the thermal treatment of the reactor might induce VPO powder peeling off the Au layer, which can also alter the structure of phase boundary. The phase boundary plays an important role in the electrochemical oxidation occurred in the EMR since the electrochemical oxidation is restricted to the region around the phase boundary, while it will not influence the conventional catalytic oxidation occurred in the CR.

Another important possible reason is that the local ratio of oxygen/butane along the axial coordinate of the VPO catalyst layer superposed on the membrane is much lower in the EMR compared to the CR, even the overall feed ratios of oxygen/butane are same. The details about the comparison of the local oxygen/butane ratio will be discussed in the following section. The reduction of VPO catalyst and the formation of carbonaceous deposits become more

likely under the low local oxygen/butane ratio, which can result in the deactivation of the catalyst as observed in the EMR.

7.5. Comparison of concentration profiles in the EMR and CR

The local oxygen/butane ratios along the axial or radial coordinate of the VPO layer are different in the EMR and the CR, even though the overall feed ratios of the oxygen/butane ratio are similar (e.g., oxygen/butane ratios are 0.97).

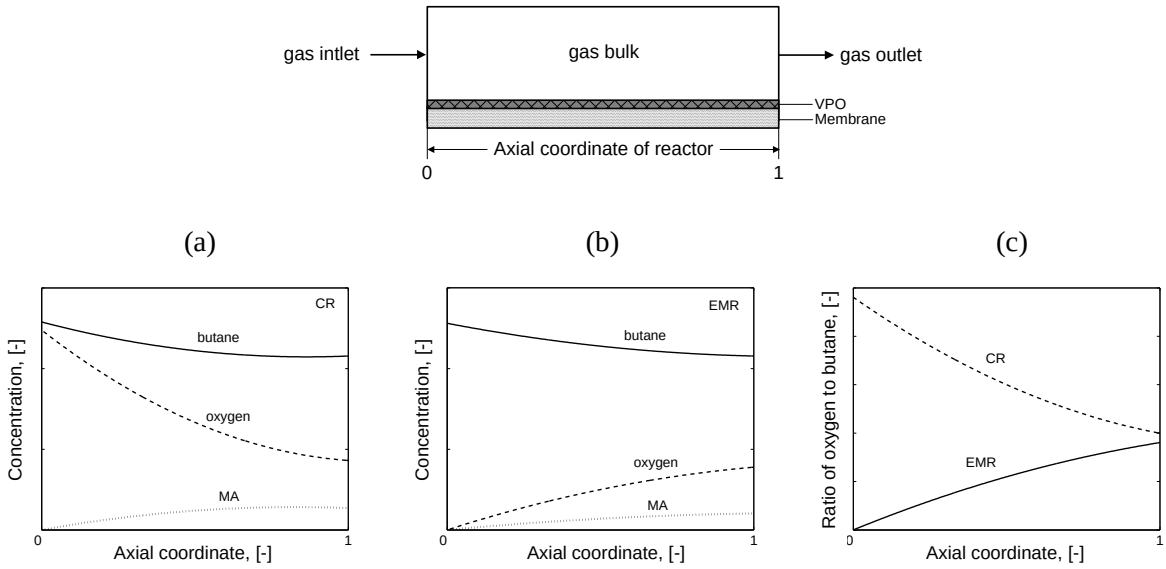

Figure 7-5 Qualitative comparison of the local concentration profiles along the axial coordinate of the VPO layer in the CR and the EMR configurations.

The concentration profiles along the axial coordinate of the VPO layer in the CR and the EMR are qualitatively illustrated in Figures 7-5a and 7-5b, and the corresponding local ratio of oxygen/butane is plotted in Figure 7-5c. Herein, “0” and “1” represent the gas inlet and outlet in the reactor, respectively, as illustrated in Figure 7-5.

In the case of the CR operation, oxygen and butane are premixed and flow together along the axial coordinate of the VPO layer. The concentrations of oxygen and butane at the inlet are higher than at the outlet (Figure 7-5a), since some oxygen and butane react on the VPO surface. In the case of the EMR operation, oxygen is supplied to the VPO layer by EOP through the YSZ membrane. The EOP provides a controlled and localized oxygen distribution to the VPO surface. Oxygen ions are consumed on the phase boundary or converted to molecular oxygen that diffuses through the catalyst layer to the bulk gas phase, which forms

an increasing oxygen concentration profile from the inlet to the outlet (Figure 7-5b). The butane concentration profile in the EMR is qualitatively similar to that in the CR since butane is fed to the reactor inlet in both cases.

Accordingly, as shown in Figure 7-5c, in the CR the ratio of oxygen/butane is higher at the inlet than the outlet and it gradually decreases along the axial coordinate of the VPO catalyst layer. In contrast, the ratio of oxygen/butane in the EMR is lower at the inlet than at the outlet and it gradually increases along the axial coordinate of the VPO catalyst layer. Moreover, since oxygen is distributed along the reactor length in the EMR, the ratio of oxygen/butane in the axial direction in the EMR is lower than that in the CR.

The concentration profiles along the radial coordinate of the VPO layer in the CR and EMR are also different, as qualitatively illustrated in Figures 7-6a and 7-6b, and the corresponding local ratio of oxygen/butane is plotted in Figure 7-6c. Herein, “0” and “1” represent the inner surface of the VPO layer close to the YSZ membrane wall and outer surface of the VPO layer exposed to the bulk gas phase, respectively, as illustrated in Figure 7-6.

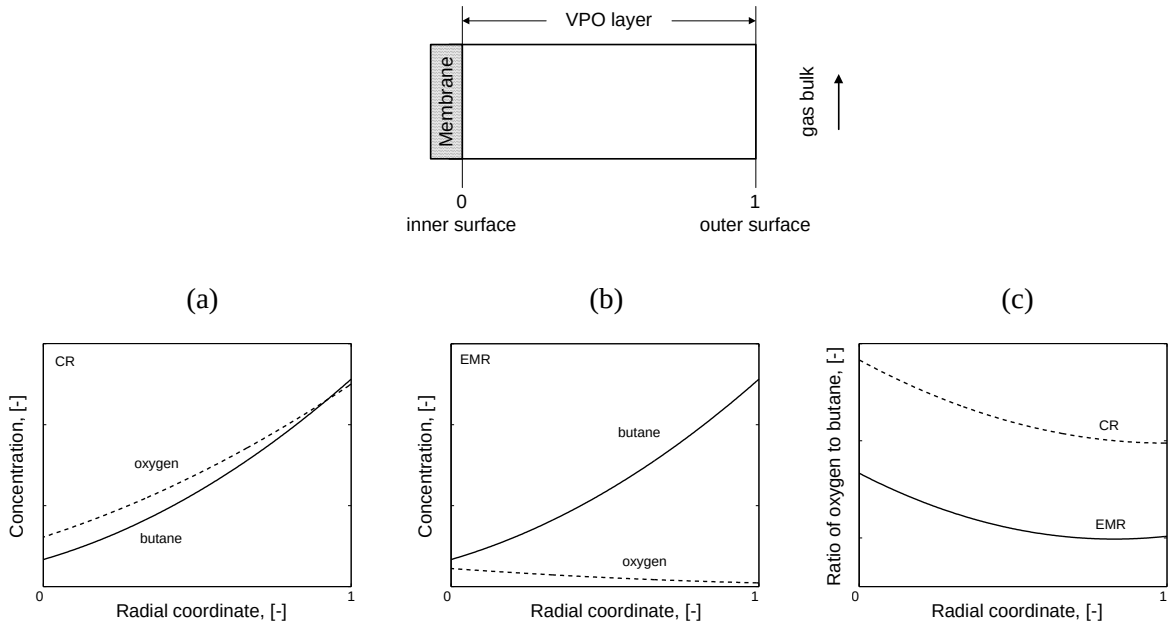

Figure 7-6 Qualitative comparison of the local concentration profiles along the radial coordinate of the VPO layer in the CR and EMR.

In the case of the CR operation, premixed oxygen and butane diffuse from the outer surface to the inner surface along the radial coordinate of the VPO layer. The concentrations of oxygen and butane at the outer surface are higher than those at the inner surface (Figure 7-6a). In the

case of the EMR operation, oxygen is pumped through the YSZ membrane towards the inner surface of the VPO layer wall and the oxygen is gradually reacted during the diffusion. Therefore, in the EMR the oxygen concentration (Figure 7-6b) at the outer surface is lower than that at the inner surface. Accordingly, in the EMR the ratio of oxygen/butane in radial direction decreases from the inner surface to the outer surface (Figure 7-6c). In the CR the ratio of oxygen/butane is assumed to be higher at the inner surface compared to the outer surface considering the fact that oxygen diffusion is faster than butane diffusion. As can be seen in Figure 7-6c, in the EMR the ratio of oxygen/butane in the radial direction is lower than that in the CR.

(a)

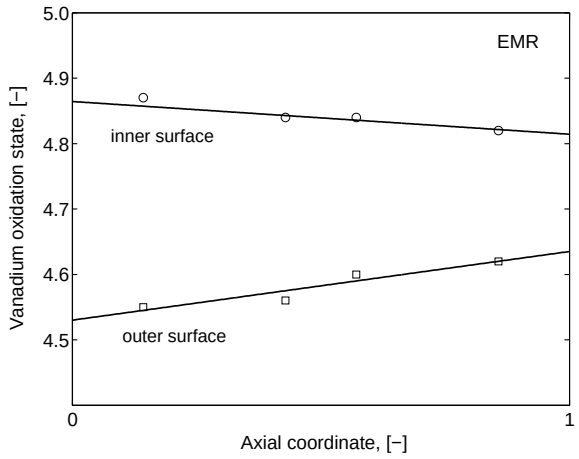

(b)

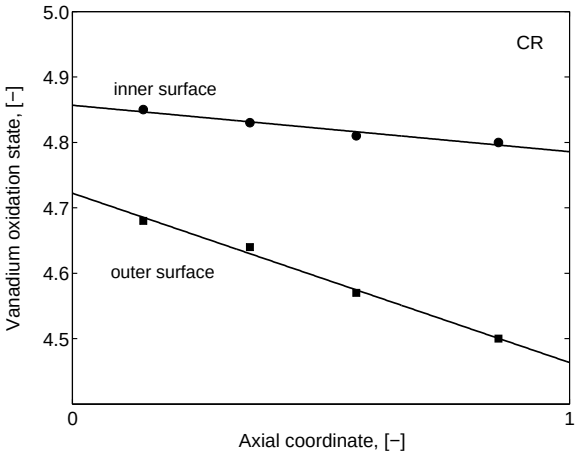

Figure 7-7 Surface vanadium oxidation states along the reactor axial coordinate with the (a) EMR and (b) CR operation.

The different spatial oxygen distributions in the EMR and CR were confirmed by the XPS analysis of the catalyst. As shown in Figure 7-7a, after the EMR operation, the vanadium

oxidation state of the catalyst at the outer surface increased along the axial coordinate of the reactor, which indicated an increasing ratio of oxygen/butane in the axial direction.

Conversely, as shown in Figure 7-7b, after the CR operation the vanadium oxidation state at the outer surface decreased along the axial coordinate of the VPO layer, which indicated a decreasing ratio of oxygen/butane in the axial direction.

Compared to the outer surface of the VPO layer exposed to the gas bulk, both of the vanadium oxidation states in the EMR and CR were higher at the inner surface of the VPO layer close to YSZ membrane (Figures 7-7a, b), which implied that the ratio of oxygen/butane in the radial direction decreased from the YSZ membrane side to the gas bulk side.

7.6. Comparison of oxygen concentration effects on the CR and EMR operations

7.6.1. Effect of oxygen partial pressure on the CR operation

In the CR, the influence of the oxygen partial pressure on the conversion, selectivity and MA yield was studied at the steady state. The investigated oxygen partial pressure varied from 0.1 to 16.7 kPa. As expected, the conversion of butane increased while the conversion of oxygen decreased with oxygen partial pressure (see Figure 7-8a).

As shown in Figure 7-8b, at the lower oxygen partial pressure range, e.g., below 0.4 kPa, the selectivity to MA increased while the selectivity to CO_x decreased with increasing oxygen partial pressure. When the oxygen partial pressure varied from 0.4 to 1.0 kPa, the selectivity to MA was essentially unaffected. At the higher oxygen partial pressure range, e.g., above 1.0 kPa, the selectivity to MA decreased but the selectivity to CO_x increased with increasing oxygen partial pressure. The MA yield increased with increasing oxygen partial pressure since more butane was reacted at higher oxygen partial pressure.

The lower MA selectivity at the very low oxygen partial pressure range (below 0.4 kPa) was mainly ascribed to the fact that the oxygen conversion was very high (above 90%) and thus the gaseous oxygen concentration on the catalyst surface was too low, which usually reduces the VPO selectivity to MA as discussed by Lorences [100] and Rubio et al. [101]. The decrease in the MA selectivity with oxygen partial pressure at the higher oxygen partial pressure range (above 1.0 kPa) can be explained by the overoxidation of MA to CO_x, which became more favorable as the oxygen concentration increased and more MA formed on the

catalyst surface. In conclusion, the highest MA selectivity could be obtained with an oxygen partial pressure of 0.4-1.0 kPa in this work. This is because the VPO selectivity to MA is strongly affected by the vanadium oxidation state [21, 103], which in turn is directly related to the oxygen concentration.

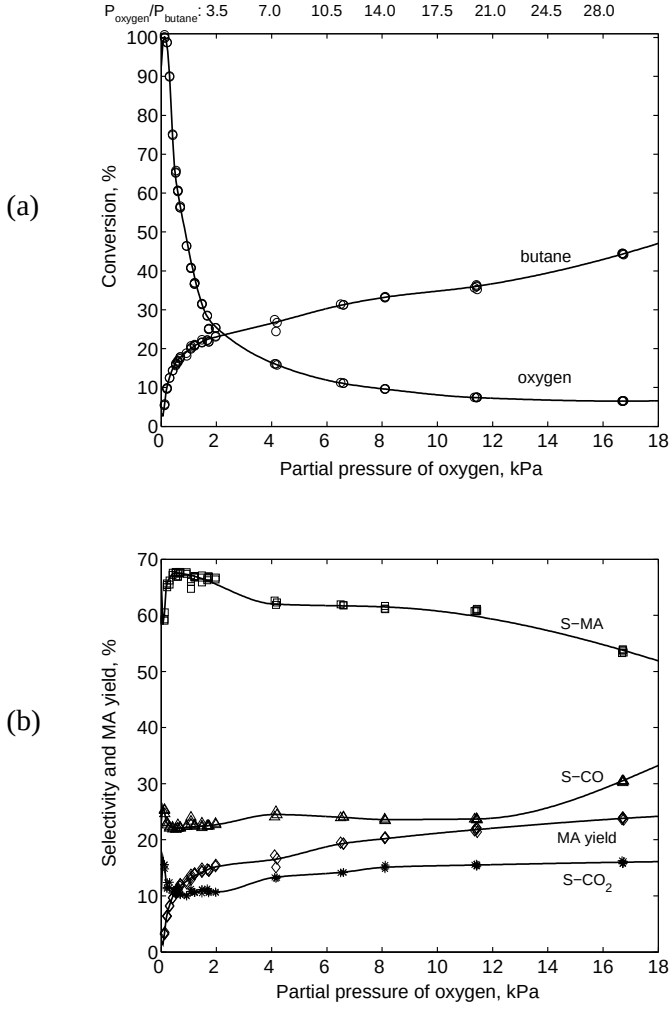

Figure 7-8 butane partial oxidation in the CR at different oxygen partial pressure. T = 753 K; anode: 0.53-0.59 mol % butane in N_2; total flow rate 35-38 ml/min (STP); VPO catalyst: 7.2 mg/cm^2.

7.6.2. Comparison of the EMR and CR operations at equal oxygen partial pressures

In order to directly compare the EMR operation to the CR operation, in the EMR both the butane and the overall oxygen partial pressures in the feed were kept as close as possible to those in the CR, i.e., equal oxygen/butane ratios. The equivalent oxygen partial pressure in the EMR was predetermined from EOP results (see Figure 5-5). For instance, with imposing a

(a)

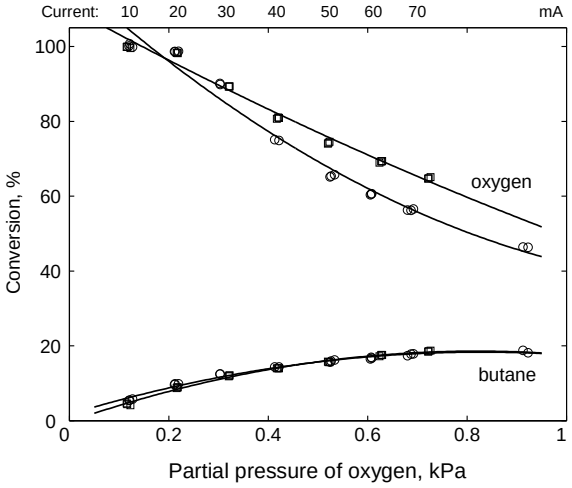

(b)

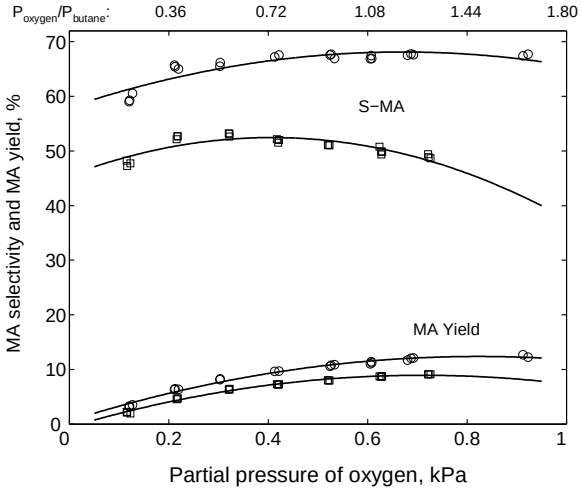

(c)

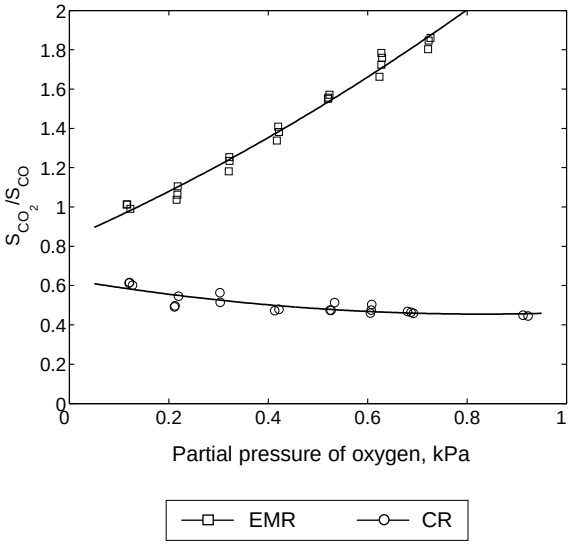

Figure 7-9 Comparison of butane oxidation in the EMR and CR at similar oxygen partial pressure. T = 753 K; anode: 0.54-0.56 mol % butane; flow rate: 35-36 ml/min; VPO loading 7.2 g/cm^2.

constant current of 50 mA to the reactor, the measured O_2 evolution rate in the exit of the reactor was 1.240×10^{-7} mol/s and thus the corresponding equivalent oxygen partial pressure was 0.52 kPa in the total flow rate of 35 ml/min. It should be noted that it was experimentally difficult to keep absolutely equal oxygen partial pressure levels in the CR and in the corresponding EMR due to limitations of the used mass-flow controllers.

Figures 7-9a and 7-9b compare the reactant conversions and the MA selectivity as well as the MA yield performed in the EMR and CR using the same prepared reactor. Both in the EMR and CR, butane conversion increased and oxygen conversion decreased with increasing oxygen partial pressure as expected. Even though the butane conversion was similar, the oxygen conversion in the EMR was higher than that in the CR as the oxygen conversion was below 100 % (see Figure 7-9a).

As can be seen in Figure 7-9b, in the CR the selectivity to MA increased with increasing oxygen partial pressure at the lower oxygen pressure range (below 0.4 kPa), while it was essentially unaffected at the oxygen partial pressure range of 0.4-1.0 kPa. In the EMR the selectivity to MA first increased with increasing current below 30 mA (i.e., equivalent oxygen partial pressure was below 0.3 kPa), then it decreased somewhat with further increasing current.

Compared to the CR operation, the EMR operation gave lower MA selectivity as well as MA yield, as can be seen in Figure 7-9b. In addition, as shown in Figure 7-9c, the selectivity ratio of CO_2 to CO (S_{CO_2}/S_{CO}) in the EMR ($S_{CO_2}/S_{CO} \geq 1$) was clearly higher than that in the CR ($S_{CO_2}/S_{CO} < 1$).

As already discussed in Section 7.5, the ratio of oxygen/butane along the axial coordinate of the reactor in the EMR was lower than in the CR (Figure 7-5c). One might expect that the low local oxygen concentration in the EMR could depress the overoxidation and thus improve the selectivity to the intermediate product MA. However, as shown in Figure 7-9b, the MA selectivity in the EMR was lower than in the CR. The unexpected behavior might be ascribed to the two following reasons.

One possible reason is that the lower local oxygen concentration in the EMR induced lower vanadium oxidation state in the VPO catalsyt. As indicated in the introduction, the vanadium oxidation state plays an important role in the catalyst activity and selectivity. Schuurman et al. [104] and Rodemerck et al. [8] observed that the desorption of MA on the more oxidized

VPO surface was faster. Rodemerck suggested that V^{5+} is the stronger Lewis acid site compared to V^{4+}. Therefore the more oxidized VPO surface with more acidic V^{5+} sites (i.e., higher vanadium oxidation state) should have a lower affinity to the acidic MA molecule, which results in a shorter contact time of MA on the VPO surface, i.e., weak adsorption. Inversely, the more reduced VPO surface with more basic V^{4+} sites (i.e., lower vanadium oxidation state) should have a higher affinity to the acidic MA molecule resulting in a longer contact time of MA on the VPO surface, i.e., strong adsorption. Accordingly, it can be inferred that the lower vanadium oxidation state in the EMR might result in a stronger MA adsorption on the VPO surface compared to the CR, which favors the overoxidation of MA to CO_2 and reduces the MA selectivity. In addition, in the EMR the MA and oxygen concentrations in the axial direction of the reactor increased simultaneously, as shown in Figure 7-5b, which also favors the overoxidation of MA to CO_2. By contrast, in the CR the MA concentration increased but the oxygen concentration decreased along the reactor length, which can depress the overoxidation of MA (see Figure 7-5a). The higher S_{CO_2}/S_{CO} ratio and higher oxygen conversion observed in the EMR than the CR (see Figure 7-9) might be also ascribed to the fact that MA was more likely overoxidized to CO_2 in the EMR.

Another possible reason is that the reaction mechanism of butane partial oxidation in the EMR is different from that in the CR, which is further discussed in Chapter 8.

7.7. Comparison of temperature effects on the EMR and CR operations

The influence of the temperature on the EMR operation was compared to that on the CR operation. As can be seen in Figure 7-10, in the CR the conversions of butane and oxygen increased linearly with increasing temperature. However, in the EMR this linear relationship was found only at the lower temperature range, e.g., below 750 K. Above 750 K, the increase of butane conversion with increasing temperature became less pronounced. The different dependencies of the conversions on temperature in the EMR and the CR are mainly due to the limitation of the oxygen supply in the EMR that in turn limits the butane conversion. As shown, in the EMR the oxygen conversion approached 100% above temperature of 760 K in the EMR, while in the CR it was below 65 % at the investigated temperature range.

As shown in Figure 7-10b, both in the EMR and the CR the selectivity to MA decreased while the selectivities to CO and CO_2 increased with increasing temperature, which indicated that the activation energy for MA formation is lower than that for the formations of CO_x, being in

(a)

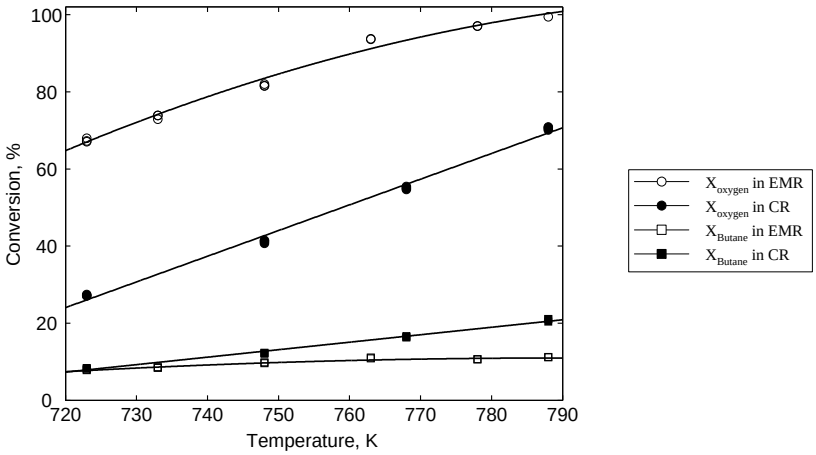

(b)

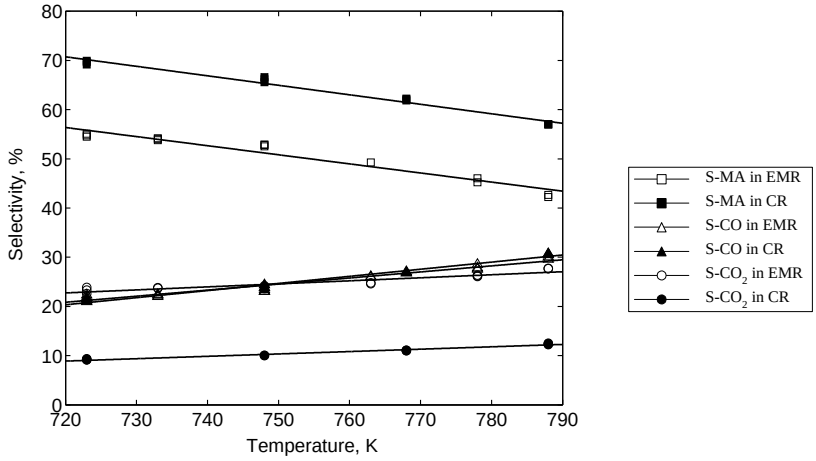

(c)

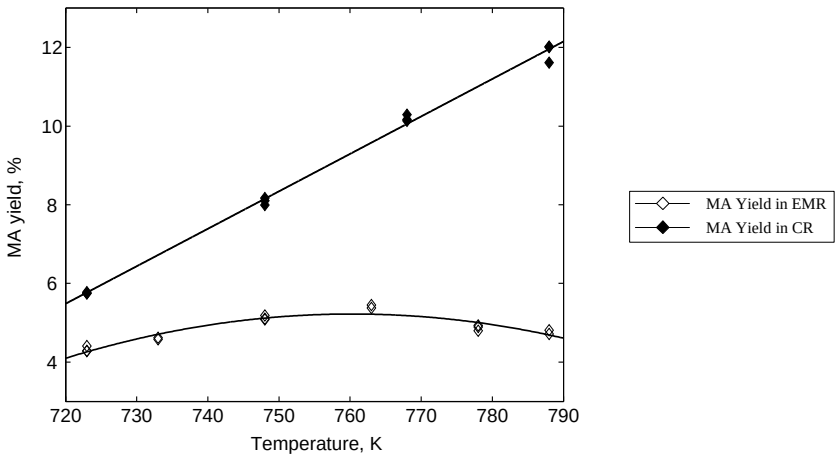

Figure 7-10. Comparison of the dependence of reaction temperature on butane oxidation in the EMR and CR. VPO catalyst: 6.6 g/cm^2; flow rate: 35-36 ml/min. EMR: 0.61 mol % butane and current 30 mA; CR: 0.62 mol % butane and 0.63 mol % gaseous oxygen.

agreement with several kinetic studies [18, 111-113]. It is interesting to note that the

decrement in MA selectivity as well as the increment in CO and CO_2 selectivity with temperature in the EMR is very similar to those in the CR. On average, 20 K temperature increase reduced the MA selectivity approximately by 4% and increased the CO and CO_2 selectivities by 2.5% and 1%, respectively. However, the MA selectivities in the EMR were generally lower than 60%, while in the CR they were higher than 60% at the investigated temperature range. The selectivities to CO were very similar in the EMR and CR, while the selectivity to CO_2 in the EMR was higher than that in the CR. Generally, the selectivity to CO_2 in the EMR was higher than 20% but it was lower than 10% in the CR. This again reveals that the EMR operation favored the total oxidation, i.e., the production of CO_2.

Unlike the CR in which the MA yield increased linearly with increasing temperature, the MA yield in the EMR first increased, after passing a maximum at around 760 K, then decreased with increasing temperature, which was mainly ascribed to the limitation of oxygen in the EMR that in turn limits the butane conversion.

7.8. Concluding remarks

The partial oxidation of *n*-butane to MA was performed in CR operation mode under periodic redox and steady-state conditions, and the results were compared to those in EMR mode. In the CR the periodic redox experiments confirmed that the reduced VPO catalyst could be re-oxidized by gas-phase oxygen. The corresponding SEP measurements qualitatively indicated the variations of the oxygen activity on the VPO catalyst surface during the periodic redox cycles. It was found that the behavior of the periodic redox cycles performed in the CR and EMR was qualitatively similar, which might suggest that the active oxygen species being involved in the reoxidation of the reduced VPO catalyst in the EMR was mainly the gas-phase oxygen.

The performance of butane oxidation in the CR was stable after 2-3 hours initial stage. Compared to the EMR, no visible deactivation was observed during the catalytic reaction in the CR. The different dynamic behavior might be due to the lower oxygen/butane ratio in the EMR compared to the CR. Additionally, in the EMR the electrical current treatment might gradually change the structure of phase boundary between Au, the YSZ membrane and the VPO catalyst layer, which can affect the electrocatalytic reaction.

In the CR, the MA selectivity was strongly influenced by the partial pressure of gaseous oxygen in the feed. Either a too high or a too low oxygen concentration reduced the MA

selectivity, and the best MA selectivity was obtained with a moderate oxygen partial pressure, i.e., 0.4-1.0 kPa in this work. Under equal feed ratios of oxygen to butane, in the EMR the oxygen conversion was higher than that in the CR while the butane conversions were similar. Unexpectedly the EMR operation gave lower MA selectivity but higher CO_2 selectivity compared to the CR. Two possible reasons were proposed for this unexpected behavior. One is that the local ratio of oxygen to butane was lower in the EMR, which favors the MA adsorption on the VPO surface and the overoxidation of MA to CO_2. Another possible reason is that butane oxidation under EOP condition in the EMR follows different reaction mechanism from that in the CR, as will be further investigated in Chapter 8.

Both in the EMR and CR, the selectivity to MA decreased while the selectivity to CO_x increased linearly with increasing temperature, which indicated that the activation energy for MA formation is lower than that for the CO_x formation. However, the EMR operation displayed lower MA selectivity but higher CO_2 selectivity compared to the CR operation at the investigated temperature range, which again confirmed that the EMR operation favors the total oxidation of hydrocarbons.

In the following work, butane partial oxidation will be investigated with mixed supply of oxygen from the gas-phase (CR) and by oxygen ion pumping (EMR). The result should be helpful for understanding the reaction mechanism in the EMR.

8. Butane Partial Oxidation with Mixed-feed Membrane Reactor Operation

In order to investigate the reaction mechanism in the EMR, a mixed-feed membrane reactor (MMR) was studied and the NEMCA effect was examined as well.

As illustrated in Figure 8-1, in the MMR, a mixture of gas-phase oxygen and butane was fed to the anode compartment and oxygen ions (O^{2-}) were simultaneously supplied to or removed from the anode by imposing a positive or negative current to the reactor.

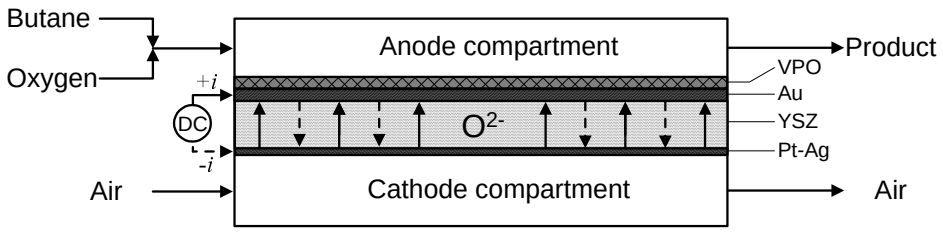

Figure 8-1 Illustration of the mixed-feed membrane reactor (MMR) for butane partial oxidation.

8.1. Galvanostatic transients

Figures 8-2a, 8-2b, 8-2c and 8-2d present galvanostatic transients in the MMR, which accordingly depicted the transient effect of a positive or negative current on the consumption rates of reactants, on the formation rates of products, on the conversion of the reactants and on the selectivities to the products. The butane and gaseous oxygen concentrations in the inlet were 0.55 and 0.56 mol %, respectively.

At $t < 0$, the reactor was initially operated under open-circuit conditions (I = 0 mA). The OCP between the anode and the cathode was E_{OCP} = −0.36 V. The consumption rates of oxygen and butane were 8.30×10^{-8} mol/s and 2.01×10^{-8} mol/s, respectively (Figure 8-2a). The corresponding conversions of oxygen and butane were $X_{0,oxygen}$ = 57.7% and $X_{0,butane}$ = 14.3% (Figure 8-2c). The product formation rates were $r_{0,MA} = 1.25\times10^{-8}$ mol/s, $r_{0,CO} = 2.12\times10^{-8}$

mol/s and r_{0,CO_2} = 9.25×10^{-9} mol/s (Figure 8-2b). The corresponding product selectivities were $S_{0,MA}$ = 62.2%, $S_{0,CO}$ = 26.3%, and S_{0,CO_2} = 11.5% (Figure 8-2d).

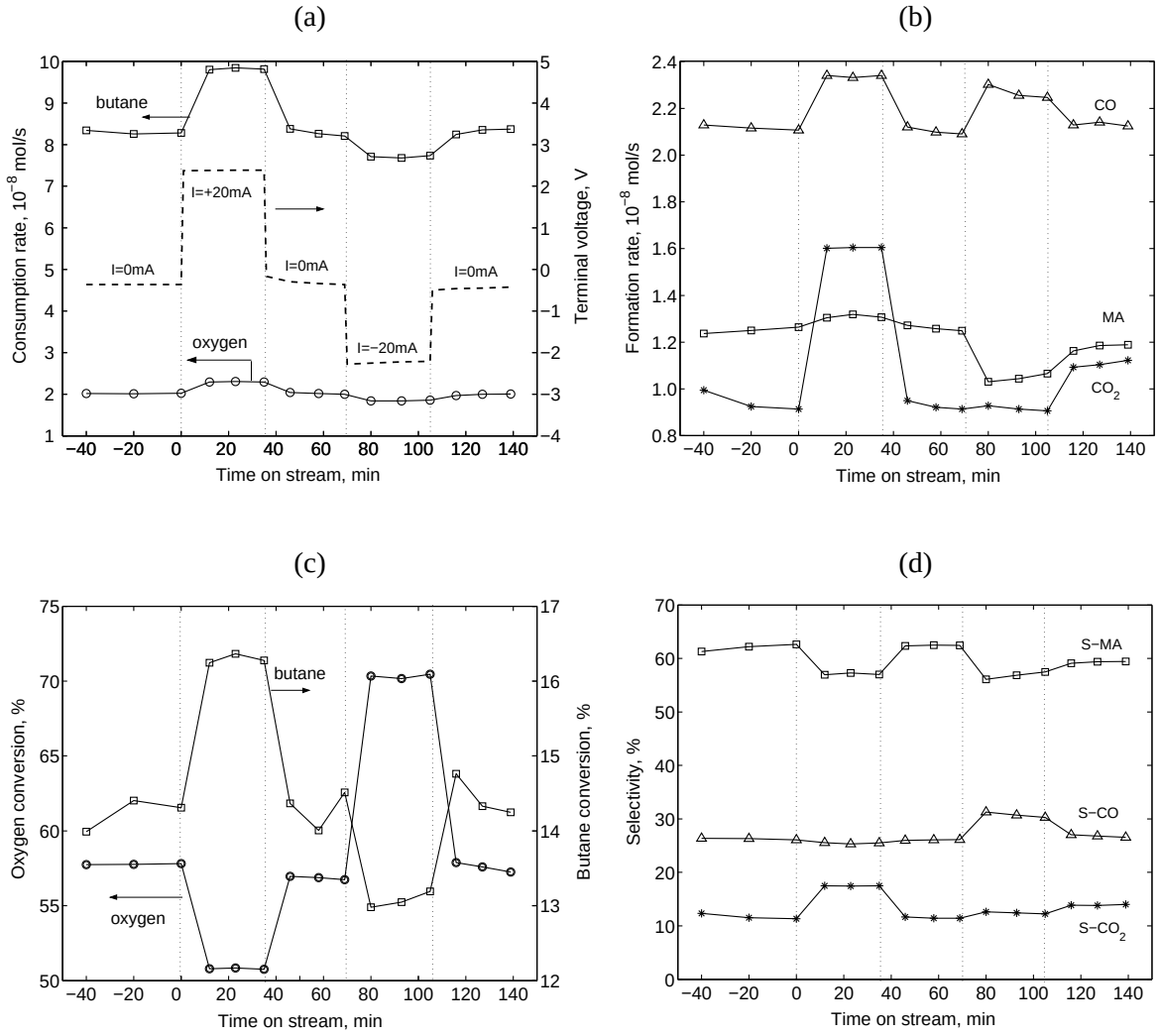

Figure 8-2 Transient effect of the electrical current changes on consumption rates of reactants (a), formation rates of products (b), conversions of reactants (c), and selectivities to products (d). T = 753 K; anode: 0.55 mol % butane and 0.56 mol % gaseous oxygen in N_2 with total flow rate 38 ml/min; VPO catalyst: 7.0 mg/cm^2.

At t = 0, a constant current (I = + 20 mA) was imposed to the reactor through the galvanostat and thereby oxygen ions were pumped towards the VPO catalyst at a rate of $I/2F = 1.04\times10^{-7}$ mol O/s. The terminal voltage between the anode and cathode rapidly jumped from –0.36 V to 2.4 V once the positive current was imposed, as shown in Figure 8-2a. Compared to the open-circuit operation, more butane and oxygen were consumed.

Correspondingly, the butane conversion increased to $X_{+,\text{butane}} = 16.3\%$ while the overall oxygen conversion (gas-phase and ionic oxygen) decreased to $X_{+,\text{oxygen}} = 50.8\%$ (Figure 8-2c).

With imposing a positive current to the MMR, the product formation rates (Figure 8-2b) increased to $r_{+,\text{MA}} = 1.30\times10^{-8}$ mol/s, $r_{+,\text{CO}} = 2.33\times10^{-8}$ mol/s and $r_{+,\text{CO}_2} = 1.60\times10^{-8}$ mol/s. Correspondingly, the enhancement ratios (calculated from Equation 1-14) resulting from the positive current were $\rho_{+,\text{MA}} = 1.04$, $\rho_{+,\text{CO}} = 1.10$ and $\rho_{+,\text{CO}_2} = 1.73$, which indicated that the positive current in the MMR mainly enhanced the CO_2 formation and this only slightly improved the MA formation. This will be discussed in detail in the following section. The MA selectivity clearly decreased to the value $S_{+,\text{MA}} = 57.0\%$ and the CO selectivity was $S_{+,\text{CO}} = 25.5\%$ being essentially unaffected compared to the open-circuit operation, while the CO_2 selectivity clearly increased to $S_{+,\text{CO}_2} = 17.5\%$ (Figure 8-2d).

Upon current interruption (I = 0 mA) at t = 36 min, all investigated variables such as consumption rates, formation rates, conversion and selectivity as well as the OCP quickly recovered their initial open-circuit values, thus the positive current effect was completely reversible.

Subsequently the reactor was imposed with a negative current (I = – 20 mA) at t = 72 min and oxygen ions were removed from the anode side at a rate of $I/2F = 1.04\times10^{-7}$ mol O/s. The terminal voltage quickly changed from –0.37 V to –2.3 V once the negative current was imposed, as shown in Figure 8-2a. Compared to the open-circuit operation, the consumption rates of oxygen and butane decreased as expected. Correspondingly, the butane conversion decreased to $X_{-,\text{butane}} = 13.0\%$ while the overall oxygen conversion increased to $X_{-,\text{oxygen}} = 70.5\%$ (see Figure 8-2c).

As can be seen in Figure 8-2b, with a negative current imposed in the MMR, the MA formation rate visibly decreased to $r_{-,\text{MA}} = 1.07\times10^{-8}$ mol/s and the CO_2 formation rate somewhat decreased to the value $r_{-,\text{CO}_2} = 9.11\times10^{-9}$ mol/s, while the CO formation rate increased unexpectedly to $r_{-,\text{CO}} = 2.24\times10^{-8}$ mol/s. So the enhancement ratios caused by the negative current were $\rho_{-,\text{MA}} = 0.86$, $\rho_{-,\text{CO}} = 1.06$ and $\rho_{-,\text{CO}_2} = 0.98$, respectively. One can

conclude from these observations that the negative current in the MMR mainly reduced the MA formation rate. Correspondingly, the MA selectivity clearly decreased to $S_{-,\mathrm{MA}} = 57.5\%$ and the CO selectivity increased to $S_{-,\mathrm{CO}} = 30.3\%$, while the CO_2 selectivity nearly remained unchanged compared to the open-circuit operation with the value $S_{-,\mathrm{CO_2}} = 12.2\%$ (Figure 8-2d).

Upon current interruption at *t* = 106 min, the formation rates of CO and CO_2 slightly increased, while the MA formation rate weakly declined. It seems that the negative current effect was not completely reversible. The OCP was –0.42 V and it was lower than the initial value -0.36 V, which implied that the oxygen surface activity decreased after the treatment of a negative current. Thus the VPO surface seems to be reduced and this might be the reason for the irreversibility. Similar irreversibility behaviour of the reaction after the current treatment was reported first by the group of Comninellis in their study on ethylene total oxidation [114].

8.2. Effect of current under steady-state

The above depiction about the influence of positive and negative currents on the catalytic performance is further clarified and confirmed in Figures 8-3, 8-4, 8-5, which demonstrate the steady-state current effect on the catalytic rate, product selectivity and apparent activation energy in the MMR, respectively.

8.2.1. Influence of current on the catalytic reaction rate

Figure 8-3a shows the influence of EOP on the formation rates of products (MA, CO and CO_2). As can be seen, the formation rates of products are linearly related to either the positive or the negative current.

When a positive current was imposed in the MMR (ionic oxygen was supplied to the anode), the formation of MA, CO and CO_2 were enhanced compared to the CR (i.e., I/2F = 0 in Figure 8-3). By increasing positive current, the formation rates of CO_x (CO, CO_2) significantly increased, while the MA formation was only slightly improved. In this case, the enhancement of the CO_2 formation rate was more significant than that of CO. Therefore, it seems that positive currents favored the total oxidation. A similar finding was also reported by the group of Vayenas in the oxidation of ethane or ethylene on metal electrodes [69, 72, 117, 118].

(a)

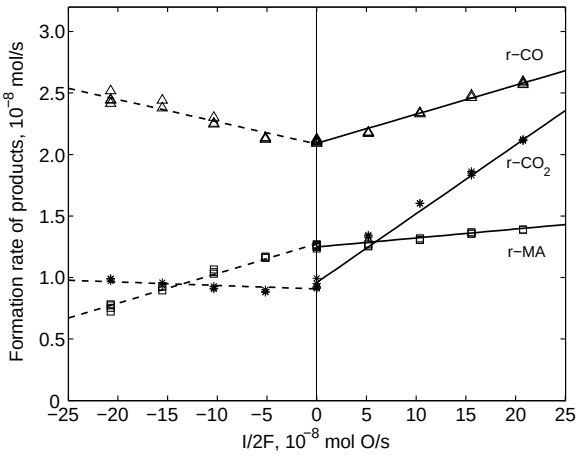

(b)

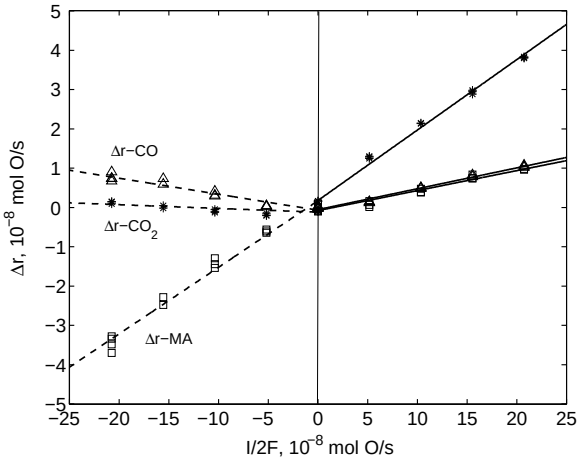

(c)

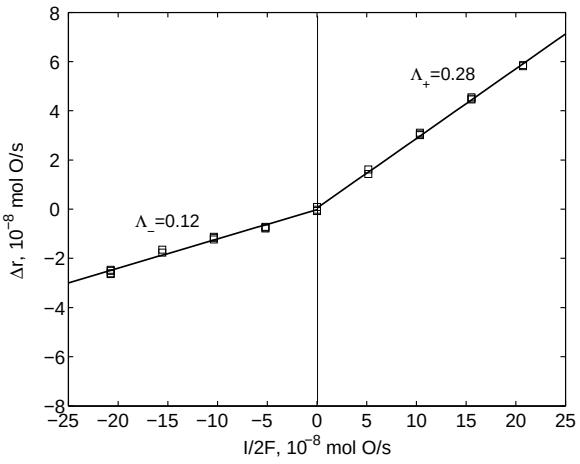

Figure 8-3 Dependence of the formation rates of products on the imposed current in the MMR. T = 753 K; anode: 0.55 mol % butane and 0.56 mol % gaseous oxygen in N_2 with total flow rate 38 ml/min; VPO catalyst: 7.0 mg/cm^2.

When a negative current was imposed in the MMR, the formation of MA was reduced compared to the CR (see Figure 8-3a) as expected, since some oxygen was removed from the reaction zone. Moreover, in the MMR the consumption of reactants and the formation of MA decreased with decreasing negative current (e.g., from –10 mA to – 40 mA). Unexpectedly, the formation rates of CO_x increased with decreasing negative current. In this case, the enhancement of the CO formation rate was more significant than that of CO_2.

The EOP effect on the catalytic rates was quantitatively expressed with a rate enhancement factor or Faradaic efficiency Λ [72] as defined in equation 1-15. The product enhancement rates Δr_{MA}, Δr_{CO} and Δr_{CO2}, with units of mol O/s, were calculated from the results shown in Figure 8-3a by using the stoichimetries of the three overall reactions:

$$C_4H_{10} + 3.5O_2 \rightarrow C_4H_2O_3 + 4H_2O \quad (8\text{-}1a)$$

$$0.25C_4H_{10} + 1.125O_2 \rightarrow CO + 1.25H_2O \quad (8\text{-}1b)$$

$$0.25C_4H_{10} + 1.625O_2 \rightarrow CO_2 + 1.25H_2O \quad (8\text{-}1c)$$

The enhancement factors for each product are defined by

$$\Lambda_i = \frac{\Delta r_i}{I/2F} \ (i = \mathrm{MA}, \mathrm{CO}, \mathrm{CO_2}) \quad (8\text{-}2)$$

The total enhancement factor for oxygen consumption, Λ, is the sum of Λ_{MA}, Λ_{CO} and Λ_{CO2}, i.e.,

$$\Lambda = \Lambda_{MA} + \Lambda_{CO2} + \Lambda_{CO} \quad (8\text{-}3)$$

As shown in Figure 8-3b, all the enhancement rates Δr were linearly related to the imposed current. The corresponding enhancement factors for MA, CO and CO_2 formation were $\Lambda_{+,MA}$ = 0.05, $\Lambda_{+,CO}$ = 0.05 and Λ_{+,CO_2} = 0.18 in the case of imposing positive currents, and $\Lambda_{-,MA}$ = 0.17, $\Lambda_{-,CO}$ = -0.04 and Λ_{-,CO_2} = -0.01 in the case of imposing negative currents. Therefore, the enhancement factors clearly revealed that a positive current in the MMR mainly improved the CO_2 formation compared to the CR, while a negative current significantly reduced the MA formation.

As shown in Figure 8-3c, the total enhancement factors were $\Lambda_+ = 0.28$ for the positive current and $\Lambda_- = 0.12$ for the negative current. Therefore, the influence of the positive current on the catalytic rates was more pronounced than that of the negative current. Since the enhancement factor was below 1 ($\Lambda < 1$) in any case, it can be concluded that both positive and negative currents in the MMR exhibited purely Faradaic effect, i.e., no NEMCA effect was present.

8.2.2. Influence of current on the selectivity

Compared to the CR operation, EOP in the MMR might influence significantly the product distribution, i.e., the selectivity to the product, as reported by Vaynas et al. in the oxidative coupling of CH_4 on Ag [115]. Figure 8-4 presents the effect of the current on the conversions of reactants and on the selectivities to products.

As shown in Figure 8-4a, with increasing both positive (e.g., from +10 mA to +40 mA) and negative (e.g., from -40 mA to -10 mA) currents, the butane conversion increased, while the overall oxygen conversion decreased. The oxygen conversion had a linear relationship with the positive current, which was not the case for the negative current. This is mainly ascribed to the limitation of oxygen in the anode since more oxygen was removed from the anode with negative current.

Figure 8-4b presents the effect of EOP on the selectivities with respect to the products. As can be seen, the selectivities show linear relationships with the imposed current. With increasing positive current, the MA selectivity obviously decreased and CO selectivity slightly declined, while the CO_2 selectivity clearly increased. With decreasing negative currents, the selectivity to MA decreased, while selectivities to CO_x increased (CO being mostly affected). In brief, compared to the CR, both positive and negative currents in the MMR reduced the selectivity to MA but increased the selectivity to CO_x, and this current effect is stronger at higher current (absolute value). The CO selectivity was significantly affected by negative currents, while the CO_2 selectivity was strongly influenced by positive currents. It should be emphasized that the influence of EOP on the MA selectivity became less pronounced at the higher anodic gaseous oxygen concentration, as can be seen from the values in Table 8-1.

(a)

(b)

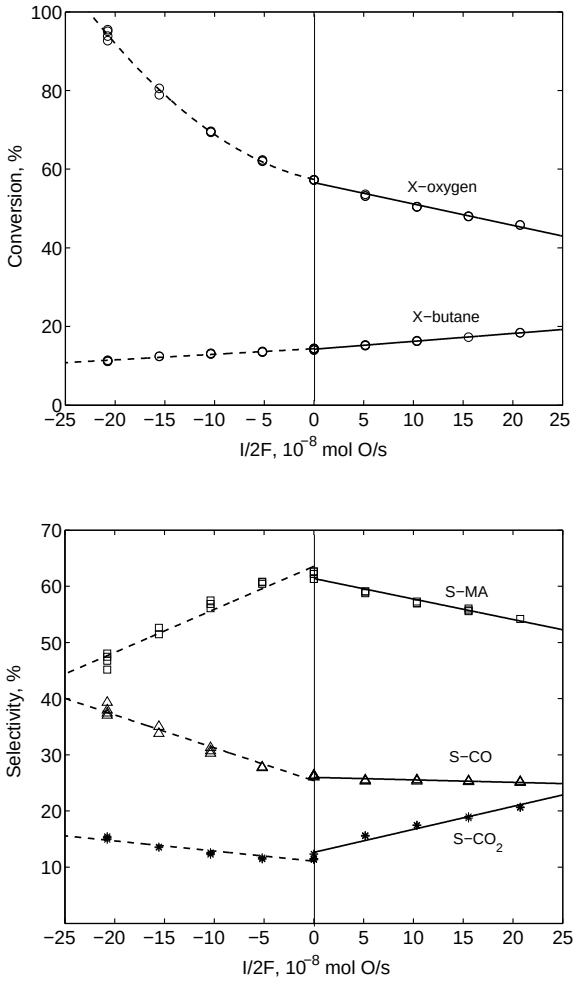

Figure 8-4 Effect of current on the conversion of reactants (a) and the selectivities to products (b). T = 753 K; anode: 0.55 mol % butane and 0.56 mol % gaseous oxygen in N_2 with total flow rate 38 ml/min; VPO loading: 7.0 mg/cm^2.

Table 8-1 Dependence of the gaseous oxygen concentration on the modification of MA selectivity by EOP. T = 753 K; anode: 0.60 mol % butane in N_2 with total flow rate 38 ml/min.

O_2 concentration (%)	$S_{0,\mathrm{MA}}$ (%)	$S_{+,\mathrm{MA}}$ (%)	$S_{-,\mathrm{MA}}$ (%)
1.8	63	60	61
0.6	65	59	60
0.2	64	54	-

Note: $S_{0,\mathrm{MA}}$, $S_{+,\mathrm{MA}}$ and $S_{-,\mathrm{MA}}$ correspond to I = 0, +20 and –20 mA, respectively.

8.2.3. Influence of current on the apparent activation energy

Figure 8-5 shows the Arrhenius plots obtained under open-circuit conditions (CR operation) and under closed-circuit conditions (MMR operation) with imposing a positive current to the reactor. The corresponding apparent activation energies for the two operation modes, calculated from the slope of the lines in Figure 8-5, are summarized in Table 8-2. As can be seen, compared to pure gas-phase oxygen supplied in the CR, the electrochemically supplied oxygen in the MMR reduced the respective apparent activation energies for CO and CO_2 with magnitude of 7.6 and 31.3 kJ/mol, while it increased that for MA formation with magnitude of 3.9 kJ/mol. So the apparent activation energy for CO_2 under the EOP condition was significantly reduced.

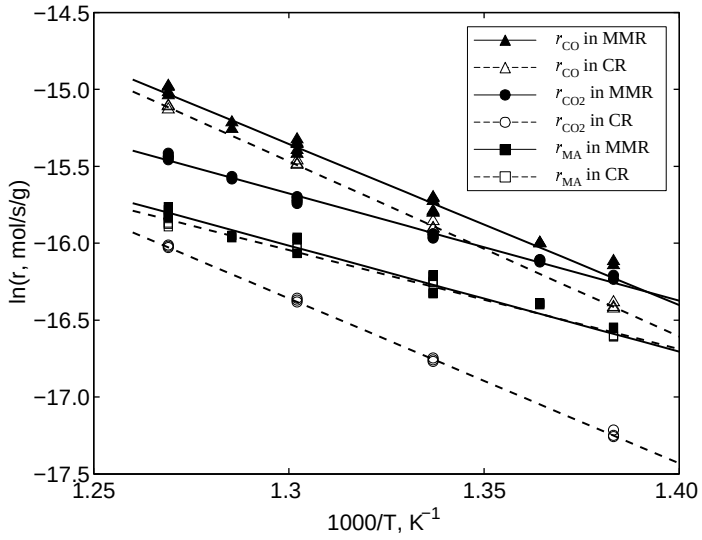

Figure 8-5 Comparison of Arrhenius plots of the CR (open-circuit with I = 0 mA) and MMR (closed-circuit with I = +30 mA). 0.61 mol % butane and 0.76 mol % O_2 in N_2 with total flow rate 38 ml/min.

Table 8-2 Apparent activation energies for products formations in CR and MMR modes.

Apparent activation energy (kJ/mol)	Open-circuit (E_{CR})	Closed-circuit (E_{MMR})	E_{MMR} - E_{CR}
E_{MA}	53.5	57.4	+3.9
E_{CO}	94.6	87.0	-7.6
E_{CO2}	89.2	57.9	-31.3

8.3. Comparison of electrochemically supplied oxygen and gas-phase oxygen

Table 8-3 compares the EMR, CR and MMR operations at the same operating temperature. It should be mentioned that the compared three operations were performed with the same reactor in order to reduce the impact of the preparation of the electrodes and the VPO catalyst as far as possible. The mole flow rates of gas-phase oxygen supplied in the CR and MMR were adjusted to be as close as possible to that supplied electrochemically in the EMR in order to make a fair and direct comparison.

Table 8-3 Comparing EMR, CR and MMR operations. T = 750 K; anode: 0.50-0.54 mol % butane in N_2 with total flow rate 38-39 ml/min.

Parameters	EMR	CR^1	MMR	CR^2
Current feed (mA)	50	-	50	-
O_2 feed (μmol/h)	-	478	446	1053
Overall oxygen feed (μmol/h)	460	478	906	1053
Butane feed (μmol/h)	515	494	480	476
Oxygen consumption (μmol/h)	305	229	350	287
Butane consumption (μmol/h)	64	56	77	70
MA productivity (μmol/h)	31.9	35.8	39.7	43.7
CO productivity (μmol/h)	53.6	53.5	67.7	70.6
CO_2 productivity (μmol/h)	81.5	27.0	83.0	34.0
MA selectivity (%)	48.6	64.0	51.3	62.8
CO selectivity (%)	20.4	23.9	21.9	25.3
CO_2 selectivity (%)	31	12.1	26.8	12.3

Note: the difference between the CR^1 and CR^2 is gas-phase oxygen feed concentration.

First, only the EMR, CR^1 and MMR listed in Table 8-3 are compared herein. Since more total oxygen (gas-phase and ionic oxygen) was supplied in the MMR, the MMR consumed expectedly more butane and more oxygen compared to the CR and the EMR. As can be seen, the consumption rate of oxygen was sequenced as $r_{O_2,MMR} > r_{O_2,EMR} > r_{O_2,CR^1}$. With the similar

overall oxygen feed rates, the oxygen consumption rate in the EMR was clearly higher than the CR, which suggested that the electrochemically supplied oxygen is more reactive than gas-phase oxygen. This conclusion can be further supported through Figure 8-6. As can be seen, at the same total oxygen feed rates in the inlet, the total oxygen consumption rates with three different operations generally increased in the order of "oxygen supplied from gas phase (CR) < oxygen supplied from gas phase and EOP (MMR) < oxygen supplied from EOP (EMR)".

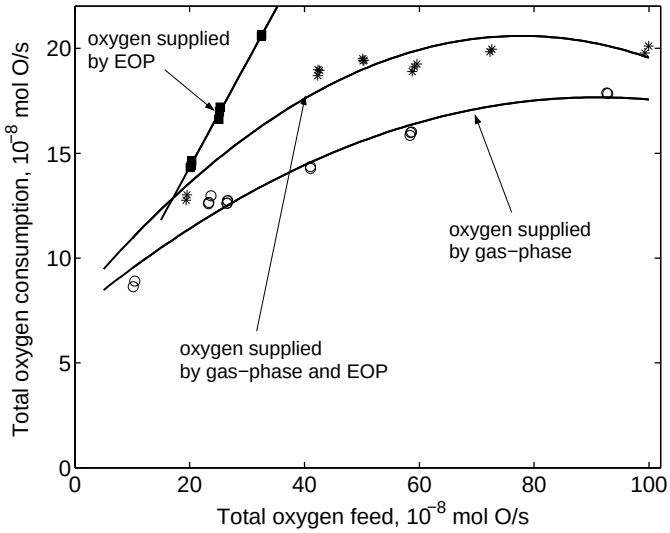

Figure 8-6 Comparison of the oxygen reactivity between gas-phase supplied oxygen and electrochemically supplied oxygen. T = 753 K; anode: 0.51 mol % butane and 0.4-1.8% gaseous oxygen; total flow rate 38-39 ml/min.

As listed in Table 8-3, the MA selectivity in three different operation modes decreased in the order $S_{MA,CR} > S_{MA,MMR} > S_{MA,EMR}$, while the CO_2 selectivity increased in the order $S_{CO_2,CR} < S_{CO_2,MMR} < S_{CO_2,EMR}$. Therefore, compared to gas-phase oxygen supplied in the CR, electrochemically supplied oxygen in the EMR and in the MMR has a lower selectivity to the intermediate product MA while a higher selectivity to the total oxidation product CO_2.

One question arises whether the decrease in the MA selectivity with the MMR operation compared to the CR operation is mainly due to the trade-off behavior of selectivity-conversion usually encountered in the partial oxidation reaction, i.e., increase of butane conversion is achieved at the sacrifice of the MA selectivity. However, according to the experimental results, this is not the case here. As reported in Figure 7-9, the MA selectivity

exhibited a very slight decrease with increasing butane conversion at the oxygen partial pressure range of 0.4-1.0 kPa. Herein, as again instanced in the columns "CR^1" and "CR^2" in Table 8-3, with increasing oxygen feed partial pressure from 0.5 kPa (CR^1) to 1.1 kPa (CR^2) the butane consumption rate increased from 56 μmol/h (CR^1) to 70 μmol/h (CR^2) and the MA selectivity only slightly decreased from 64.0% (CR^1) to 62.8% (CR^2). However, when a current of 50 mA was imposed, the overall oxygen partial pressure increased from 0.5 kPa (CR^1) to 1.0 kPa (MMR) and the MA selectivity clearly decreased from 64.0% to 51.3% as the butane consumption rate increased from 56 μmol/h (CR^1) to 77 μmol/h (MMR).

In Chapter 7, it was reported that the EMR operation gave lower MA selectivity than the CR operation unexpectedly and it has been suggested that this unexpected behavior might be ascribed to two reasons. One possible reason is the different reaction mechanism between the CR and EMR operations. Another reason is the different local ratio of oxygen to butane in the CR and EMR. When the overall oxygen/butane ratios in the feed are close in the CR and the EMR, the local oxygen/butane ratio along the reactor length in the EMR is lower. The low local oxygen/butane ratio can reduce the MA selectivity due to the stronger adsorption of MA on the VPO surface under reducing reaction atmosphere as already discussed in Section 7.2.5.

If the reaction mechanism with electrochemically supplied oxygen were identical to that with gas-phase oxygen and the different local oxygen concentrations between the EMR and CR were the main reason for the lower MA selectivity in the EMR, one could easily infer that the MA selectivity operated in MMR mode should be higher than or at least comparable to that in the CR under similar feed rates of gas-phase oxygen and butane, since additional ionic oxygen is added to the MMR from EOP and the local oxygen concentration along the reactor in the MMR is higher than that in the CR. However, as reported in Table 8-3, the fact is that the MMR gave a significantly lower MA selectivity than the CR (see Table 8-3). Therefore, it can be concluded that the electrochemically pumped oxygen follows a different butane oxidation mechanism from the gas-phase supplied oxygen, which is more likely the main reason for the low MA selectivity obtained in the EMR.

8.4. Catalytic and electrocatalytic butane oxidation in the SEMR

8.4.1. Roles of Au and YSZ in the SEMR

Compared to a conventionally operated catalytic reactor, two additional materials, i.e., YSZ

and Au, were used in the present SEMR. Attributed to the saturated structure of butane, no direct oxidation of butane was observed with co-feeding butane and gas-phase oxygen in the blank SEMR Au/YSZ/Pt-Ag (i.e., CR operation). Moreover, the catalytic rates of the direct oxidation of butane to CO_2 in the blank SEMR under EOP (i.e., EMR operation) was negligible compared to the SEMR VPO/Au/YSZ/Pt-Ag. So the direct conversion of butane on the Au or YSZ surface can be ignored. Nevertheless, the roles of Au and YSZ surface in the further oxidation of the partial oxidation products (all possible intermediates such as furan, MA, CO and so on) formed by initially activating butane on the VPO catalyst surface could not be simply precluded, since the partial oxidation products usually have unsaturated structures and thus are easily over-oxidized by any available oxygen species on the Au or YSZ surface according to either a Langmuir-Hinshelwood or a Rideal-Eley mechanism. Eng et al. [119] has shown that YSZ is a good catalyst for the partial oxidation of CH_4 to C_2 hydrocarbons and CO_2 at high temperature. Herein, the partial oxidation products MA and CO which can be detected in this work were used to prove the overoxidation of the partial oxidation products on the Au or YSZ surface.

To test the catalytic activity of Au and YSZ surface in CR mode, gas-phase oxygen (O_2) and MA (or CO) was co-fed to the reactor Au/YSZ/Pt-Ag. The vapour MA was obtained by melting the crystal MA in the inlet of the reactor. As shown in Figure 8-7a, the CO was over-oxidized to CO_2 on the Au or YSZ surface as co-feeding O_2 and CO, and the formation rates of CO_2 increased with increasing O_2 concentration. It is likely that the CO_2 formation occurred only on the Au surface since no CO_2 was found when CO and O_2 were co-fed to the blank YSZ surface. As can be seen in Figure 8-7b, the co-feeding of MA and O_2 to the reactor Au/YSZ/Pt-Ag resulted in the formation of CO_x (CO_2 dominated). Both the CO and CO_2 formation rates increased with the O_2 concentration. The catalytic oxidation of MA not only occurred on the Au surface but also on the YSZ membrane surface, which was observed by the detection of CO and CO_2 as co-feeding MA and O_2 to the blank YSZ surface. It is worth mentioning that the oxidation of CO or MA is not a homogeneous gas phase reaction. This was concluded from the preliminary experimental result by co-feeding CO (or MA) and O_2 to a blank quartz reactor, where only traces of CO_2 were detected and they were negligible compared to the catalytic reactivity of the Au and YSZ surfaces.

The overoxidation of MA or CO by electrochemically pumped oxygen species in the blank SEMR (Au/YSZ/Pt-Ag) operated in EMR mode can be seen in Figures 8-7c and 8-7d, both the MA and CO overoxidation rates proportionally increased with increasing current and

more CO_2 than CO was formed in the MA overoxidation (see Figure 8-7d).

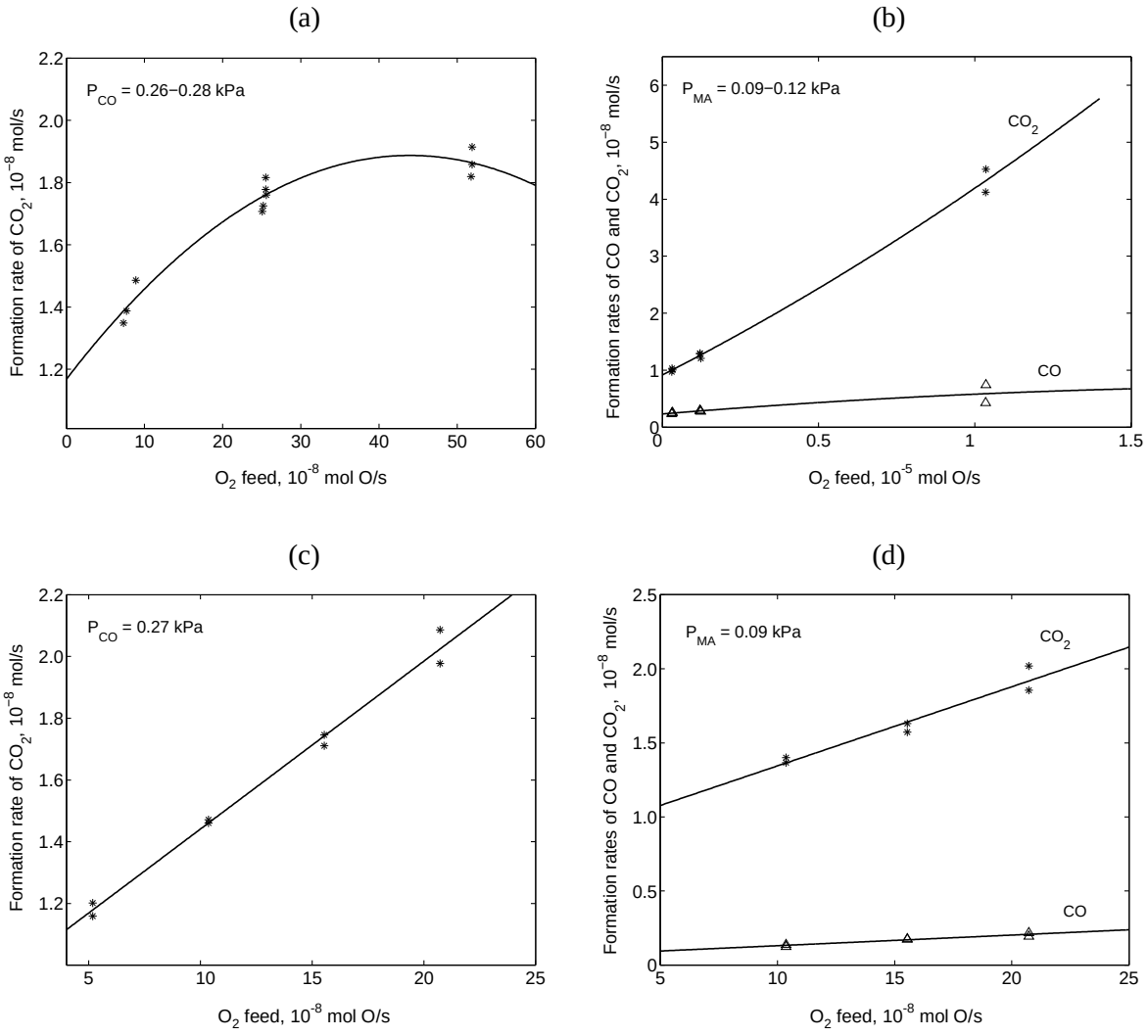

Figure 8-7 Oxidation of CO and MA with (a, b) gas-phase oxygen and (c, d) electrochemically supplied oxygen in the reactor Au/YSZ/Pt-Ag. T = 753 K; total flow rate: 36-38 ml/min balanced with N_2.

The oxygen species involved in the overoxidation of MA and CO on the Au and YSZ surface with electrochemically pumped oxygen are likely more complicated than those with gas-phase oxygen. Once oxygen ions are pumped to the anode, they might quickly combine to form molecular oxygen (O_2) (see Equation 8-4) at the three-phase boundary (3PB) formed between YSZ membrane, Au anode and reaction gas.

$$O^{2-} \xrightarrow{3PB} \frac{1}{2}O_2 + 2e^- \qquad (8\text{-}4)$$

Thus formed O_2 can further oxidize MA or CO on the Au and YSZ surface following the same catalytic overoxidation mechanism as gas-phase oxygen.

On the other hand, electrophilic intermediate oxygen species such as O_2^-, O_2^{2-} and O^- (denoted as $O^{\delta-}$) might be produced in the oxidation of O^{2-} to O_2 at the 3PB, as described in Equation 8-4:

$$O^{2-} \xrightarrow{3PB} O^{\delta-} + (2-\delta)e^- \qquad (8\text{-}5)$$

Therefore the electrocatalytic overoxidation of MA or CO at the 3PB with O^{2-} and electrophilic oxygen $O^{\delta-}$ could not be precluded. The electrophilic oxygen species ($O^{\delta-}$) have been found to be very active in total oxidations [98].

Table 8-4 Comparison of the CO_x formation rates in oxidation of CO and MA with EMR, CR and MMR operations in the reactor Au/YSZ/Pt-Ag. T = 753 K, total flow rate 36-39 ml/min.

	Parameters	EMR	CR[1]	MMR	CR[2]
CO oxidation	Current feed (mA)	30	-	30	-
(P_{CO} = 0.26-0.28 kPa)	O_2 feed (μmol/h)	-	415	431	931
	Overall oxygen feed (μmol/h)	280	415	711	931
	CO_2 formation rates	61.6	57.5	87.3	74.5
MA oxidation	Current feed (mA)	30	-	30	-
(P_{MA}=0.09-0.10 kPa)	O_2 feed (μmol/h)	-	561	558	2165
	Overall oxygen feed (μmol/h)	280	561	838	2165
	CO_2 formation rates (μmol/h)	56.6	37.0	72.8	46.6
	CO formation rates (μmol/h)	6.2	9.0	13.0	10.3
	Rate ratio of CO_2 to CO	9.1	4.1	5.6	4.5

The electrocatalytic overoxidation of MA or CO with electrochemically supplied oxygen was proved to be true by means of comparing the overoxidation rates in EMR, CR and MMR operation modes. As can be seen in Table 8-4, the overall oxygen feed with different operations was in the increasing order of $F_{O_2,EMR} < F_{O_2,CR^1} < F_{O_2,MMR} < F_{O_2,CR^2}$. As described in Figures 8-7a and 8-7b, the CO_2 formation rates in the oxidation of CO and MA increased with the oxygen concentration. If the overoxidation of MA and CO with electrochemically pumped

oxygen only followed the catalytic oxidation path as same as gas-phase oxygen, the formation rates of CO_2 would likely increase in the order of $r_{CO_2,EMR} < r_{CO_2,CR^1} < r_{CO_2,MMR} < r_{CO_2,CR^2}$. Unexpectedly, the observed CO_2 formation rates increased in the sequences of $r_{CO_2,CR^1} < r_{CO_2,CR^2} < r_{CO_2,EMR} < r_{CO_2,MMR}$ in the oxidation of MA and $r_{CO_2,CR^1} < r_{CO_2,EMR} < r_{CO_2,CR^2} < r_{CO_2,MMR}$ in the oxidation of CO. Therefore, the electrochemically supplied oxygen was more reactive to produce CO_2, and the overoxidation of MA or CO with electrochemical oxygen species followed a different mechanism from the catalytic overoxidation with gas-phase oxygen. This conclusion is in line with that of butane partial oxidation in the SEMR with the configuration VPO/Au/YSZ/Pt-Ag.

It is also interesting to note that the ratio of the formation rates of CO_2 to CO in the overoxidation of MA with electrochemically supplied oxygen was 9.1 in EMR mode, while it was 4.1 with gas-phase oxygen in CR mode. This is consistent with the observation in butane oxidation performed in the SEMR with the configuration VPO/Au/YSZ/Pt-Ag as shown in Figure 7-9c (higher S_{CO_2}/S_{CO} in the EMR than the CR). Therefore, the fact that the EMR operation for butane oxidation gave lower MA selectivity but higher oxygen conversion than the CR operation (see Figure 7-9) seems partly due to the electrocatalytic overoxidation of MA to CO_2 with very active electrochemical oxygen species such as O^{2-}, $O^{\delta-}$ at the 3PB. Accordingly, butane oxidation in the SEMR under the EOP condition (i.e., EMR) involved not only the catalytic reaction with conventional oxygen species such as O_2, O^* and O_O^X (lattice oxygen in VPO catalyst) but also the electrocatalytic reaction with electrochemical oxygen species (O^{2-}, $O^{\delta-}$).

8.4.2. Proposal for the catalytic and electrocatalytic reaction-mechanism scheme in the EMR VPO/Au/YSZ/Pt-Ag

Despite extensive research on butane partial oxidation to MA, the mechanism of butane oxidation over VPO catalyst is still unclear [3]. One important reason is that butane oxidation over the VPO catalyst is a multistep reaction involving many intermediates, e.g., butenes, butadiene, crotonlactone, furan and ethylene [120, 121]. Another is that the respective roles of the active oxygen species in the conversion of *n*-butane to MA and CO_x are very difficult to clarify as indicated in the introduction. For the sake of simplification, hereafter the discussion of the mechanism of butane partial oxidation in the SEMR is based on the following

assumption: The catalytic oxidation of butane over the VPO catalyst in a conventional reactor occurs according to a Mars-van Krevelen or redox mechanism involving lattice oxygen [23, 29]. In short, butane is oxidized with the lattice oxygen located on the surface of the oxidized VPO catalyst (VPO_{ox}), and the reduced VPO catalyst (VPO_{red}) is in turn oxidized by gas-phase oxygen (O_2).

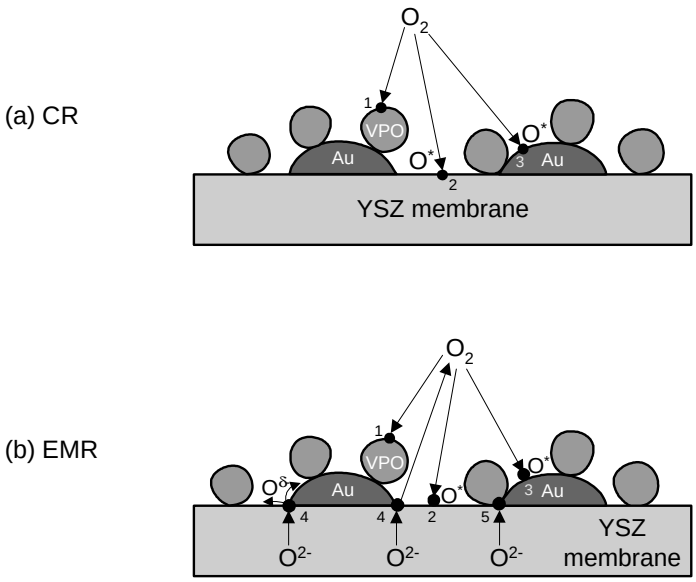

Figure 8-8 Illustration of reaction sites and active oxygen species for butane oxidation carried out in the (a) CR and (b) EMR.

Figures 8-8a and 8-8b illustrate the possible reaction sites and active oxygen species for butane oxidation occurring in the CR and in the EMR, respectively. As can be seen in Figure 8-8a, in the CR the possible reaction sites for the catalytic butane oxidation are (1) VPO catalyst surface, (2) underlying YSZ surface and (3) underlying Au surface. The possible active oxygen species involved in the catalytic reaction are (a) gas phase oxygen (O_2), (b) lattice oxygen located on the surface of VPO catalyst, and (c) adsorbed oxygen species (O^*) on the underlying Au or YSZ surface. Correspondingly, the catalytic reaction mechanism is proposed as described in Figure 8-9a. Herein, the lattice oxygen in the VPO catalyst is assumed to be responsible for the direct oxidation of butane to partial oxidation products (e.g., MA and CO) as well as CO_2 and the further oxidation of MA over the VPO catalyst is not considered. Moreover, some partial oxidation products can be further over-oxidized to CO_2 on the Au or YSZ surface with adsorbed oxygen species. The reduced VPO catalyst is re-oxidized with gas-phase oxygen. In brief, the catalytic reaction can be described as follows:

$$C_4H_{10} + VPO_{ox} \longrightarrow \text{Oxidized products (MA, CO, } CO_2) + VPO_{red} \quad (8\text{-}6)$$

$$\text{MA or CO} + O^* \xrightarrow{\text{Au-YSZ}} CO_2 \quad (8\text{-}7)$$

$$\frac{1}{2}O_2 + VPO_{red} \longrightarrow VPO_{ox} \quad (8\text{-}8)$$

where the overoxidation of MA or CO was used as the exemplification of the over-oxidizing partial oxidation products to CO_2 on the Au or YSZ surface (denoted as Au-YSZ).

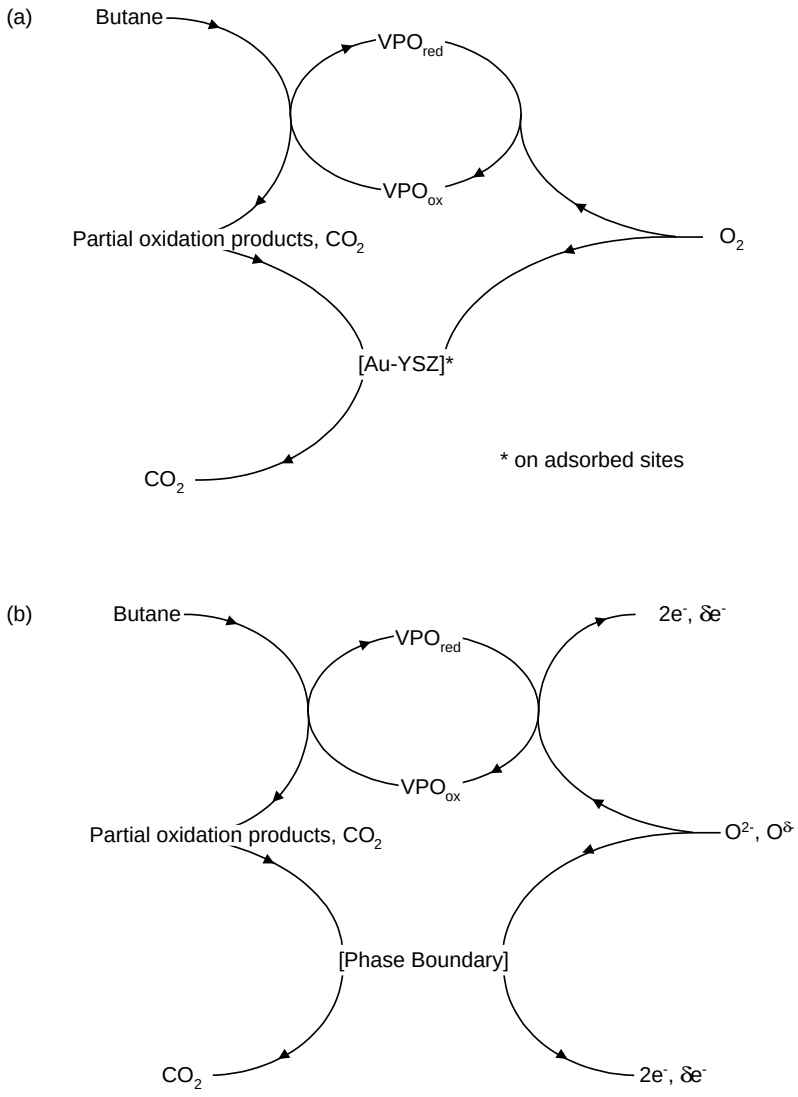

Figure 8-9 Proposed (a) catalytic and (b) electrocatalytic reaction mechanisms for butane partial oxidation performed in an SEMR.

Considering that butane oxidation in the EMR involved not only the catalytic reaction but also the electrocatalytic reaction, in the EMR the possible reaction sites for butane oxidation are as

follows: (1) VPO catalyst surface, (2) underlying YSZ surface, (3) underlying Au surface, (4) 3PB, and (5) four-phase boundary (4PB) formed as the contact point between YSZ membrane, Au electrode, VPO catalyst and reaction gas. Under EOP conditions, the possible active oxygen species are: (a) lattice oxygen located in the surface of VPO catalyst, (b) oxygen ions (O^{2-}) at the 3PB or 4PB, (c) gas-phase oxygen (O_2) generated from oxidizing O^{2-} at the 3PB as described in Equation 8-4, (d) adsorbed oxygen species (O^*) on the underlying Au or YSZ surface, and (e) electrophilic oxygen species ($O^{\delta-}$) such as O_2^-, O_2^{2-} and O^- at the 3PB or 4PB via reaction 8-5.

The catalytic reactions in the EMR are the same as those described in the CR, so Figure 8-9a can also represent the catalytic reaction mechanism occurred in the EMR (only O_2 is generated from the oxidation of O^{2-} at the 3PB via Equation 8-4). The proposed electro-catalytic reaction mechanism in the EMR can be seen in Figure 8-9b. The electrochemical oxygen species such as O^{2-} and electrophilic oxygen $O^{\delta-}$ might directly fill the oxygen vacancy on the surface of the VPO catalyst located at the 4PB with simultaneous release of electrons. Moreover, the electrochemical oxygen species could further oxidize the partially oxidized products to CO_x (more likely CO_2) at the phase boundary. The electrocatalytic reactions taking place in the EMR can be simply described by Equation 8-5 and Equations 8-9 to 8-12.

$$O^{2-} + VPO_{red} \xrightarrow{4PB} VPO_{ox} + 2e^- \quad (8\text{-}9)$$

$$O^{\delta-} + VPO_{red} \xrightarrow{4PB} VPO_{ox} + \delta e^- \quad (8\text{-}10)$$

$$MA \text{ or } CO + O^{2-} \xrightarrow{3PB \text{ or } 4PB} CO_2 + 2e^- \quad (8\text{-}11)$$

$$MA \text{ or } CO + O^{\delta-} \xrightarrow{3PB \text{ or } 4PB} CO_2 + \delta e^- \quad (8\text{-}12)$$

The schemes in Figure 8-9 together represent the complete reaction mechanism for butane oxidation performed in the studied SEMR under EOP conditions, i.e., EMR or MMR operation. The electrocatalytic reaction under EOP conditions directly induced a lower MA selectivity and a higher oxygen conversion in the EMR than the CR. However, the role of O^{2-} and electrophilic $O^{\delta-}$ involved in the electrocatalytic reaction needs further detailed investigations.

8.5. Concluding remarks

The effect of the electrical current in the MMR operation on the catalytic reaction rates and on the product selectivity as well as on the apparent activation energy was investigated. It was found that in MMR mode both positive and negative currents reduced the selectivity to MA compared to the CR mode. Moreover, EOP in the MMR was found to clearly reduce the apparent activation energy for CO_2 formation while increase the apparent activation energy for MA formation. Since the enhancement factor in the studied SEMR was below unity with both positive and negative currents, the current effect is a pure Faradaic effect without any NEMCA effect.

Based on the direct comparison of the EMR, CR and MMR operations, it was concluded that the electrochemically supplied oxygen in the oxidation of butane was more reactive but less selective to product MA than gas-phase oxygen, and it was inferred that the electrochemically supplied oxygen follows a different butane oxidation mechanism from gas-phase oxygen. The butane partial oxidation carried out in the EMR involved not only the same catalytic reaction with conventional oxygen species (O_2, O^*, O_O^X) as in the CR but also the electrocatalytic reaction with electrochemical oxygen species such as O^{2-}, O_2^-, O_2^{2-} and O^-. The electrocatalytic reaction directly leads to a lower MA selectivity in the EMR and in the MMR compared to the CR. A simplified reaction-mechanism scheme is proposed for the butane partial oxidation occurred in the studied SEMR under the EOP condition, which specially takes the overoxidation of partially oxidized products to CO_2 on the Au or YSZ surface into account. The electrochemical oxygen species was found to be very active for the overoxidation of MA and CO to CO_2 compared to conventional oxygen species (O_2, O^*, O_O^X). However, the respective role of O^{2-} and electrophilic $O^{\delta-}$ in the electrocatalytic reaction are difficult to characterize and to identify.

9. General Conclusions and Outlook

The partial oxidation of *n*-butane to MA in a SEMR was studied experimentally in this work. The results can be summarized as follows:

After investigating the oxygen ion conductivity of several solid electrolyte candidates with 2-probe ac impedance spectroscopy, 13% YSZ was chosen as the membrane material to be used for the SEMR due to its higher oxygen ion conductivity at low temperature (< 773 K) and good stability under reducing atmosphere.

The electrical conductivity of VPO catalyst, measured with 2-probe impedance spectroscopy, was rather low. Therefore, the VPO catalyst could not be directly used as the anode. Finally, an oxide-covered porous metal anode was designed in the studied SEMR.

The measured I-V curve of the investigated SEMR prior to butane partial oxidation suggested that the SEMR at low temperature should be operated in EOP mode in order to obtain a high oxygen flux to the anode. The oxygen flux through the membrane under EOP was found to agree very well with Faraday's law at low currents, while it deviated slightly at high currents.

The periodic redox and steady-state experiments for butane partial oxidation performed in the SEMR under the EOP condition clearly demonstrated that the MA synthesis in an EMR is feasible. Butane partial oxidation in the EMR was strongly influenced by the imposed current, reaction temperature and butane feed concentration as well as anodic flow rate. The selectivity to MA was 50-53% and the butane conversion was 15-18% with MA yield of 8-10% in the studied EMR at 753 K. The catalyst-mass-based and membrane-area-based MA productivity of this reactor were 1.22×10^{-4} $mol/(h\cdot g_{cat})$ and 0.017 $mol/(m^2\cdot h)$, respectively.

The direct comparison between the EMR and co-feed reactor in this work was realized by investigating a CR with the same configuration as the EMR. Under steady-state condition, in both the EMR and the CR the selectivity to MA decreased while the selectivity to CO_x increased with increasing temperature, which suggested that the activation energy for MA formation was lower than that for CO_x formation in both operation modes. At the same oxygen/butane feed ratios, the EMR operation gave a higher oxygen conversion but a lower

MA selectivity than the CR operation, which are unexpected. Two possible reasons were suggested for this behavior: (1) the lower local oxygen/butane ratio in the EMR than in the CR and (2) different reaction mechanisms dominating in the EMR and in the CR.

The second reason for the lower MA selectivity in the EMR operation was proved by means of the MMR operation. The results of the MMR operation revealed that both positive and negative currents reduced the selectivity to MA compared to the CR operation. In addition, the enhancement factor in the studied SEMR was below unity both with positive and negative currents, which revealed that the current effect is a pure Faradaic effect without any NEMCA effect.

From the direct comparison between the EMR, CR and MMR operation modes, it was found that EOP in the EMR and the MMR clearly led to a higher oxygen consumption but to a lower MA selectivity compared to the CR and thus it was concluded that electrochemically supplied oxygen in the oxidation of butane was more reactive but less selective to MA compared to gas-phase oxygen. Based on the comparison, it was further inferred that electro-chemically supplied oxygen follows different butane oxidation mechanism from gas-phase oxygen, which is likely the main reason for the lower MA selectivity in the EMR compared to the CR.

Butane partial oxidation is a very complex reaction. The investigated reactor concept in this work is absolutely new. The working principle of this new type of reactor was realized successfully. New knowledge obtained in the present study may also contribute to the investigation of other hydrocarbons oxidation performed in the SEMR. However, some problems are still to be resolved and further improvements have to be achieved:

(1) A composite anode should be developed in order to further reduce the electrical resistance of the electrodes and thus increase the oxygen flux to the anode.
(2) The active oxygen species involved in the electrocatalytic reaction in the EMR might be characterized by means of modern spectroscopic techniques.

References

[1] Kirk-Othmer on-line, Encyclopedia of Chemical Technology, (2001).

[2] www.gobi.co.uk/pdfs/Anhydride.PDF (2000).

[3] G. Centi, F. Trifiro, Chem. Rev. 88 (1988) 55.

[4] F. Cavani, F., Trifiro, Catalysis 11 (1994) 246.

[5] K.E. Birkeland, S.M. Babitz, G.K. Bethke, H.H. Kung, J. Phys.Chem. B 101 (1997) 6895.

[6] P.L. Gai, K. Kourtakies, Science 267 (1995) 661.

[7] G.J. Hutchings, A. Desmartln-Chomel, R. Oller, J.C. Volta, Nature 368 (1994) 41.

[8] G.K. Kwentus, European Patent Application 0189261 (1983).

[9] R.C. Edwrads, C.A. Udovich, U.S. Patent 4,649,205 (1987).

[10] R.M. Contractor, European Patent Application 01899261 (1986).

[11] R.M. Contractor, D.I. Garnett, H.S. Horowitz, H.E. Bergna, G.S. Patience, J.T. Schwartz, G.M. Sisler. In *New Developments in Selective Oxidation II*, (Eds.), V. Cortes Corberan, S. Vic Bellon. Elsevier, 1989, p.233.

[12] R.A. Keppel, V.M. Franchetti, U.S. Patent 4,632,915 (to Monsanto) 1986.

[13] J.T. Wrobleski, J.W. Edwards, C.R. Graham, R.A. Keppel, M. Raffelson, U.S. Patent 4,562,268 (to Monsanto) 1985.

[14] R.M. Contractor, Chem. Eng. Sci. 54 (1999) 5627.

[15] W.J. Johnson, C.J. David, J.J. Allan, F.B. John, J. Am. Chem. Soc. 106 (1984) 8123.

[16] C. J. Kiely, A. Burrows, S. Sajip, G. J. Hutchings, M.T. Sananes, A.Tuel and J.C. Volta, J. Catal. 162 (1996) 31.

[17] N. Harrouch-Batis, H. Batis, A. Ghorbel, J.C. Vedrine and J.C. Volta, J. Catal. 128 (1991) 248.

[18] J.S. Buchanan, S. Sundaresan, Appl. Catal. 26 (1986) 211.

[19] G. Bergeret, M. David, J.P. Broyer, J.C: Volta, G. Hecquet, Catal. Today 1 (1987) 37.

[20] V.A. Zazhigalov, A.I. Pyatnitskaya, I.V. Bachetokova, G.A. Komashko, G. Ladwig, V.M. Belousov, Kinet. Catal. Lett. 23 (1983) 119.

[21] U. Rodemerck, B. Kubias, H.-W. Zanthoff, G.-U. Wolf, M. Baerns, Appl. Catal. A: General 153 (1997) 217.

[22] M. Abon, K.E. Bere, A. Tuel, P. Delichere, J. Catal. 156 (1995) 28.

[23] M.A. Pepera, J.L. Callahan, M.J. Desmond, E.C. Milberger, P.R. Blum, N.J. Bremer, J. Am. Chem. Soc. 107 (1985) 4883.

[24] F. Trifiro, C. Banfi, G. Caputo, P. Forzatti and I. Pasquon, J. Catal. 30 (1973) 393.

[25] Yu.A. Kruchinin, Yu.A. Mishcenko, P.P. Nechiporuk, A.I. Golbshtein, Kinet. Catal. 25 (1984) 328.

[26] M. Misono, K. Miyamoto, K. Tsuji, T. Goto, N. Mizuno, T. Okuhara, in *New Developments in Selective Oxidation*, eds. G. Centi and T. Trifiro, Elsevier, Amsterdam, 1990, p.605.

[27] J.T. Gleaves, J.R. Ebner, T.C. Kuechler, Catal. Rev. - Sci. Eng. 30 (1988) 49.

[28] U. Rodemerck, B. Kubias, H.-W. Zanthoff, M. Baerns, Appl. Catal. A: General 153 (1997) 203.

[29] M. Abon, K.E. Bere, P. Delichere, Catal. Today 33 (1997) 15.

[30] D. Wang, M.A. Barteau, Catal. Lett. 90 (2003) 7.

[31] V.A. Zazghigalov, Yu.P. Zaitsev, V.W. Belousov, N. Wyustnek, H. Wolf, React. Kinet. Catal. Lett. 24 (1984) 375.

[32] J. Coronas, J. Santamaria, Catal. Today 51 (1999) 377.

[33] A. Seidel-Morgenstern, In *Integrated Chemical Processes*, (Eds.), K. Sundmacher, A. Kienle, A. Seidel-Morgenstern, Wiley-VCH, 2005, p.359.

[34] A. M. Ramachandra, Y.Lu, Y.H. Ma, W.R. Moxer, A.G. Dixon, J. Mem. Sci. 116 (1996) 253.

[35] F. Klose, T. Wolff, S. Thomas, A. Seidel-Morgenstern, Appl. Catal. A: General257 (2004) 193.

[36] P. Kölsch, M. Noack, R. Schäfer, G. Georgi, R. Omorjan, J. Caro, J. Mem. Sci. 198 (2002) 119.

[37] C. Tellez, M. Menendez, J. Santamaria, AIChE J. 43 (1997) 777.

[38] R. Mallada, M. Menéndez, J. Santamaria, Catal. Today 56 (2000) 191.

[39] R. Mallada, M. Pedernera, M. Menéndez, J. Santamaria, Ind. Eng. Chem. Res. 39 (2000) 620.

[40] J.G. Sanchez-Macano, T.T. Tsotsis, Catalytic Membranes and Membrane Reactors, Wiley-VCH, Weinheim, 2002.

[41] A. Julbe, D. Farruseng, C. Guizard, J. Mem. Sci. 181 (2001) 320.

[42] T. Kudo, in The CRC Handbook of Solid State Electrochemistry, eds. P.J. Gellings and H.J.M. Bouwmeester, CRC press, Boca Raton, 1997, p.195.

[43] M. Stoukides, Catal. Rev. Sci. Eng. 42 (2000) 1.

[44] H. Iwahara, Y., Asakura, K., Katahira, M. Tanaka, Solid State Ionics 168 (2004) 299.

[45] K. Sundmacher, L.K. Rihko-Struckmann, V. Galvita, Catal. Today 104 (2005) 185.

[46] C. Wagner, Adv. Catal. 21 (1970) 323.

[47] C.G. Vayenas, H.M. Saltsburg, J. Catal. 57 (1979) 296.

[48] M. Stoukides, C.G. Vayenas, J. Catal. 64 (1980) 18.

[49] C.G. Vayenas, J. Catal. 90 (1984) 371.

[50] M. Stoukides, Ind. Eng. Chem. Res. 27 (1988) 1745.

[51] H.G. Lintz, Solid State Ionics 136-137 (2000) 727.

[52] P.D. Petrolekas, I.S. Metcalfe, J. Catal. 152 (1995) 147.

[53] E.M. Breckner, S. Sundaresan, J.B. Benziger, Appl. Catal. 30 (1987) 277.

[54] G. Lu, X. Zuo, Catal. Letters 58 (1999) 67.

[55] P.G. Debenedetti, C.G. Vayenas, Chem. Eng. Sci. 38 (1983) 1817.

[56] C.G. Vayenas, R.D. Farr, Nature 208 (1980) 593.

[57] T. Ishiara, T. Yamada, T. Akbay, Y. Takita, Chem. Eng. Sci. 54 (1999) 1535.

[58] T. Tagawa, K.K. Moe, M. Ito, S. Goto, Chem. Eng. Sci. 54 (1999) 1553.

[59] S. Hamakawa, R. Shiozaki, T. Hayakawa, K. Suzuki, K. Murata, K. Takehira, M. Koizumi, J. Nakamura, T. Uchijima, J. Electrochem. Soc. 144 (2000) 839.

[60] S. Hamakawa, T. Hayakawa, K. Suzuki, K. Murata, K. Takehira , S. Yoshino, J. Nakamura , T. Uchijima, Solid State Ionics 136-137 (2000) 761.

[61] S. Hamakawa, K.Sato, T.Hayakawa, A.P.E, York, T.Tsunoda, K.Suzuki, M. Shimizu, K.Takehira, J. Electrochem. Soc. 144 (1997) 1.

[62] K. Takehira, T. Komatsu , N. Sakai, H. Kajioka, S. Hamakawa, T. Shishido, T. Kawabata, K. Takaki, Appl. Catal. A: General 273 (2004) 133.

[63] N. Lapeña-Rey, P.H. Middleton, Appl. Catal. A: General 240 (2003) 207.

[64] R. Wang, M. Xie, P. Li, C. Ng, Catal. Letters 24 (1994) 67.

[65] C.G. Vayenas, S.I. Bebelis, I.V. Yentekakis, H.-G. Lintz, Catal. Today 11 (1992) 303.

[66] C. Pliangos, I.V. Yentekakis, X. Verykios, C.G. Vayenas, J. Catal. 154 (1995) 124.

[67] I.V. Yentekakis, C.G. Vayenas, J. Catal. 149 (1994) 238.

[68] M. Makri, A. Buekenhoudt, J. Luyten, C.G. Vayenas, Ionics 2 (1996) 282.

[69] C. Pliangos, I.V. Yentekakis, S. Ladas, C.G. Vayenas, J. Catal. 159 (1996) 189.

[70] P.D. Petrolekas, S. Balomenou, C.G. Vayenas, J. Electrochem. Soc. 145 (1998) 1202.

[71] C.G. Vayenas, M.M. Jaksic, S.I. Bebelis, S.G. Neophytides, in: J.O. M. Bockris, B.E. Conway, E. White (Eds.), Modern Aspects of Electrochemistry, Vol. 29, Plenum Publishing Co, New York, 1995, pp. 57.

[72] S. Bebelis, M. Makri, A. Buekenhoudt, J. Luyten, S. Brosda , P. Petrolekas, C. Pliangos, C.G. Vayenas, Solid State Ionics 129 (2000) 33.

[73] P. Delichere, K.E. Bere, M. Abon, Appl. Catal. A: General 172 (1998) 295.

[74] Y. Suchorski, L. Rihko-Struckmann, F. Klose, Y. Ye, M. Alandjiyska, K. Sundmacher, H. Weiß, Applied Surface Science, 249 (2005) 231.

[75] T. Van Dijk, A. J. Burggraff, Phys. Stat. Sol. 63 (1981) 229.

[76] R. Waser, R. Hagenbeck, Acta Mater. 48 (2000) 797.

[77] S.P.S. Badwal, F. T. Ciacchi, D.V. Ho, J. Appl. Electrochem. 21 (1991) 721.

[78] M. Mogensen, D. Lybye, N. Bonanos, P.V. Hendriksen, F.W. Poulsen, Solid State Ionics 174 (2004) 279.

[79] P.J. Gellings, H.J.M. Bouwmeester, the CRC Handbook of Solid State Electro-chemistry, CRC Press, New York, 1997.

[80] P.S. Manning, J.D. Sirman, R.A. De Souza, J.A. Kilner, Solid State Ionics, 100 (1997) 1.

[81] H. Inaba, H. Tagawa, Solid State Ionics, 83 (1996) 1.

[82] S.P.S. Badwal, F. T. Ciacchi, D.milosevic, Solid State Ionics, 136-137 (2000) 91.

[83] O. Yamamoto, Y. Arati, Y. Takeda, N. Imanishi, Y. Mizutani, M. kawai, Y. Nakamura, Solid State Ionics 79 (1995) 137.

[84] S. Loridant, L. Abello, E. Siebert, G. Lucazeau, Solid State Ionics 78 (1995) 249.

[85] J.-M. Herrmann, in: B. Imelik, J.C. Vedrine, (Eds.), Catalyst Characterization, Plenum Press, New York, 1994, p. 559.

[86] J.-M. Herrmann, P. Vernoux, K. E. Bere, M. Abon, J. Catalysis 167 (1997) 106.

[87] G.C. Bond, Heterogeneous Catalysis: Principles and Applications, 2nd ed., Oxford Univ. Press, Oxford, 1987.

[88] G. Busca, Cataly. Today 27 (1996) 457.

[89] J. Ross Macdonald, Impedance Spectroscopy: Emphasizing Solid Materials and Systems, John Wiley & Sons, Inc., New York, 1987.

[90] G.M. Ingo, J. Am. Ceram. Soc. 74 (1991) 381.

[91] X. Guo, Solid State Ionics 99 (1997) 143.

[92] S. Furukawa, M. Okada, Y. Suzuki, Energy Fuels 13 (1999) 1074.

[93] J. H. Park, R.N. Blumental, J. Am. Ceram. Soc. 72 (1989) 1485.

[94] J. Soria, J.S. Moya, J. Am. Ceram. Soc. 71 (1988) C479.

[95] X. Guo, Y.Q. Sun, K. Cui, Sensors and Actuators B 31 (1996) 139.

[96] D.X. Wang, M.A. Barteau, Appl. Catal. A: General 223 (2002) 205.

[97] M. Brown, S. Primdahl, M. Mogensen, J. Electrochem. Soc. 147 (2000) 475.

[98] A. Bielanski, J. Haber, Catal. Rev. - Sci. Eng. 19 (1973) 1.

[99] M. Abon, J.M. Herrmann, J. C. Volta, Catal. Today 71 (2000) 121.

[100] M.J. Lorences, Ph.D. Thesis, University of Oviedo, Oviedo, Spain, 2000.

[101] O. Rubio, R. Mallada, J. Herguido, M. Menéndez, Ind. Eng. Chem. Res. 41 (2002) 5181.

[102] M.J. Lorences, G.S. Patience, F.V. Díez, J. Coca, Ind. Eng. Chem. Res. 42 (2003) 6730.

[103] K. Ait-Lachgar, A. Tuel, M. Brun, J.M. Herrmann, J.M. Krafft, J. R. Martin, J.C. Volta, M. Abon, J. Catal. 177 (1998) 224.

[104] Y. Schuurman, J.T. Gleaves, Catal. Today 33 (1997) 25.

[105] S. Hess, PhD Thesis, University of Erlangen, 2002.

[106] B. Munder, Y. Ye, L. Rihko-Struckmann, K. Sundmacher, Catal. Today 104 (2005) 138.

[107] R. Mallada, S. Sajip, C.J. Kiely, M. Menéndez, J. Santamaría, J. Catal. 196 (2000) 1.

[108] J. van Herle, A.J. McEvoy, Ber. Bunsenges. Phys. Chem. 97 (1993) 470.

[109] G. Marnellos, M. Stoukides, Solid State Ionics 175 (2004) 597.

[110] F.H. van Heuveln, H.J.M. Bouwmeester, J. Electrochem. Soc. 144 (1997) 134.

[111] G. Centi, G. Fornasari, F. Trifiro, Ind. Eng. Chem. Prod. Res. Dev. 24 (1985) 32.

[112] S.K. Bej, M.S. Rao, Ind. Eng. Chem. Res. 30 (1991) 1829.

[113] R.K. Sharma, D.L. Cresswell, E.J. Newson, AIChE J. 37 (1991) 39.

[114] J. Nicole, D. Tsiplakides, S. Wodiunig, Ch. Comninellis, J. Electrochem. Soc. 144 (1997) L312.

[115] P. Tsiakaras, C. G. Vayenas, J. Catal. 144 (1993) 333.

[116] E. Ivers-Tiffee, A. Weber, D. Herbstritt, J. Europ. Ceram. Soc. 21(2001) 1805.

[117] C. Pliangos, C. Raptis, Th. Badas, D. Tsiplakides, C.G. Vayenas, Electrochimica Acta 46 (2000) 331.

[118] A. Kaloyannis, C.G. Vayenas, J. Catal. 171 (1997) 148.

[119] D. Eng, M. Stoukides, Catal. Lett. 9 (1991) 47-54.

[120] B. Kubias, U. Rodemerck, H.-W. Zanthoff, M. Meisel, Catal. Today 32 (1996) 243-253.

[121] B. Chen, E. J. Munson, J. AM. Chem. Soc. 124 (2002) 1638-1652.

Appendices

Appendix I. GC analysis

As shown in Figure A1, there are two serial channels “A” and “B” with five capillary columns and three 6-way valves as well as one 10-way valve (see Figure A2) in the used Agilent 6890 GC. valves 1 and 4 are the gas sampling valves, while valves 2 and 3 are switching valves. The “A” channel includes columns 4 and 5 and it is equipped with a FID, while the “B” channel includes columns 1, 2 and 3 and it is equipped with a TCD.

In the “A” channel, the MA and other hydrocarbons such as butane and butene are separated by column 4 (HP-1, 10 m, 0.53 mm I.D.). Subsequently, the MA first elutes from column 4 and it is directly transferred to the FID by switching on valve 2 at 0.55 min (see Table A1). At 2.0 min, valve 2 is switched off and hydrocarbons without MA from column 4 pass into column 5 (FFAP, 50 m, 0.32 mm I.D.) where different hydrocarbons are separated from each other and detected by FID.

In the “B” channel, the gas sample is initially separated into an inert gas mixture [N_2, O_2, CO] and CO_2 as well as H_2O in column 2 (PLOT-Q, 30 m, 0.53 mm I.D.) after flushing MA back with column 1 (HP-1, 10 m, 0.53 mm I.D.). Subsequently, with switching on the valve 3 at 3.2 min, CO_2 directly flows into the TCD due to its short residence time in column 2. At 4.3 min, the valve 3 is switched off again and the inert gas mixture [N_2, O_2, CO] is separated in column 3 (MS 5A). Finally, at 8.2 min the valve 3 is again switched on and thus H_2O is introduced from column 2 directly into the TCD.

The oven temperature program is plotted in Figure A3 and a typical GC spectrum is given for instance in Figure A4. The program of valve switching time described in Table A1 is used for on-line sampling.

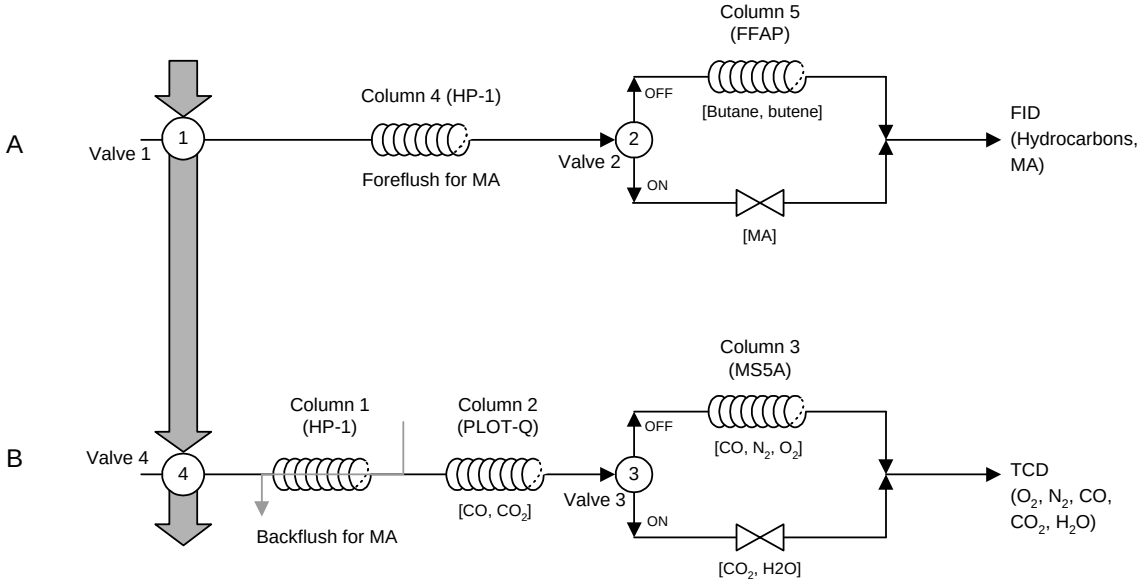

Figure A1 GC analysis for butane partial oxidation.

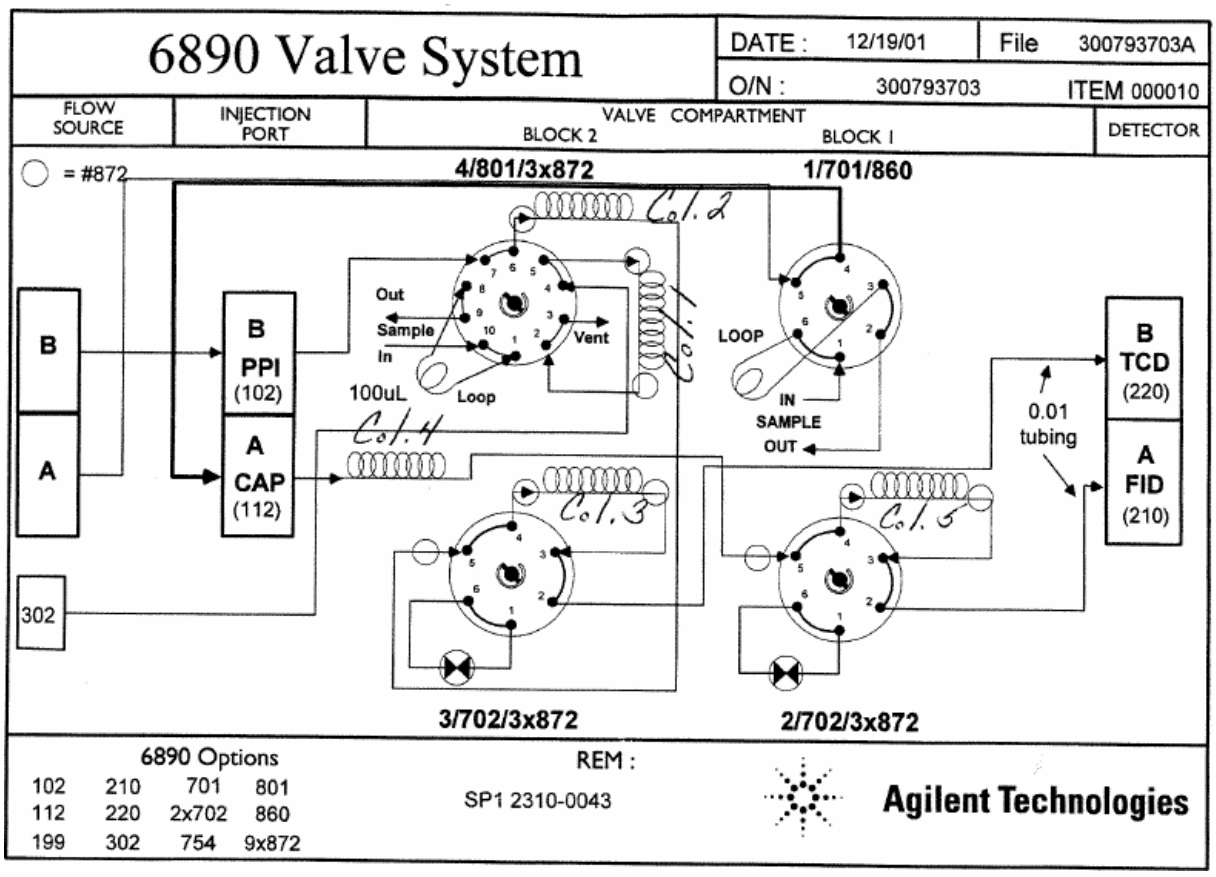

Figure A2 GC valve system.

Table A1 Program of valves used in GC.

Valve	Time (min)	Setpoint
V2	0	OFF
V3	0	OFF
V2	0.55	ON
V2	2.0	OFF
V3	3.2	ON
V3	4.3	OFF
V3	8.2	ON
V3	12.5	OFF

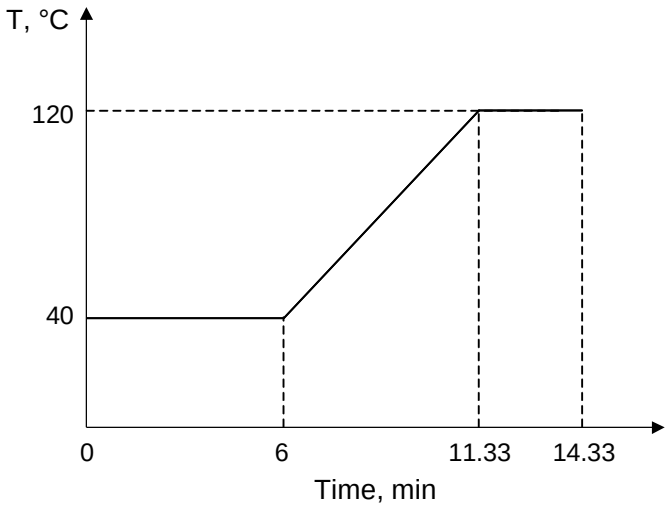

Figure A3 Temperature program applied to GC analysis.

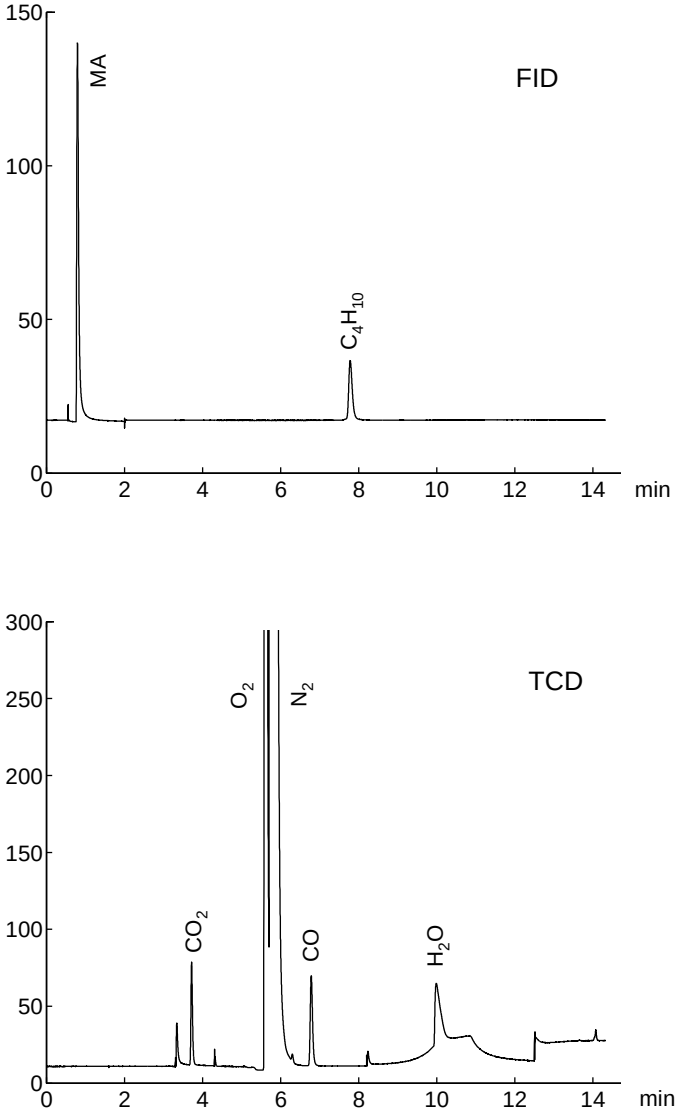

Figure A4 Examples of the GC analysis.

Appendix II. Kröger-Vink notation

Table A2 Kröger-Vink notation for point defects in Crystals [79].

Type of defect	Symbol	Remarks
Vacant M site	V_M''	Divalent ions are chosen as example with MX as compound formula
Vacant X site	$V_X^{\bullet\bullet}$	M^{2+}, X^{2-}: cation and anion
Ion on lattice site	M_M^X , X_X^X	^{x}: unchanged
L on M site	L_M'	L^+ dopant ion
N on M site	$N_M^{\bullet}$	N^{3+} dopant ion
Free electron	e'	
Free (electron) hole	$h^{\bullet}$	
Interstitial M ion	$M_i^{\bullet\bullet}$	$^{\bullet}$: effective positive charge
Interstitial X ion	X_i''	$'$: effective negative charge

Appendix III. Publication list

Journal Publications:

1. Ye Y., Rihko-Struckmann L., Munder B., Rau H., Sundmacher K., Feasibility of an electrochemical membrane reactor for partial oxidation of *n*-butane to maleic anhydride. *Industrial & Engineering Chemistry Research*, 2004, **43**: 4551-4558.
2. Ye Y., Rihko-Struckmann L., Munder B., Sundmacher K., Partial oxidation of *n*-butane in a solid electrolyte membrane reactor: Periodic and steady-state operations. *Applied Catalysis A: General*, 2005, **285** (1-2): 86-95.
3. Ye Y., Rihko-Struckmann L., Munder B., Sundmacher K., Partial oxidation of *n*-butane in a solid electrolyte membrane reactor: Influence of electrochemical oxygen pumping. *Journal of The Electrochemical Society*, 2006, **153** (2): D21-D29.
4. Munder B., Ye Y., Rihko-Struckmann L., Sundmacher K., Solid electrolyte membrane reactor for controlled partial oxidation of hydrocarbons: model and experimental validation. *Catalysis Today*, 2005, **104**: 138-148.
5. Rihko-Struckmann L. Ye Y., Chalakov L., Suchorski Y., Weiß H., Sundmacher K., Characterisation of VPO catalyst used in an electrochemical membrane reactor. *Catalysis Letters*, 2006, in press.
6. Suchorski Y., Rihko-Struckmann L., Klose F., Ye Y., Alandjiyska M., Sundmacher K., Weiß H., Evolution of oxidation states in vanadium-based catalysts under conventional XPS conditions, *Applied Surface Science*, 2005, **249**: 231-237.

Conference Contributions:

7. Sundmacher K., Rihko-Struckmann L., Munder B., and Ye Y., Elektrochemische Charakterisierung von Festoxidmembranen für Partial Oxidationsprozesse, DECHEMA-Arbeitsausschuss “Technische Reaktionen”, 13-14 January, 2003, Frankfurt am Main, Germany.
8. Rihko-Struckmann L., Ye Y., Munder B., Sundmacher K., Chalakov L., Schulz M., Rau H., Kontrollierte Partialoxidation von Butan in einem elektrochemischen Membranreaktor, *XXXVI Jahrestreffen Deutscher Katalytiker*, 19-21 March 2003, Weimar, Germany.
9. Ye Y., Rihko-Struckmann L., Munder B. and Sundmacher K., Electrochemical characterization of VPO catalyst for butane partial oxidation, *EuropaCat VI*, 31 August - 4 September 2003, Innsbruck, Austria.
10. Munder B., Rihko-Struckmann L. Ye Y. and Sundmacher K., Electrochemical membrane reactor for controlled partial oxidation of hydrocarbons: model-based analysis of reactor

dynamics, *4th European Congress of Chemical Engineering*, 21-25 September 2003, Granada, Spain.

11. Ye Y., Rihko-Struckmann L., Munder B. and Sundmacher K., Experimental study on electrochemical membrane reactor for n-butane partial oxidation, *16th International Conference on Chemical Reactors*, 1-5 December 2003, Berlin, Germany.
12. Rihko-Struckmann L., Ye Y., Munder B., Chalakov L. and Sundmacher K.: Vanadyl-pyrophosphatkatalysator (VPO) als Anodenkomponente in elektrochemischen Membran-reaktoren, *XXXVII. Jahrestreffen Deutscher Katalytiker*, 17-19 March 2004, Weimar, Germany.
13. Frömmichen R., Chalakov L., Rihko-Stuckmann L., Ye Y., Munder B. and Sundmacher K., Electrochemical membrane reactors for partial oxidation of light hydrocarbons, *13th International Congress on Catalysis*, 11-16 June 2004, Paris, France.
14. Munder B., Ye Y., Rihko-Struckmann L., Sundmacher K., Electrochemical membrane reactor for controlled partial oxidation of hydrocarbons: model and experimental validation, *6th International Conference on Catalysis in Membrane Reactors*, 6-9 July 2004, Lahnstein, Germany.
15. Ye Y., Rihko-Struckmann L., Munder B., Sundmacher K., Conversion and selectivity behaviour of an electrochemical membrane process, *16th International Congress of Chemical and Process Engineering (CHISA 2004)*, 22-26 August 2004, Prague, Czech Republic.
16. Rihko-Struckmann L., Ye Y., Chalakov L., Suchorski Y., Weiß H. and Sundmacher K., Charakterisierung von anodischen Vanadylpyrophosphatkatalysatoren (VPO) in elektro-chemischen Membranreaktoren, *XXXVIII Jahrestreffen Deutscher Katalytiker*, 16-18 March 2005, Weimar, Germany.
17. Suchorski Y., Rihko-Struckmann L., Ye Y., Sundmacher K. and Weiß H., XPS-mapping of a membrane reactor surface: Vanadium oxidation state variations, *IWSP-2005*, 10-13 September 2005, Polanica Zdroj/Wroclaw, Poland.
18. Ye Y., Rihko-Struckmann L., Munder B. and Sundmacher K., Influence of electro-chemical oxygen pumping on the performance of butane partial oxidation to maleic anhydride in a solid electrolyte membrane reactor. *EuropaCat-VII*, 28 August-01 September, 2005, Sofia, Bulgaria.